

REPORT DOCUMENTATION PAGE			Form Approved OMB No. 0704-0188	
<small>Public reporting burden for this collection of information is estimated to average 1 hour per response, including the time for reviewing instructions, searching existing data sources, gathering and maintaining the data needed, and completing and reviewing the collection of information. Send comments regarding this burden estimate or any other aspect of this collection of information, including suggestions for reducing this burden, to Washington Headquarters Services, Directorate for Information Operations and Reports, 1215 Jefferson Davis Highway, Suite 1204, Arlington, VA 22202-4302, and to the Office of Management and Budget, Paperwork Reduction Project (0704-0188), Washington, DC 20503.</small>				
1. AGENCY USE ONLY (Leave blank)		2. REPORT DATE 5.Sep.02		3. REPORT TYPE AND DATES COVERED DISSERTATION
4. TITLE AND SUBTITLE A STUDY OF MAGNETIC STROM CURRENT SYSTEMS BY THE APPLICATION OF WAVELET ANALYSIS TO GROUND-BASED MAGNETOGRMS			5. FUNDING NUMBERS	
6. AUTHOR(S) MAJ CADE WILLIAM B III				
7. PERFORMING ORGANIZATION NAME(S) AND ADDRESS(ES) UTAH STATE UNIVERSITY			8. PERFORMING ORGANIZATION REPORT NUMBER CI02-512	
9. SPONSORING/MONITORING AGENCY NAME(S) AND ADDRESS(ES) THE DEPARTMENT OF THE AIR FORCE AFIT/CIA, BLDG 125 2950 P STREET WPAFB OH 45433			10. SPONSORING/MONITORING AGENCY REPORT NUMBER	
11. SUPPLEMENTARY NOTES				
12a. DISTRIBUTION AVAILABILITY STATEMENT Unlimited distribution In Accordance With AFI 35-205/AFIT Sup 1			12b. DISTRIBUTION CODE	
13. ABSTRACT (Maximum 200 words)				
<div style="font-size: 2em; font-weight: bold;">20021028 005</div>				
14. SUBJECT TERMS			15. NUMBER OF PAGES 135	
			16. PRICE CODE	
17. SECURITY CLASSIFICATION OF REPORT	18. SECURITY CLASSIFICATION OF THIS PAGE	19. SECURITY CLASSIFICATION OF ABSTRACT	20. LIMITATION OF ABSTRACT	

A STUDY OF MAGNETIC STORM CURRENT SYSTEMS BY THE APPLICATION
OF WAVELET ANALYSIS TO GROUND-BASED MAGNETOGRAMS

by

William B. Cade III

A dissertation submitted in partial fulfillment
of the requirements for the degree

of

DOCTOR OF PHILOSOPHY

in

Physics

Approved:

Jan Sojka
Major Professor

Bela Fejer
Committee Member

Piotr Kokoszka
Committee Member

Charles Torre
Committee Member

Lie Zhu
Committee Member

Thomas Kent
Dean of Graduate Studies

UTAH STATE UNIVERSITY
Logan, Utah

2002

Copyright © William B. Cade III 2002

All Rights Reserved

ABSTRACT

A Study of Magnetic Storm Current Systems by the Application of
Wavelet Analysis to Ground-Based Magnetograms

by

William B. Cade III, Doctor of Philosophy


Utah State University, 2002

Major Professor: Dr. Jan J. Sojka
Department: Physics

Ground-based magnetograms are used to measure the intensity of magnetic storms, yet the relative contributions of the current systems involved have been debated for decades. Wavelet analysis is a technique to analyze signals with complex content and is well suited to the analysis of time-series data. I applied wavelet analysis to ground magnetograms to extract information about magnetic storms current systems. The analysis showed three components at low- and mid-latitudes: 3-6 hours, 12-25 hours, and >30 hours, with each most likely associated with different current systems. Wavelet analysis also enabled the separation of directly driven and unloading components in high-latitude magnetic data. This allowed a comparison of low- and high-latitude substorm measurements to calculate the configuration of the substorm current wedge. Reasonable wedge configurations were found that matched the magnetic measurements.

(135 pages)

DEDICATION

This work is dedicated to my family: 

ACKNOWLEDGMENTS

I would like to thank Jan Sojka for being the best advisor anyone could have. His guidance, enthusiasm, and support have made my research a truly enjoyable experience. Thanks to Lie Zhu for providing his expertise to my work whenever asked. Thank you to Dr. Yohsuke Kamide of the Solar Terrestrial Environment Laboratory, Nagoya University, Japan, for the great interaction in Greece, the interest in and support of my work, and for the data that made this work possible. Thanks to the Utah Article Delivery Service (UTAD), without which Chapter 3 would not have been possible. The Physics and CASS staff members (Deborah, Karalee, Sharon, James, Marilyn, Shawna, and Melanie) have been so friendly and helpful (even though I took unauthorized binder clips) – they made this effort so much easier. A special thanks to Deborah as the shepherd of the process.

Thanks to my parents, Nelwyn and Jack Strain and Bancker and Lana Cade, for their support and encouragement.

Most of all, I want to thank the most important people in my life, my family – Beth, Kelsi, and Kyle. You have been so wonderful and supportive of me and I appreciate it so much. We make a great team!

The views expressed in this work are those of the author and do not reflect the official policy or position of the United States Air Force, Department of Defense, or the U.S. Government.

CONTENTS

	Page
ABSTRACT	iii
DEDICATION	iv
ACKNOWLEDGMENTS	v
LIST OF TABLES	viii
LIST OF FIGURES	ix
INTRODUCTION	1
DATA DESCRIPTION	4
Geomagnetic Indices.....	4
January-June 1979 Data Set.....	7
REVIEW OF CURRENT CONTRIBUTIONS TO LOW- AND MID-LATITUDE MAGNETIC MEASUREMENTS.....	10
Ring Current.....	10
Magnetopause Current.	17
Tail Current	22
Partial Ring Current	27
Field-Aligned Currents	44
Other Currents.....	55
BASICS OF WAVELET ANALYSIS	62
The Fourier Transform and Its Limitations	62
The Short-Time Fourier Transform and Its Limitations	64
Wavelet Analysis	67
WAVELET ANALYSIS OF LOW- AND MID-LATITUDE DATA	73
Storm Data Selection	73
Wavelet Analysis of Magnetograms.....	76
WAVELET ANALYSIS OF HIGH-LATITUDE DATA	87
Substorm Current Wedge and Electrojet Theory.....	87
Separation of Electrojet Components via DWT	88

Substorm Current Wedge Calculations.....	90
CONCLUSIONS AND FURTHER STUDY	99
Conclusions.....	99
Areas For Further Study.....	100
REFERENCES	103
CURRICULUM VITAE	123

LIST OF TABLES

Table	Page
1 Coordinates of the magnetic stations of the <i>Dst</i> network.....	5
2 Observatories for the data set used in this study	8
3 Ratios of internal-to-external magnetic field components found by various authors	56
4 Ratios of internal-to-external magnetic field components found by various authors and the corresponding correction factors to remove induction from ΔH	58
5 Time periods selected for study from the Jan-Jun 1979 data set	73
6 Level and scale information for DWT analysis on 1-minute data using the Reverse Biorthogonal 2.8 wavelet	88
7 Data selected for current wedge calculations.....	96

LIST OF FIGURES

Figure	Page
1 The chain of <i>AE</i> stations.....	6
2 Low- and mid-latitude data for a magnetic storm during 10-13 Mar 79.....	9
3 High-latitude data for a magnetic storm during 10-13 Mar 79	9
4 Chapman and Ferraro's bridge current, which would produce a westward ring current as a result of charges building up on the magnetopause surface	11
5 a) Spiral and bounce motion and b) gradient-drift motion proposed by <i>Singer</i> [1957] as the causes of the ring current	13
6 Ring current distribution calculated by <i>Akasofu and Chapman</i> [1961].....	15
7 Chapman and Ferraro's depiction of currents flowing on the front of a plasma cloud interacting with the Earth's magnetic field	18
8 Magnetic field at the Earth's equator due to the magnetopause current	19
9 The current loops of the tail current system modeled by <i>Alexeev et al.</i> [1996].....	25
10 Equatorial magnetic field effect of the tail current calculated by <i>Iyemori and Rao</i> [1996] based on the <i>Tsyganenko</i> 1987 magnetic field model	26
11 Contribution of the ring and tail currents to <i>Dst</i> as theorized by <i>Ohtani et al.</i> [2001]	27
12 The atmospheric current system of <i>Chapman</i> [1927] to explain magnetic storm surface field measurements	28
13 Comparison of <i>DS</i> and <i>Dst</i> evolution during magnetic storms reported by <i>Sugiura and Chapman</i> [1960].....	29
14 Magnetic storm current system proposed by <i>Alfvén</i> [1940].....	30
15 Partial ring current system proposed by <i>Cummings</i> [1966] to explain the low-latitude asymmetry in the <i>H</i> disturbance field	31
16 Proposed partial ring current and westward electrojet current systems [<i>Fukushima</i> 1972].	34

17	Relative contributions of partial ring current elements to the surface H disturbance as calculated by <i>Crooker and Siscoe</i> [1974].....	35
18	Updated magnetospheric current system proposed by <i>Harel et al.</i> [1981b] including a midnight-centered partial ring current.....	36
19	Diagram of how a rotation of the Region 1 current system produces a net downward current at noon and a net upward current at midnight.....	37
20	Total ring current density distribution calculated by <i>De Michelis et al.</i> [1997] for different AE activity ranges	39
21	Combination of (a) a symmetric ring current and (b) a two-loop quadrupole system to produce a partial ring current system (c) [<i>Tsyganenko</i> 1993].....	41
22	Field-aligned current systems proposed by <i>Birkeland</i> [1908] to explain polar magnetic disturbances	44
23	<i>Boström's</i> [1964] two types of field-aligned current systems	46
24	The substorm current wedge (top), its equivalent current system (bottom right), and its magnetic signature at 30° latitude (bottom left) as studied by <i>Clauer and McPherron</i> [1974].....	48
25	The Region 1 and Region 2 currents reported by <i>Iijima and Potemra</i> [1978].....	49
26	Current system for polar magnetic substorms proposed by <i>Kamide et al.</i> [1976]	50
27	Substorm current system proposed by <i>Chen et al.</i> [1982]	52
28	Main phase contributions to 1-minute Dst by conjugate substorm current wedges with ionospheric closure at 52.5° latitude as calculated by <i>Friedrich et al.</i> [1999]	54
29	Example showing how a signal composed of sinusoidal components of four frequencies is decomposed by a Fourier Transform	62
30	Periodograms derived from performing a Fast Fourier Transform (FFT) on sinusoidal signals with progressively increasing frequencies	63
31	Signal composed of impulses and the resulting FFT periodogram.....	64
32	Analysis of a sinusoidal signal of increasing frequency with the Short-Time Fourier Transform (STFT) with two different window sizes.....	65

33	STFT with two different windows of a two-frequency signal with two imbedded impulses.....	66
34	(a) The Second Derivative Gaussian, or Mexican Hat, Wavelet. The effect of (b) scale and (c) translation upon the Mexican Hat Wavelet when compared to a sinusoidal signal	68
35	Absolute value of the CWT coefficients resulting from analyzing a sinusoidal signal with the Mexican Hat wavelet.....	68
36	Some possible wavelets: (a) Mexican Hat wavelet, (b) Morlet wavelet, (c) 1 st -derivative Gaussian wavelet, and (d) Haar wavelet.....	69
37	CWT analysis of a sinusoidal signal of increasing frequency using the Morlet wavelet.....	70
38	Absolute value of the CWT coefficients resulting from analyzing an aperiodic impulsive signal with the Mexican Hat wavelet	71
39	Absolute value of the CWT coefficients resulting from analyzing a signal containing a steady low frequency, an increasing high frequency, and several discontinuities.....	71
40	Magnetograms and <i>SYMH</i> for the period 0000 UT/20 Feb 79 – 1315 UT/23 Feb 79.....	74
41	Magnetograms and <i>SYMH</i> for the period 0030 UT/10 Mar 79 – 1345 UT/13 Mar 79	74
42	Magnetograms and <i>SYMH</i> for the period 1725 UT/2 Apr 79 – 0640 UT/6 Apr 79.....	75
43	Magnetograms and <i>SYMH</i> for the period 0000 UT/24 Apr 79 – 1315 UT/27 Apr 79.....	75
44	The Reverse Biorthogonal 2.8 wavelet	76
45	Absolute value of the CWT coefficients for the 20-23 Feb 79 storm	77
46	Absolute value of the CWT coefficients for the 10-13 Mar 79 storm	77
47	Absolute value of the CWT coefficients for the 2-6 Apr 79 storm.....	78
48	Absolute value of the CWT coefficients for the 24-27 Apr 79 storm.....	78
49	Absolute value of the CWT coefficients for the 20-23 Feb 79 storm	80

50	Absolute value of the CWT coefficients for the 10-13 Mar 79 storm	80
51	Absolute value of the CWT coefficients for the 2-6 Apr 79 storm.....	81
52	Absolute value of the CWT coefficients for the 24-27 Apr 79 storm.....	81
53	Time average of the square of the CWT coefficients for pseudo-periods up to 52 hours	82
54	Time average of the square of the CWT coefficients for pseudo-periods up to 5 hours	82
55	FFT of the four storm times for periods up to 52 hours.....	83
56	Reconstructed magnetograms with only periods > 36 hours retained	85
57	Reconstructed magnetograms with only periods > 18 hours retained	85
58	Leirvogur magnetogram analyzed with the SWT denoising technique to remove high frequencies	89
59	Example of how the SWT denoising separates the directly driven (middle) and unloading (bottom) components from a substorm signature (top)	90
60	Example of a mid-latitude local time profile of a substorm.....	91
61	Multiple signatures of a substorm found in magnetograms during the 2-6 Apr 79 storm	92
62	Plot of Kp versus the electrojet latitudes that provide a self-consistent current wedge solution to the low- and high-latitude measurements in Table 7	96
63	Plot of Kp versus the median distance of the wedge tail current closure corresponding to the electrojet latitudes calculated in Figure 62	97
64	Plot of Kp versus the median electrojet current intensity values that provide a self-consistent current wedge solution to the low- and high-latitude measurements in Table 7	98

CHAPTER 1

INTRODUCTION

Geomagnetic storms are a subject of great importance in the space physics community, as well as for others such as satellite operators, power companies, and communication system users who suffer from the impacts of these disruptive events. During geomagnetic storms, electric currents are flowing in various regions of the magnetosphere and ionosphere. These currents produce changes in the Earth's magnetic field at the surface that are measured by ground-based magnetometers. The derived magnetograms will be a combination of the signatures of various current systems with different characteristic times, the relative contributions of which are determined by the latitude and local-time location of the magnetometer. These magnetograms are also used to create geomagnetic activity indices, such as *Dst* and *AE*. One long-standing debate in the space physics community is the issue of what current systems contribute to the *Dst* index. This index, derived from averaged low- and mid-latitude ground magnetometers, is supposed to represent the growth and decay of the symmetric ring current. However, it is likely other currents influence these magnetometers and therefore the *Dst* index [Kamide *et al.*, 1998]. In particular, Campbell [1996] argues that *Dst* may instead represent a lognormal distribution of inputs from various currents with differing time scales. Chapter 2 will present a discussion of the nature of these magnetograms and the derived indices, as well as the data set provided by Dr. Yohsuke Kamide of the Solar Terrestrial Environment Lab at Nagoya University, Japan. This data set will be used in this study.

Chapter 3 will discuss the main current systems contributing to ground magnetic perturbations and how these currents affect low- and mid-latitude magnetic measurements and *Dst*. The magnetopause current flows around the outside surface of the magnetosphere and is driven primarily by the speed and density of the solar wind. The tail current flows across the center of the Earth's magnetotail region and responds to various solar wind parameters. The ring current flows around the Earth, primarily in the near-Earth equatorial plane, and is driven mostly by magnetospheric convection. Ionospheric currents flow in the auroral zone in response to changes in magnetospheric currents, convection, and changes in ionospheric conductivity. Field-aligned currents connect the magnetospheric and ionospheric currents and respond to changes in all of these. The partial ring current exists within a portion of the ring current region, and views of its cause vary from current imbalances in the field-aligned current to asymmetric injection of protons from the magnetotail into the near-Earth environment. The substorm current wedge results from a portion of the tail current being diverted into the ionosphere via field-aligned current. Of particular interest is the effect of the substorm current wedge on *Dst* [Friedrich *et al.*, 1999].

Chapter 4 will discuss the similarities and differences of Fourier and wavelet analysis and why wavelet analysis is better suited to geomagnetic storm studies. Fourier analysis has been used in the past to analyze magnetograms to determine the spectral components, but there are some inherent problems with its use. While Fourier analysis is good for spectrum analysis of signals with more or less constant frequency components, its usefulness is limited when signals with impulsive components are

involved. Wavelet analysis, on the other hand, is perfectly suited to finding frequency components that may not be sinusoidal, such as with pulsed signals. From this perspective, wavelets have a promising potential when applied to geophysical systems, such as magnetic storm records, which are composed of impulsive inputs of a non-sinusoidal nature, such as intense substorms during the main phase of magnetic storms. It should, in principle, be possible to extract the magnetogram components of different characteristic scales.

In Chapter 5, I discuss the results of applying wavelet analysis to low- and mid-latitude magnetograms, in the hopes of finding out if these measurements are truly composed of current systems with different characteristic time scales, and if so, what these time scales are. In particular, it is hoped that within a storm lasting a day or more, substorm signatures (on the order of 3 hours) can be identified. Chapter 6 presents the results of applying wavelet analysis to high-latitude substorm measurements to differentiate between the directly-driven and loading-unloading electrojet components (the loading-unloading component corresponds to the substorm current wedge). The loading-unloading component is then compared to the positive perturbations at low-latitude near local midnight to determine if these two measurements can provide a self-consistent picture of the theorized substorm current wedge and confirm these low-latitude signatures correlate to substorms. A by-product of this effort will be relationships among various substorm parameters: the geomagnetic activity index Kp , latitude of the ionospheric electrojet current, location of wedge closure in the magnetotail, and current intensity.

CHAPTER 2

DATA DESCRIPTION

Geomagnetic Indices

Dst Index

The *Dst* index was first derived both by *Sugiura* [1964] and *Kertz* [1964] and was conceived as a measure of the intensity of the equatorial ring current (see Chapter 3). Since the ring current is assumed to be mostly a symmetric, equatorial zonal current, its magnetic field at the surface is parallel to the dipole axis and is seen mainly in the horizontal component (H) of the magnetic field [*Rangarajan*, 1989]. The method of *Sugiura* is essentially in use today, in which the disturbance of the horizontal field is made up of two parts: 1) a universal-time part *Dst*; and 2) a local-time dependent part *DS*. For a uniform longitudinal distribution of stations, the mean value of D at any instant will not be contaminated by *DS* (assuming that *DS* has a global average of zero), so that essentially *Dst* is measured. Under the assumption the spatial and temporal variations in ring current intensity are not rapid, a dense network of stations is not needed. Currently, *Dst* is measured by four stations (Table 1) located far enough from the magnetic equator so they are not affected by the equatorial electrojet, yet close enough to the equator to minimize auroral effects [*Rangarajan*, 1989]. Other currents, however, may still effect *Dst*, as has been increasingly recognized by more researchers. This issue is discussed at length in Chapter 3.

Table 1. Coordinates of the magnetic stations of the *Dst* network.

Station	Geographic Latitude	Geographic Longitude	Magnetic Latitude	Magnetic Longitude
Honolulu	21.32	202.00	21.46	268.57
San Juan	18.38	293.88	29.36	5.21
Hermanus	-34.42	19.23	-33.73	82.67
Kakioka	36.23	140.18	26.62	207.77

In computing the index, the hourly average of H is recorded at each station. The diurnal solar-quiet (Sq) variation is computed at each station for each month for the five quietest days, and then subtracted from the original hourly values. The reference level at each station is determined by a parabola fitted to the annual means of H for the five quietest days each month. The hourly H disturbance value for each station is then obtained by subtracting the Sq value and the reference level. These disturbance values are then corrected for latitude to obtain the equatorial equivalent, and then averaged to determine the hourly *Dst* value [Mayaud, 1980].

Auroral Indices

The auroral indices AE , AL , AU , and AO (hereafter called the AE indices) were first introduced by Davis and Sugiura [1966] to measure the auroral electrojets and are discussed in detail by Mayaud [1980]. Using a chain of 12 auroral stations (Figure 1), a quiet time reference level is derived for each month at each station from the five quietest days. This level is subtracted from the 2.5 or 1-minute H data for each station, the data is superposed in universal time, and the extreme positive and negative values at each instant define AU and AL , respectively. Ideally, AL should measure the intensity of the westward

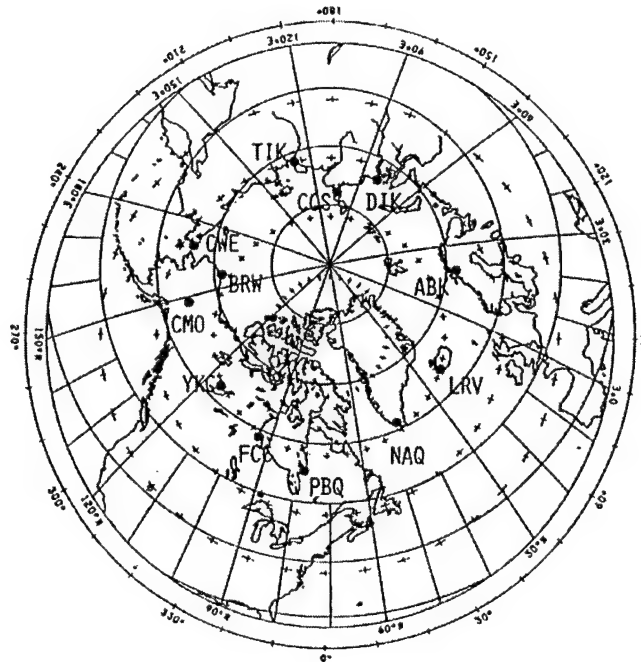


Figure 1. The chain of *AE* stations. Geographic coordinates are indicated by solid lines, and geomagnetic coordinates are shown by plus signs [from *Data Book 21*, WDC-C2 for Geomagnetism, Kyoto, Japan, 1992].

electrojet, while *AU* should measure the intensity of the eastward electrojet. These indices most likely contain contributions from any other zonal currents. Therefore *AE* is defined as $AU - AL$ to remove any symmetric zonal contribution. *AO*, defined as $(AU + AL)/2$, is then intended to be an approximate measure of the equivalent zonal current. However, since there is asymmetry between the eastward and westward electrojets, *AO* really measures this asymmetry plus any zonal current effects. Unlike the currents that drive the *Dst* index, the auroral electrojets are relatively close to the Earth (~ 100 - 200 km) and so the *AE* indices are extremely sensitive to the positions of these currents.

While the *AE* indices can be considered to be more closely tied to a physical system (the auroral electrojets), there are still other factors that can influence these indices. Other currents, including currents induced within the conducting Earth, can contribute. In particular, the effect of induced currents can be extremely complex and variable [Boström, 1971; Kisabeth and Rostoker, 1977]. Also, the daily regular variation of *H* is not eliminated as it is for *Dst*. Although this is not significant during active periods (the daily variation is tens of nT, while the electrojet variations are hundreds of nT), the daily variation itself can define *AU* and *AL* during quiet periods [Mayaud, 1980].

January-June 1979 Data Set

Dr. Yohsuke Kamide of the Solar Terrestrial Environment Lab at Nagoya University, Japan, has provided a data set for use in this study. The set consists of 5-minute resolution magnetic observations from the six low- to mid-latitude stations listed in Table 2 for the time period January 1 – June 30, 1979. These observations are also used to compute the *SYM H* index, which is calculated in the same way as *Dst* except it is at 5-minute resolution instead of 1-hour. *SYM H* can be considered as an improved, higher time resolution *Dst* index [Ohtani *et al.*, 2001]. The data set has been quality controlled by Dr. Kamide and he has used his own procedures to remove the quiet-time baseline. The set contains five storm periods where *Dst* drops below -100 nT. An example of data from a magnetic storm period is shown in Figure 2. Notice each individual station shows more variability than the *SYM H* index.

Table 2. Observatories for the data set used in this study.

Station	Geographic Latitude	Geographic Longitude	Magnetic Latitude	Magnetic Longitude
Low- and Mid-Latitude Stations (5-minute resolution)				
San Juan (SJG)	18.38	293.88	29.36	5.21
Hermanus (HER)	-34.42	19.23	-33.73	82.67
Tashkent (TKT)	41.33	69.62	32.51	145.52
Kakioka (KAK)	36.23	140.18	26.62	207.77
Honolulu (HON)	21.32	202.00	21.46	268.57
Boulder (BOU)	40.13	254.77	48.88	319.04
High-Latitude Stations (1-minute resolution)				
Narssarssuaq (NAQ)	61.20	314.60	70.60	38.66
Leirvogur (LRV)	64.18	338.30	69.71	71.98
Abisko (ABK)	68.36	18.82	65.88	115.50
Dixon Island (DIK)	73.55	80.57	63.36	162.45
Cape Chelyuskin (CCS)	77.72	104.28	66.72	177.41
Tixie Bay (TIK)	71.58	129.00	60.99	192.81
Cape Wellen (CWE)	66.17	190.17	62.36	239.37
Barrow (BRW)	71.30	203.25	69.10	243.67
College (CMO)	64.87	212.17	65.10	259.23
Yellow Knife (YLK)	62.47	245.53	69.14	296.56
Fort Churchill (FCC)	58.80	265.90	68.53	325.60
Poste-de-la-Baleine (PBQ)	55.30	287.25	66.31	357.38

The set also includes 1-minute data from the 12 high-latitude stations (see Table 2) that comprise the *AE* network, along with the derived *AE* indices. Figure 3 shows the measurements from the *AE* stations for the same storm as shown in Figure 2. In general high-latitude magnetograms show much more variability and on smaller time scales than lower-latitude measurements.

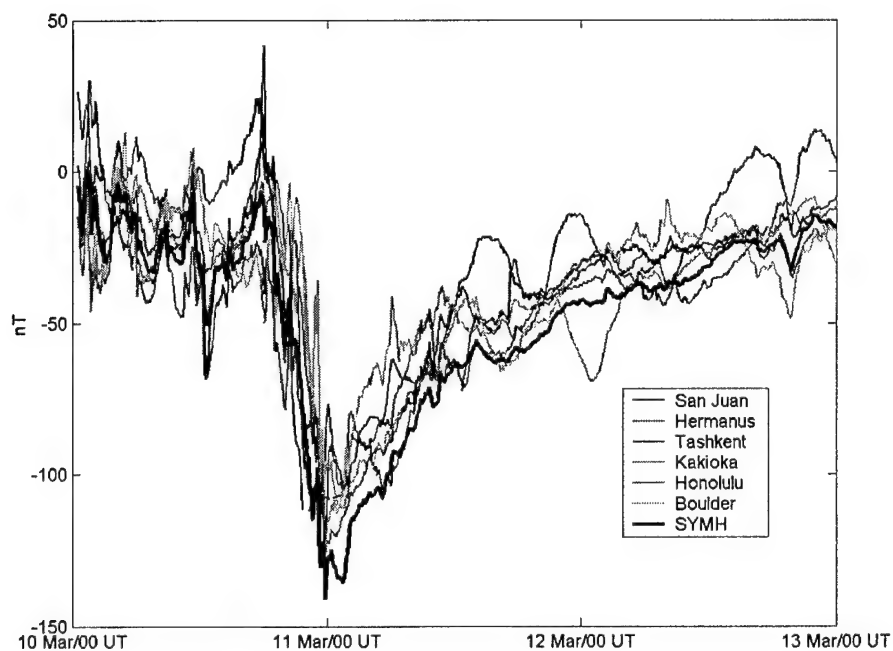


Figure 2. Low- and mid-latitude data for a magnetic storm during 10-13 Mar 79.

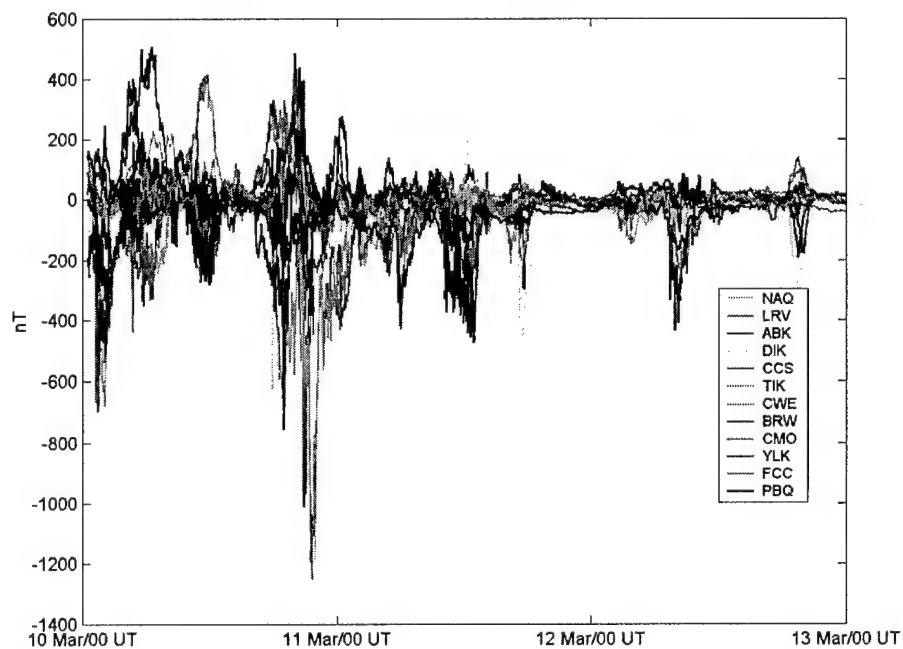


Figure 3. High-latitude data for a magnetic storm during 10-13 Mar 79.

CHAPTER 3

REVIEW OF CURRENT CONTRIBUTIONS TO LOW- AND MID- LATITUDE MAGNETIC MEASUREMENTS

Ring Current

Many geophysicists at the turn of the century theorized a current ring encircling the Earth as a possible cause of the worldwide main phase magnetic depression during a magnetic storm (a phenomena first studied extensively by *Birkeland* [1908] and *Moos* [1910]). *Birkeland* [1908], theorizing on what he called the negative equatorial perturbation, postulated a current ring based on his terella experiments showing it was possible to trap a ring of electrons around a magnetized sphere. Following the work of *Birkeland*, *Störmer* [1910] discussed the existence of a permanent ring current of trapped charges of one sign, mainly to explain the equatorward movement of the auroral zone during a magnetic storm, and *Schmidt* [1917] talked about an equatorial ring current fed by particles from the sun as relating to both the aurora and to low-latitude storm perturbations. In a series of papers, *Chapman* [1918, 1927] discussed the characteristics and possible causes of magnetic storms and, believing currents could not exist outside the atmosphere, attributed storms to currents flowing in the upper atmosphere, first as a result of vertical motions [1918] and then to horizontal currents [1927]. Later, in their landmark work on magnetic storms, *Chapman and Ferraro* [1933] attributed the storm depression to the penetration of ions into the cavity formed by the interaction of solar plasma cloud with the Earth's magnetic field. Ions would drift across the cavity on the

night side, dragging electrons behind them, with a velocity differential creating a westward current across the gap (Figure 4), with the current closure being uncertain but presumably creating a current ring around the Earth. Modeling it as a simple circular current, they showed it could be maintained for days before breaking up. *Chapman* [1935] was a continuation of his 1918 and 1927 papers on magnetic storms and discussed the issue of atmospheric versus extraterrestrial currents. He concluded the evidence favored atmospheric currents, but if there was an extraterrestrial ring current, he favored the Chapman and Ferraro model over that of Störmer. *Vestine and Chapman* [1938] still favored atmospheric currents, but acknowledged a ring current could exist at $\sim 2 R_e$ due to differential ion and electron velocities. *Forbush* [1938], studying the effect of magnetic storms on cosmic ray measurements, concluded his data was consistent with the existence of an extraterrestrial ring current at a distance $> 2 R_e$. *Chapman and Bartels* [1940] also

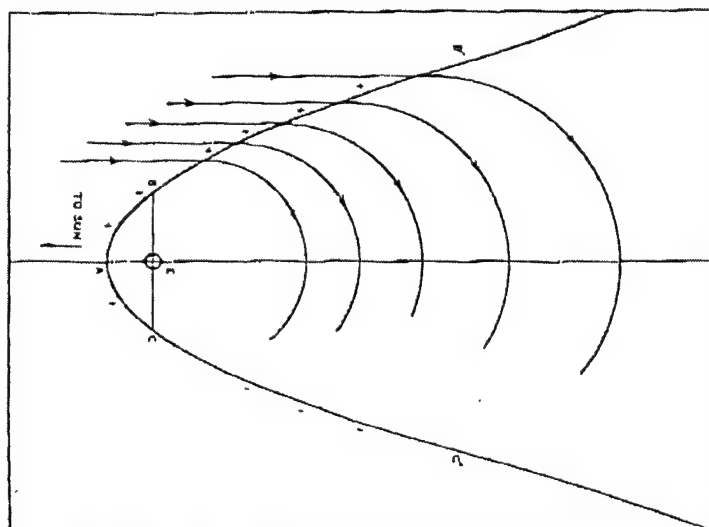


Figure 4. Chapman and Ferraro's bridge current, which would produce a westward ring current as a result of charges building up on the magnetopause surface [*Chapman and Ferraro*, 1933].

favored the Chapman and Ferraro bridge current over that of Störmer. Still somewhat skeptical of currents flowing above the atmosphere, they noted if the current is of one sign (as in Störmer's theory), it could not hold together. If the current is of both signs (as in the Chapman and Ferraro model), the formation mechanism breaks down. In the end they left the question open. *Chapman and Ferraro* [1941] studied the stability of their theoretical ring current (using a simple cylindrical current sheet model) and deduced it could be stable at a distance of $\sim 7-9 R_e$. *Martyn* [1951], expanding on the work of *Chapman and Ferraro* [1931, 1932, 1933], applied hydrodynamic considerations to the formation of the hollow around the Earth (the magnetosphere) and ring current stability and found a stable ring current at $5-6 R_e$ with a width of $2 R_e$. He included this ring current as part of a larger system of currents that flowed from the ring, into the auroral zone, meridionally across the auroral zone, and back into the ring. *Alfvén* [1939, 1940, 1950, 1955] developed a theory of magnetic storm currents based on the interaction of a solar plasma cloud's electric field with the Earth, and the subsequent differential ion/electron drift, to produce a ring current connected to the ionosphere through field-aligned currents.

Using hydromagnetic theory, *Parker* [1956, 1958a, 1958b] tried to show it was impossible for a ring current to cause the storm main phase. According to his calculations, it would take months or years for magnetic field changes from the ring current to diffuse to the Earth's surface through the medium between. His views were countered by *Hines* [1957] and *Hines and Storey* [1958] who tried to show the diffusion time could be as little as a few seconds. The essential differences between their two

views were addressed in a joint paper [Hines and Parker, 1958]. Meanwhile, Singer [1957] had developed his ideas, which would become fundamental to ring current theory. He proposed the ring current was distributed throughout the trapping region in the Earth's magnetic field, as suggested by the terella pictures of Birkeland [1908, 1913] and the calculation of forbidden regions by Störmer [1955]. In his theory, these trapped particles would spiral along magnetic field lines, be reflected, and would gradient drift (protons westward and electrons eastward – an idea originally discussed by Alfvén [1939, 1940]) to produce a net westward ring current that was largely permanent (Figure 5). Particles would be lost through pitch angle scattering. Two years later Dessler and Parker [1959], based largely on the work of Parker [1957a, 1957b, 1958c] (and now accepting the ring current as the main phase source), developed a detailed hydromagnetic formulation describing the physics of particles trapped in the Earth's magnetic field during a magnetic storm. Their description explained the initial and main phase perturbations in terms of stresses set up in the geomagnetic field, the main phase being mainly due to outward stresses from the centrifugal force of protons as they oscillate along magnetic field lines.

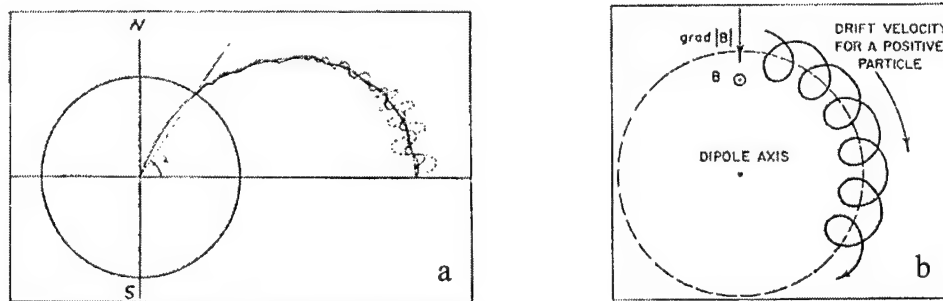


Figure 5. a) Spiral and bounce motion and b) gradient-drift motion proposed by Singer [1957] as the causes of the ring current.

They assumed a trapping environment at 3-5 R_e . They also formulated the still-used relation $\Delta B/B_o = -2E/3E_m$ for the magnetic field intensity at the Earth's center (ΔB) due to a ring current with particles of total energy E (B_o is the intensity of the Earth's main field and E_m is the total energy of the Earth's field). This relation was later shown to be valid under general conditions by *Sckopke* [1966] and is now called the Dessler-Parker-Sckopke (DPS) relation (recently re-verified by *Greenspan and Hamilton* [2000] and *Ebihara and Ejiri* [2000] as corrected by *Vasyliunas* [2001] and *Ebihara and Ejiri* [2001]).

The discovery of the radiation belts and the realization there was a permanent population of trapped particles confirmed the existence of a permanent ring current and located it at a distance of a few R_e . Space-based measurements were used to construct ring current models [e.g., *Smith et al.*, 1960] and ring current theories were quickly refined [e.g., *Akasofu*, 1960; *Akasofu and Chapman*, 1961; *Akasofu et al.* 1961; *Apel et al.*, 1962; and *Hoffman and Bracken*, 1965], extending the theories of *Parker* [1957b], *Singer* [1957], *Dessler and Parker* [1959], and incorporating the pioneering plasma physics work of *Alfvén* [1950]. Based on these studies, it became apparent pressure gradients in the trapped particle environment (not the particle drift) were the most important terms determining the current intensity (this fact had been shown years earlier to be true in general for a magnetically immobilized plasma by *Tonks* [1955]). In the ring current environment, It was found the pressure gradient distribution actually induced an eastward current on the inner edge of the region and a much more dominant westward current further out (Figure 6), a distribution verified by magnetospheric magnetic field

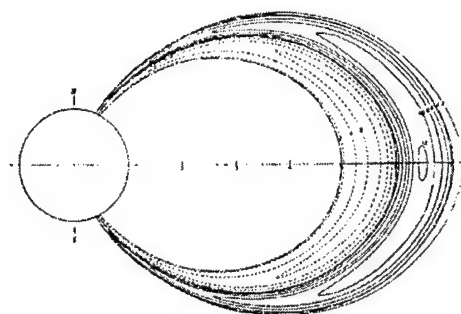


Figure 6. Ring current distribution calculated by *Akasofu and Chapman* [1961]. Solid contours indicate a westward current and dashed contours indicate an eastward current.

measurements. Most placed the current center at about $6 R_e$ and assigned protons as the primary current carrier.

After the ring current's existence was verified and the basic physics had been developed, the ring current was widely accepted as the cause of the symmetric part of the storm main phase depression at low latitudes. The focus of many researchers shifted to investigating the injection, energization, and decay processes, the particle sources and composition, and the particle energy spectra [e.g., *Lyons and Williams*, 1980; *Williams*, 1983; *Williams*, 1985; *Williams*, 1987]. A detailed description of these is beyond the scope of this paper, but a recent review of the advancements in these areas is provided by *Daglis et al.* [1999]. Trying to study and model the ring current's behavior during storms became another area of research interest [e.g., *Lui et al.*, 1987; *Hamilton et al.*, 1988; *Wrenn*, 1989; *Takahashi et al.*, 1990; *Feldstein et al.*, 1990; *Feldstein*, 1992; *Ebihara and Ejiri*, 2000; *Fok et al.*, 2001].

It has always been well known the ring current alone does not produce the low-latitude main phase depression. Typically the magnetic signature is divided between a symmetric component (attributed to the symmetric ring current and represented by *Dst*)

and an asymmetric component (usually attributed to a partial ring current). It was even recognized that other currents contribute to the symmetric component (i.e. the magnetopause current, induced Earth currents, the tail current, and even the partial ring current) but the ring current was by far the dominant contributor [e.g., *Lui et al.*, 1987]. Recently, however, some researchers have begun to dispute this view. *Campbell* [1996] created a stir by proposing the *Dst* storm signature was not due to a ring current but instead was produced by a conglomeration of varying currents with varying time constants, as exhibited by the lognormal distribution-like nature of the typical *Dst* profile. *Belova and Maltsev* [1994], *Alexeev et al.* [1996], *Dremukhina et al.* [1999], and *Kalegaev and Dmitriev* [2000] all stated the contribution of the tail current is equal to that of the ring current. *Roeder et al.* [1996a,b] found for one particular storm the observed ring current particle fluxes could only account for 40-70% and 30-50% of *Dst* respectively, indicating other current systems could be important. *Turner et al.* [2001] also reported results of storm studies showing ring current ions produce about 50% of the *Dst* depression. These results are contradicted by others [*Yokoyama and Kamide*, 1997; *McPherron*, 1997; *Rostoker et al.*, 1997b; *Jorgensen et al.*, 1997; *Noël*, 1997; *Jordanova et al.*, 1998; *Ebihara and Ejiri*, 2000; *Greenspan and Hamilton*, 2000; *Reeves and Henderson*, 2001] who still believe *Dst* is predominately reflective of the growth and decay of the ring current. However even within this area, most agree there is a significant asymmetric ring current contribution during the storm main phase, indicating the partial ring current, not just the symmetric ring current, is important. *Grafe* [1999] has gone further and suggested there is no evidence a symmetric ring current even exists, only an

asymmetric one. In a review of our current understanding of magnetic storms by the most prominent researchers in the field, *Kamide et al.* [1998] recognized “the present *Dst* value includes significantly an artificially symmetric value resulting from asymmetric perturbations.” Whether *Dst* is an accurate reflection of the growth and decay of the ring current is still a controversial issue.

Magnetopause Current

In response to the predominate theory of the time (as seen, for example, in *Chapman* [1918]) magnetic storms were due to clouds from the sun composed of particles of one charge, *Lindemann* [1919] was the first to propose magnetic storms were produced by a neutral plasma interacting with the Earth. *Chapman and Ferraro* [1931, 1932, 1940] were the first to rigorously model a neutral plasma interacting with the Earth’s magnetic field, assuming space was a void only occasionally interrupted by a streaming plasma from the sun. Using a simple model of a conducting planar sheet approaching the Earth, they were able to infer current patterns (Figure 7), a roughly parabolic shape of the boundary, and the existence of cusp regions (referred to as horns). They used this model’s currents to explain the initial phase of geomagnetic storms, where ground magnetic measurements show a sudden increase of up to 100 nT in *H*. Since that time, magnetopause currents have been recognized as the source of the storm initial phase.

As the solar wind became recognized as a permanent feature, many researchers began detailed analysis of the nature of the solar wind-magnetosphere interaction [e.g.,

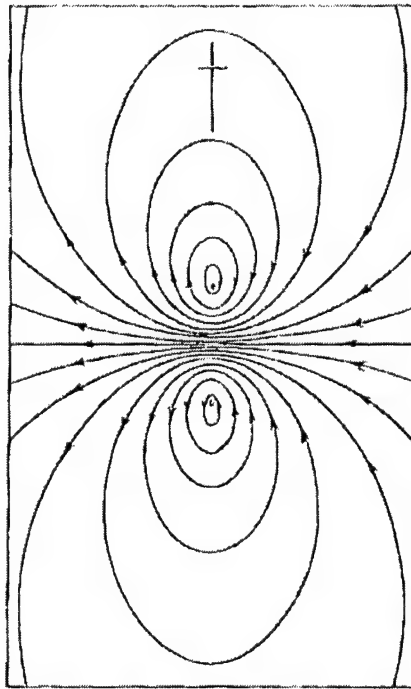


Figure 7. Chapman and Ferraro's depiction of currents flowing on the front of a plasma cloud interacting with the Earth's magnetic field. The view is from the Earth towards the sun [Chapman and Ferraro, 1932].

Ferraro, 1960a and 1960b; *Beard*, 1960; *Dungey*, 1961; *Spreiter and Briggs*, 1962; *Beard*, 1962; *Midgley and Davis*, 1963; *Midgley*, 1964; *Mead*, 1964; *Mead and Beard*, 1964]. Most of these authors were interested in finding the shape of the magnetopause by pressure balance methods, and as a by-product, the magnetopause current system was found that would cause the Earth's field outside the magnetosphere to be zero. *Midgley and Davis* [1963] used a moment technique to find the magnetopause boundary and integrate over the current on this surface to derive an expression for the magnetic field near Earth due to this current (for a solar wind of velocity 500 km/sec and density 2.5 ions/cc, equatorial values were 30.8 nT at noon and 26.1 nT at midnight). *Mead* [1964] used the magnetopause current calculated by *Mead and Beard* [1964] to express the

geomagnetic potential inside the magnetosphere in terms of a spherical harmonic series. By taking the negative gradient of this potential, Mead was able to derive expressions for the magnetic field due to the current anywhere within the magnetosphere, particularly at the Earth's surface, as a function of magnetopause boundary distance (Figure 8). Mead stated values of around 25 nT for a boundary at $10 R_e$ and 115 nT for a boundary at $6 R_e$. It is interesting to note that *Mead* gives the equation $B = 0.0305\sqrt{nv}$ (n is solar wind density and v is solar wind velocity) as an approximate expression for the field at the Earth's surface due to magnetopause currents. At the suggestion of Mead, *Midgley* [1964] reanalyzed the work of *Midgley and Davis* [1963] to obtain a scalar potential in terms of a spherical harmonic series, and found their magnetic fields agreed with *Mead* to within 0.1 to 0.4% through most of the inner magnetosphere. *Davis and Sugiura* [1966] estimated the magnetopause current surface field with $(0.25/r_b^3)\cos\theta$ gauss (r_b is the magnetopause distance in R_e and θ is latitude; r_b of 10 gives 20 nT at the equator).

Both *Midgley and Davis* [1963] and *Mead* [1964] assumed no dipole tilt relative to the solar wind direction. *Olson* [1969] extended the calculations of *Mead and Beard*

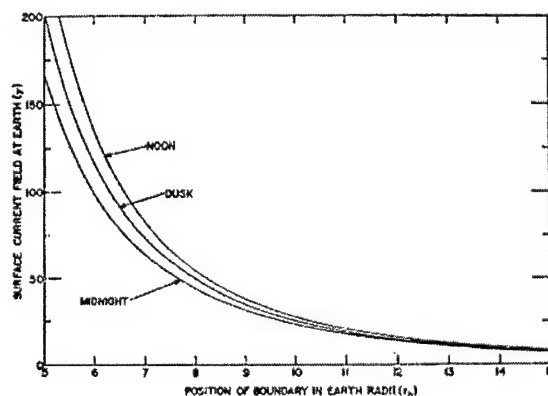


Figure 8. Magnetic field at the Earth's equator due to the magnetopause current [*Mead*, 1964].

[1964] to include dipole tilt. *Olson* [1970] used the *Olson* [1969] model of the magnetosphere to show magnetopause currents could be responsible for the quiet-time variations in the Earth's magnetic field measurements (daily, semiannual, and annual). He was able to show the magnetopause current reproduces the variability properly, but only about 20% of the amplitude. *Choe et al.* [1973] used a self-consistent iteration method (similar to *Mead and Beard* [1964]) to calculate the magnetopause surface for various dipole tilt angles. *Choe and Beard* [1974] (later corrected by *Halderson et al.* [1975]) used the *Choe et al.* model to integrate over the magnetopause current and derive a scalar potential (expanded in spherical harmonics) to represent the magnetic field. They presented results similar to those of *Mead* [1964] in Figure 5.

Several authors [*Siscoe et al.*, 1968; *Ogilvie et al.*, 1968; *Verzariu et al.*, 1972; *Su and Konradi*, 1975) studied the relationship $B = K\sqrt{nv}$ proposed by *Mead* [1964] for the field at the Earth due to the magnetopause current and found varying values of the constant K . *Verzariu et al.* [1972] compared \sqrt{nv} (from solar wind data) to Dst during quiet times and found a linear correlation, confirming the interpretation positive Dst fluctuations are caused by magnetopause boundary currents associated with the solar wind. *Su and Konradi* [1975] analyzed the relation in a slightly different form,

$$Dst = K \times 10^4 R_s^{-3} + \Delta B_r$$

(R_s is the magnetopause subsolar distance and is proportional to $(nv^2)^{-1/6}$, ΔB_r is the magnetic field depression due to the ring and tail currents).

Comparing Dst to solar wind values, they determined ΔB_r to be -19 nT for quiet times and -44 nT for slightly disturbed times, while K did not change (their value was 1.4 times *Mead's* value). *Burton et al.* [1975] rearranged this relation in another form,

$Dst_0 = Dst - b(P_d)^{1/2} + c$ (where Dst_0 is the Dst corrected to remove the effects of magnetopause currents, P_d is the solar wind pressure, and c is the quiet-day ring current contribution), which has become known as the Burton equation. Since that time, numerous authors have used this equation to correct Dst for solar wind effects, with varying values of b and c [e.g., *Gonzalez et al.*, 1989; *Feldstein*, 1992; *Valdivia et al.*, 1999; *Ebihara and Ejiri*, 2000].

While interest continued since the 1970's in creating more refined models of the magnetosphere, most have focused on modeling the magnetic field throughout the magnetosphere (and not at the surface) with ever-increasing complexity and contributions from all current sources. Little has been done in refining calculations of the magnetic field at the Earth's surface due to magnetopause currents as most storm researchers seemed content to use the Burton equation. Recently, however, there has been some renewed interest in computing the relative contribution of magnetopause currents to magnetic measurements at the surface. *Arykov and Maltsev* [1994], in their analysis of three magnetic storms, indicated the magnetopause currents could in some cases offset the ring current contribution to Dst . *Belova and Maltsev* [1994], *Dremukhina et al.* [1999], and *Kalegaev and Dmitriev* [2000] all reached the same conclusion. In a brief review of various current contributions to Dst , *Greenspan and Hamilton* [2000] state during quiet times, the magnetopause current contribution is ~ 10 to ~ 40 nT while during storms, the Burton equation is typically used to estimate its magnitude.

Tail Current

The possibility of the tail current contributing to ground magnetic perturbations has been recognized for some time. Shortly after the permanence of the solar wind became known, *Piddington* [1960, 1962] indicated the reduction in magnetic pressure in the tail, related to the formation of the tail and tail currents, could be responsible for the storm main phase. *Piddington* [1963] concluded the *Dst* main phase is caused by the combined effects of the ring current and tail processes in varying proportions. His argument was based on analysis of the nature of *Dst* versus *DS*, showing a ring current could not account for a small *Dst* change and a *DS* change nine times larger at the same time. He proposed tail formation as the main source for *DS* variations. He used the two-step decay of the *Dst* as evidence that both the ring current and tail contribute in different ways. *Axford et al.* [1965], in their discussion of the magnetotail, indicated since the field from the tail current should be about the same at the Earth's equator as it is in the tail, the tail current might contribute substantially to the main phase. *Behannon and Ness* [1966] compared magnetic field measurements in the tail to the *H* component of low-latitude ground magnetic measurements and found both correlation and anti-correlation during several storms, with the amplitude of the tail field at 25-35 nT while *Dst* was in the 100 nT range. *Davis and Sugiura* [1966] estimated the tail current effect at ~15 nT at the Earth. *Campbell* [1973] studied midnight magnetic field measurements at low-latitudes and believed the general behavior of the data showed characteristics more closely related to a tail current than a ring current.

Siscoe [1966] used a force balance perspective to look at the magnetopause current, ring current, and tail current effects on the Earth's geomagnetic environment. Using a semi-infinite cylinder model of the tail, he concluded the non-storm time tail current contributes ~ 3 nT to the ground magnetic field. He did not try to estimate the storm time contribution citing the large uncertainties involved and concluded that the H depression was "probably due mainly to the ring current."

In analyzing the magnetic field depression due to quiet-time magnetopause currents, both *Verzariu et al.* [1972] and *Su and Konradi* [1975] stated one must keep in mind that Dst measures magnetic effects from the ring current, magnetopause current, and the tail current. *Olson* [1974] made similar observations in his attempt to model the ring current and tail current as a continuous, distributed current system. *Grafe* [1974] studied the asymmetry of the equatorial magnetic field and considered it as a possible consequence of the tail current.

The issue of the tail current contribution then seemed to go dormant for some time. Not until *Arykov and Maltsev* [1994] was the tail current again looked at from this perspective. *Arykov and Maltsev* used a two-region model of the magnetosphere to study three different geomagnetic storms. The regions consisted of an inner (closed-drift trajectory) region and an outer (open-drift trajectory) region. They used solar wind pressure to calculate the magnetopause current contribution, the magnetotail magnetic flux to calculate the tail current contribution, and the DPS relation to calculate the ring current contribution to Dst . They determined the ring current, tail current, and magnetopause current all contribute roughly the same order of magnitude to Dst . They

also showed the expected change in the tail current with solar wind changes agreed with the observed rate of *Dst* change during the main phase, indicating the tail current is a key contributor to *Dst*. *Belova and Maltsev* [1994] used the same model to study the tail current contribution during the February 1986 storm, arriving at the value of -220 nT (the corresponding *Dst* being -257 nT). With the solar wind pressure contributing 251 nT and the ring current -262 nT, they concluded the tail current, solar wind compression term, and the ring current contributions were all roughly equal. This model was used again by *Maltsev et al.* [1996] and similar calculations (using magnetotail magnetic flux) were used to show the tail current can explain the *Dst* dependence on southward IMF (Interplanetary Magnetic Field) since the magnetotail magnetic flux depends on dayside reconnection. *Arykov and Maltsev* [1996] used the two-region model and formulas of *Arykov and Maltsev* [1994] to build formulas for dH/dt and the injection functions of the ring current and tail current. They made the case that magnetic flux transport from dayside reconnection to the tail (associated with the tail current) can explain the *H* depression growth.

Alexeev et al. [1996] used a paraboloid magnetospheric model [*Alexeev*, 1978] to calculate the relative contributions of magnetopause currents, the ring current, and the tail current to *Dst*. This dynamic model determines the total magnetic field due to magnetopause currents, the tail current system including closure (Figure 9), and the ring current. The tail current intensity depends on the magnetopause subsolar distance, distance to the inner edge of the current sheet, the tail lobe magnetic flux, and AL . Their analysis showed 1) the tail current is necessary to account for the rapid (~1 hour)

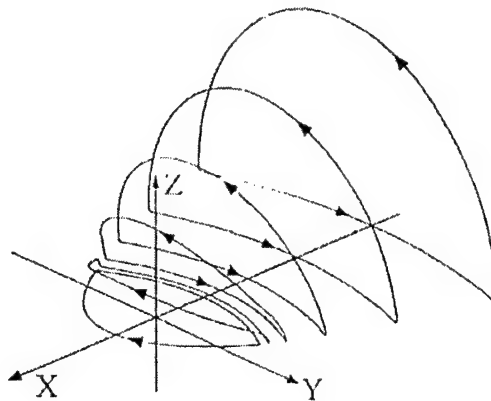


Figure 9. The current loops of the tail current system modeled by *Alexeev et al.* [1996].

variations in Dst that the ring current cannot produce; and 2) the contribution of the tail current can be equal to or greater than that of the ring current. It is interesting to note near the Earth, their tail current model (Figure 9) closely resembles a ring current.

Maltsev et al., *Arykov and Maltsev*, and *Alexeev et al.* all cited the fact that the auroral oval expands equatorward with decreasing Dst as further proof of the importance of the tail current (since the crosstail current, not the ring current, controls the auroral oval location). *Dremukhina et al.* [1999] again used the paraboloid model to study four geomagnetic storms and showed during the main phase, the magnetopause current, tail current, and ring current contributions are all of equal magnitude, while during the recovery phase the ring current dominates. *Kalegaev and Dmitriev* [2000] also used the paraboloid model to show during a November 1986 storm the magnetopause current, tail current, and ring current contributions are all the same order of magnitude.

Some recent authors [e.g., *Maltsev et al.*, 1996; *Arykov and Maltsev*, 1996] have also argued that the tail current (and magnetopause closure) contribution to Dst is

approximately equal to the B_x component in the tail lobes (similar to the claim made by *Axford et al.* [1965]). During quiet times $B_x \approx 20$ nT but in disturbed periods can be 100 – 300 nT [*Arykov and Maltsev*, 1996]. This subject has yet to be explored in detail.

Iyemori and Rao [1996] calculated the equatorial surface effect of the tail current using the Tsyganenko 1987 geomagnetic field model [*Tsyganenko*, 1987] for various K_p values. Their results are shown in Figure 10. *McPherron* [1997] claimed the effect of the tail current on Dst can justifiably be ignored. He gave results of calculations with a simple current sheet model that the tail effect is ~ -10 nT at quiet times and ~ -30 nT at very disturbed times. He also estimated even with a more complex model that includes Region 1 current, the effect would be a fraction of -100 nT. In their study of the substorm current wedge effect on Dst , *Friedrich et al.* [1999] concluded the wedge closure current in the magnetospheric equatorial plane is the primary source of an H perturbation from the wedge. This would imply that the tail current system as a whole could have a significant effect on Dst , but this concept was not explored further.

Turner et al. [2000] specifically analyzed the effect of the tail current on Dst using the Tsyganenko 89 and 96 magnetic field models. The models' surface field values

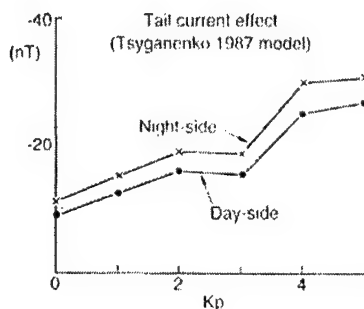


Figure 10. Equatorial magnetic field effect of the tail current calculated by *Iyemori and Rao* [1996] based on the Tsyganenko 1987 magnetic field model.

were used to replicate Dst with and without the tail current. The tail current was calculated by defining a box in the tail containing the tail current and taking the curl of the magnetic field to get the current flowing through the box. The effect of this current was subtracted before Dst calculation to determine the effect of the tail current. They arrived at an average value of about 25% for the tail current component of Dst . Ohtani *et al.* [2001] arrived at a similar value (20-25%) as a minimum contribution of the tail current to Dst (in their case $SYM-H$) at Dst minimum. Also, they attributed the initial Dst recovery to a reduction in tail current (due to substorm current disruption) and not decay of the ring current (Figure 11).

Partial Ring Current

Moos [1910] was one of the first to do a detailed analysis of the low-latitude storm-time magnetic field. Comparing the character of storm perturbations at different local times, he found a pattern of maximum perturbation at dusk and minimum

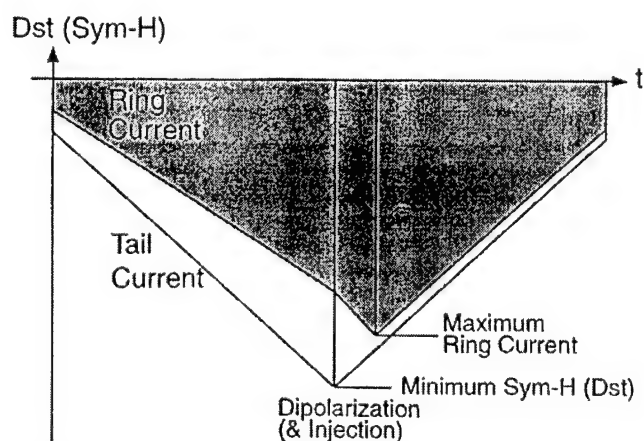


Figure 11. Contribution of the ring and tail currents to Dst as theorized by Ohtani *et al.* [2001].

perturbation at dawn. In a series of magnetic storm studies, *Chapman* [1918, 1919a, 1927] found there was a global component depending only on storm-time, and a local component that varied with local time. This local-time component, at low- and mid-latitudes, tended to have a maximum at around 1800 LT and a minimum around 0600 LT. Believing that currents could only exist in the atmosphere, he proposed an atmospheric current system that could produce these components, with the electrojets closing through the mid- and low-latitude ionosphere (Figure 12). Patterns similar to this would be the accepted cause of the local-time variation for the next forty years. *Chapman* [1935] devised the term S_D (disturbance daily variation) to designate the local-time part, created more detailed current diagrams, and made calculations of atmospheric current intensities. *Vestine* [1938] studied mostly auroral asymmetries, also attributed them to atmospheric currents, and reaffirmed the correctness of *Chapman*'s proposed current system. *Vestine and Chapman* [1938] and *Fukushima and Oguti* [1953] also confirmed the theory only atmospheric currents were necessary to reproduce S_D . In a detailed analysis of geomagnetic storm morphology, *Chapman* [1952] defined Dst as the storm-time

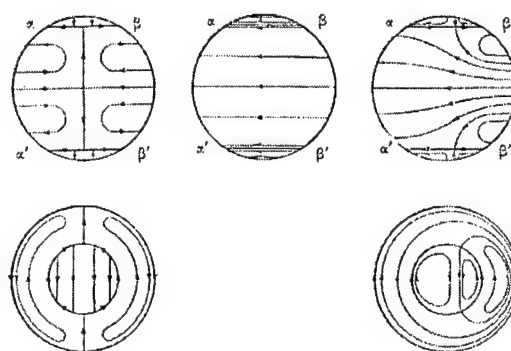


Figure 12. The atmospheric current system of *Chapman* [1927] to explain magnetic storm surface field measurements.

component and DS as the disturbance local time inequality. While both DS and S_D were defined in terms of subtracting the storm time part from the overall field, they differed in that S_D was defined over a 24-hour period while DS could be defined for each instant in time (S_D basically being the 24-hour average of DS). One of the characteristics Chapman found was DS developed and decayed faster than Dst . It is interesting to note Chapman's original Dst and DS were defined as averages over several storms to remove individual storm characteristics and find average storm behavior – Dst and DS for an individual storm had no meaning. *Sugiura and Chapman [1960]* continued the series of storm morphology studies. They provided a more in-depth report on the systematic phase shift of the DS axis, as well as early development and decay of DS compared to Dst (Figure 13).

Alfvén [1939, 1940, 1950, 1955] developed a completely different idea to explain the S_D asymmetry. Alfvén's theory of magnetic storm currents included a detailed explanation of how protons and electrons from the sun would drift in the Earth's

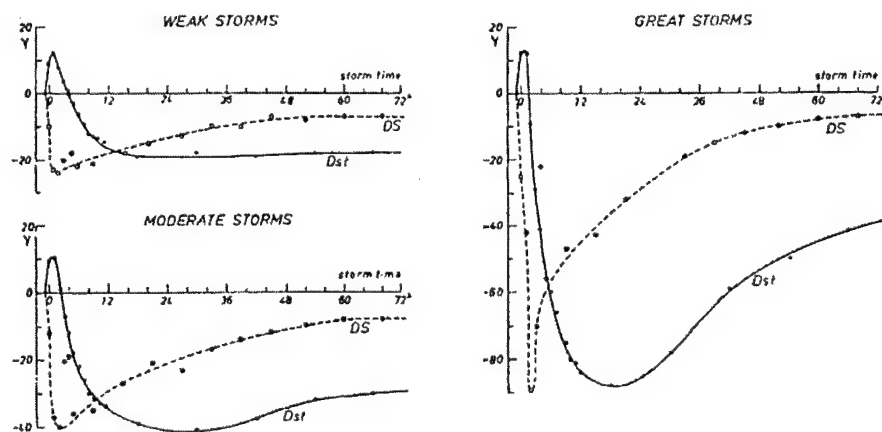


Figure 13. Comparison of DS and Dst evolution during magnetic storms reported by *Sugiura and Chapman [1960]*.

magnetic field. These drift patterns, with electrons going one way and protons the other, would create the ring current but would also lead to a build-up of space charge that would discharge along magnetic field lines into the auroral zone – in essence the first asymmetric ring current model (Figure 14). He claimed this asymmetric ring current could produce the S_D asymmetry. *Martyn* [1951] expanded upon the ring current work of *Chapman and Ferraro* [1933] by adding a field-aligned current segment to connect the ring current to the auroral ionospheric current to help explain SD . This concept was also similar to later partial ring current models. However, *Kirkpatrick* [1952] analyzed *Alfvén's* current system and found it insufficient to explain S_D . *Fejer* [1961, 1964] introduced a ring current asymmetry, but only as a mechanism to generate the needed ionospheric current system necessary to explain DS and the electrojets.

Akasofu and Chapman [1964] studied several large storms and saw main phase asymmetry even with no significant electrojet activity. This led them to realize DS was not entirely ionospheric and theorize the ring current had a nightside gap, with current diverted into the low- and mid-latitude ionosphere, which created the asymmetry. *Parker*

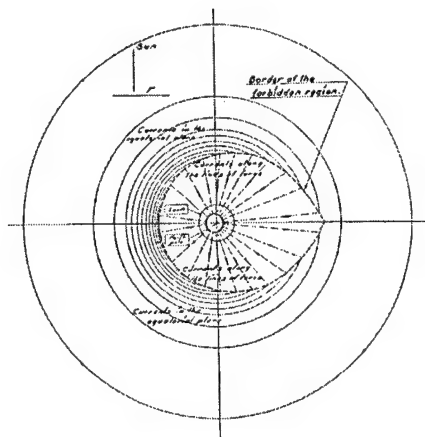


Figure 14. Magnetic storm current system proposed by *Alfvén* [1940].

[1966] developed a theoretical formulation for the effect of an asymmetric trapped particle population and showed since the asymmetry dissipates much faster than the symmetric part, the asymmetry could only exist during the active part of a storm.

Cummings [1966] was the first to propose a partial ring current (with partial ring current + symmetric ring current = asymmetric ring current). *Cummings* suggested a partial current system (Figure 15) centered at 1800 LT but slowly drifting westward, composed mainly of protons, and located at $\sim 4 R_e$. *Cummings* also indicated this system would decay more rapidly than the symmetric ring current. *Akasofu and Chapman* [1967a,b] reaffirmed *DS* was extra-ionospheric and supported an asymmetric ring current as the cause, with *Akasofu and Chapman* [1967b] noting the westward shift of the asymmetry center was most likely due to the westward drift motion of an asymmetric proton injection. *Sugiura* [1968] studied the westward drift of the asymmetry in more detail and attributed it to westward-drifting protons of energy 10-15 KeV. *Kavanaugh et al.* [1968] used an electric field model to simulate proton and electron drifts in the magnetosphere and showed that *Alfvén's* original work was basically correct – the different drift paths could produce the asymmetric ring current. *Schiold et al.* [1969] also showed *Alfvén's* basic physics of charge separation and field-aligned current generation

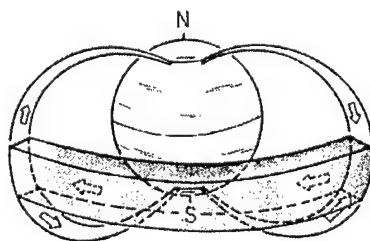


Figure 15. Partial ring current system proposed by *Cummings* [1966] to explain the low-latitude asymmetry in the *H* disturbance field.

were correct but needed to be reformulated in terms of magnetospheric convection.

Langel and Sweeney [1971] and *Kawasaki and Akasofu* [1971] showed the low-latitude *DS* must be due to distant (not ionospheric) current and concluded it was most likely due to the asymmetric ring current and, according to *Kawasaki and Akasofu*, also the tail current.

During this time of increased partial ring current speculation, observational evidence of the partial ring current's existence began to mount. *Cahill* [1966] studied the storm of April 17, 1965 using ground and satellite magnetic data and found the main phase was due to an asymmetric introduction of charged particles into the 18-00 LT sector centered at $3 R_e$. After rapid loss of the asymmetric population, the slow recovery phase began, characterized by a symmetric population centered at $3.5 R_e$. *Cahill* [1970] provided further satellite evidence of asymmetric particle injections during storms. *Frank* [1970] reported the first direct satellite observation of asymmetric proton enhancements in the evening sector during early storm development and seemed to show correlations of these enhancements with asymmetric ground magnetic measurements. Further satellite confirmation was presented by *Bogott and Mozer* [1973].

As the existence of the partial ring current became more certain, researchers began looking for a connection between it and the auroral electrojets, which seemed natural based on the geometry. *Swift* [1967, 1968] used numerical simulations based on the guiding-center Vlasov equation to show the asymmetric ring current could drive the auroral electrojets. *Akasofu and Meng* [1968, 1969] discarded Chapman's old *DS* pattern and concluded the eastern electrojet did not close through the ionosphere but through the

asymmetric ring current. They went on to propose these two current systems were so closely connected that asymmetric ring current growth was the cause of substorms. *Crooker and Siscoe* [1971] performed a Fourier analysis on the low-latitude H component, equating the zeroth harmonic as Dst and comparing the first harmonic (equated to the asymmetric component) to AE , finding a very close correlation. They also found the center of greatest negative H to be around 1800 LT. *Crooker* [1972] performed the same Fourier analysis but with higher resolution data (2.5-min. instead of the 1-hour data of Crooker and Siscoe) and found similar results. *Clauer and McPherron* [1978, 1980], however, examined the relationship between the partial ring current (as measured by the mid-latitude magnetic perturbation at dusk) and both substorms and the interplanetary dawn-dusk electric field (correlated to B_z). They found a much higher correlation with the interplanetary electric field and also found several partial ring current enhancements that occurred prior to substorm onset. This led them to conclude the solar wind was the most important driver of the partial ring current.

Kamide and Fukushima [1971] created new indices for the asymmetric ring current – the DR indices (DRS for symmetric ring current perturbation, DRP for partial ring current perturbation, T for local time center of the partial ring current, and W for the longitudinal width of the partial ring current) – and analyzed several storms with them. They theorized during the first few hours of a storm, westward drifting protons produce DRP , and are then gradually converted to DRS . Based on their model of the partial ring current (similar to Figure 15) they were the first to quantify the magnetic effect of the partial ring current system. They showed the equatorial segment and the field-aligned

currents were both important at low- and mid-latitudes, and at its maximum, *DRP* could be comparable in magnitude to *DRS*. They also found *DRP* develops and decays earlier than *DRS* and *T* starts in the evening sector and moves slowly westward. Kamide and Fukushima further proposed the partial ring current was connected to the eastward electrojet. This view of partial ring current closure was reasserted by Kamide and Fukushima [1972], Fukushima [1972], and Crooker and McPherron [1972], all of whom agreed the westward electrojet was not connected to the partial ring current but part of a separate circuit, possibly connected to the tail current (Figure 16). Grafe [1974] presented evidence countering any substorm connection to the low-latitude asymmetry and also cautioned not to necessarily attribute the asymmetry to only an asymmetric ring current and it could be due to the tail current.

Fukushima and Kamide [1973a] conducted a detailed study of partial ring current theory and currents. They discounted ring current eccentricity as a cause of low-latitude asymmetry and calculated the partial ring current's field-aligned current contributed twice as much to the asymmetry as the eastward electrojet or the westward equatorial

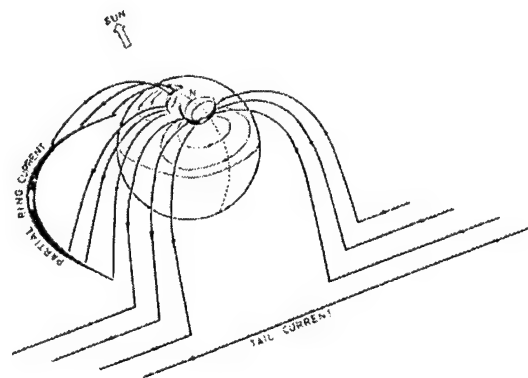


Figure 16. Proposed partial ring current and westward electrojet current systems [Fukushima 1972].

segment (10^6 amps flowing from $4 R_e$ produced 45 nT in their model). This result was further confirmed by *Fukushima and Kamide* [1973b]. *Crooker and Siscoe* [1974] developed a detailed mathematical model of the partial ring current to determine contributions from all possible components. Their results are shown in Figure 17. Like Fukushima and Kamide, they also concluded that the field-aligned current contributes most to the mid- and low-latitude disturbance, with little effect due to the uncertainty in ionospheric closure. These results were in direct opposition to *Siscoe and Crooker* [1974] who reasoned with symmetry arguments the field-aligned current contribution averaged out to zero.

After the discovery of the Region 1 & 2 current systems, researchers began to tie them to the partial ring current. In one of the first computer simulations of the inner magnetosphere during a substorm, *Harel et al.* [1981a, b] argued the classic dusk-centered partial ring current model needed to be updated to a midnight-centered model

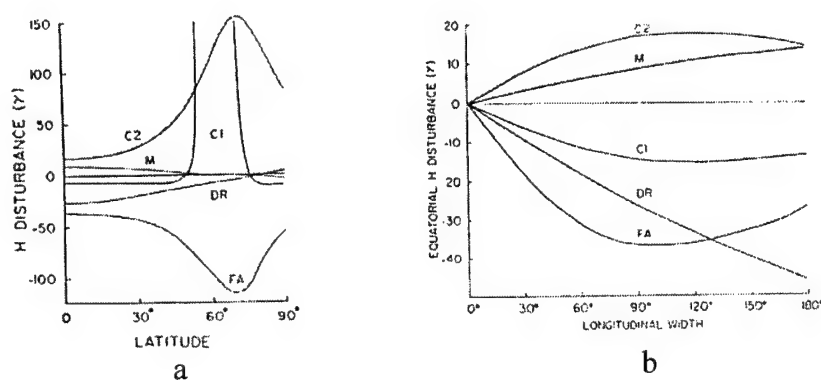


Figure 17. Relative contributions of partial ring current elements to the surface H disturbance as calculated by *Crooker and Siscoe* [1974]. The current elements are the drift current (DR), field-aligned current (FA), ionospheric electrojet closure (C1), distributed ionospheric closure (C2), and magnetization current (M). (a) shows the contributions along the central meridian for a partial ring current of width 90° . (b) shows the equatorial disturbance for different partial ring current widths.

(Figure 18) that closes through Region 2 currents (*Sugiura [1975]* and *Kamide et al. [1976]* had proposed earlier a midnight-centered equatorial current was the most likely closure for the Region 2 currents). Their rationale was: 1) this picture better fit the observed Birkeland current pattern (symmetric about the noon-midnight meridian); 2) their simulation showed the maximum/minimum ring current strength at midnight/noon; and 3) it is the net result of the Region 1 & 2 currents (downward at noon and upward at midnight) that produces the low-latitude asymmetry. *Crooker and Siscoe [1981]* examined this idea in more detail. Based on a simple model of the Region 1 & 2 currents, they too concluded it was the net Birkeland current that produced the low-latitude asymmetry. In their model (Figure 19), the divergence of the Hall current due to the auroral oval's conductivity discontinuity caused an eastward rotation of the Region 1 current system. This rotation then produced a net downward current at noon and an upward current at midnight. Their model gave a value of about 30 nT for the equatorial disturbance for the net Birkeland current, with the value dependent upon the Hall

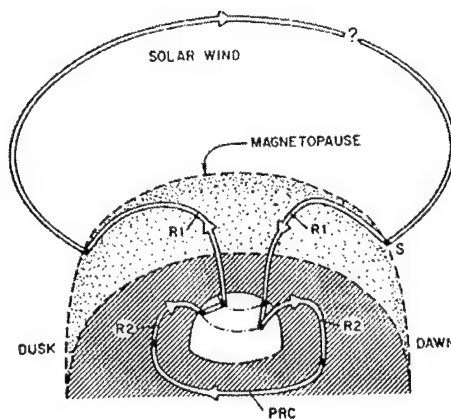


Figure 18. Updated magnetospheric current system proposed by *Harel et al. [1981b]* including a midnight-centered partial ring current.

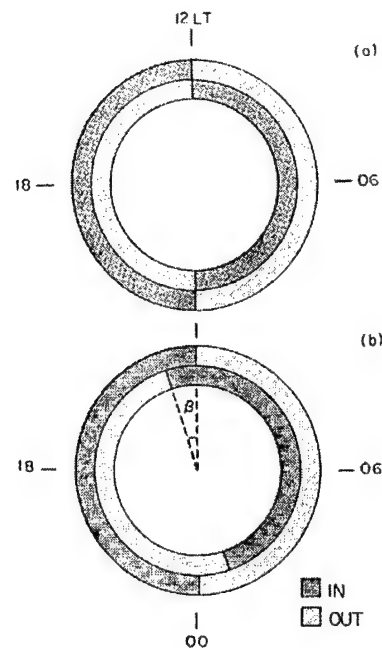


Figure 19. Diagram of how a rotation of the Region 1 current system produces a net downward current at noon and a net upward current at midnight [Crooker and Siscoe 1981].

conductivity in the auroral oval and the cross polar cap potential (which would explain the asymmetry dependence upon southward IMF found by Clauer and McPherron [1980]).

Some observational evidence supported this new midnight-centered view of the partial ring current. Grafe *et al.* [1986] produced local time profiles from 3-minute magnetometer data and showed better agreement with ones calculated from the Crooker and Siscoe model than from the classical particle ring current picture. Roelof [1987] offered confirmation of a noon-midnight asymmetry in the ring current from energetic neutral atom (ENA) imaging of the inner magnetosphere, with the asymmetry as high as 20:1 during storms. Roelof [1989] went on to show the ion pressure distribution from this

observed asymmetry could produce the expected Region 2 current pattern. Looking at AMPTE CCE magnetic field data, *Iijima et al.* [1990] found a pronounced noon-midnight asymmetry in the westward equatorial current, with the nightside greater than the dayside by a factor of two to three. This current drove field-aligned currents with a positive divergence from 1600 to 2100 LT and a negative divergence from 0200 to 0700 LT. These patterns matched the new partial ring current model and *Iijima et al.* used this as proof of the partial ring current-Region 2 current connection. *Nakabe et al.* [1997] used magnetometer data from the DE-1 satellite and also found a noon-midnight asymmetry in the inner magnetosphere corresponding to the asymmetry in the ring current. Although acknowledging the tail and magnetopause currents could contribute, they concluded the asymmetry was large enough to deduce the ring current was much stronger on the nightside than the dayside. They also determined the dawn-dusk asymmetry measured on the ground was due almost completely to net field-aligned currents, in agreement with *Crooker and Siscoe* [1981]. Determining average ring current characteristics from AMPTE CCE data, *De Michelis et al.* [1997] found both a dawn-dusk asymmetry and a stronger midnight-noon asymmetry, but gave alternate reasons for them. They attributed the dawn-dusk asymmetry to the different proton trajectories (low-energy protons drift to the dawnside while higher energy protons drift to the duskside) and the midnight-noon asymmetry to the magnetospheric configuration (more compressed on the noonside). The average total ring current density (Figure 20) showed the peak current density at 2300 LT, and was attributed to the effects of storm/substorm injections. With these measurements they were able to explain the asymmetries without invoking field-aligned

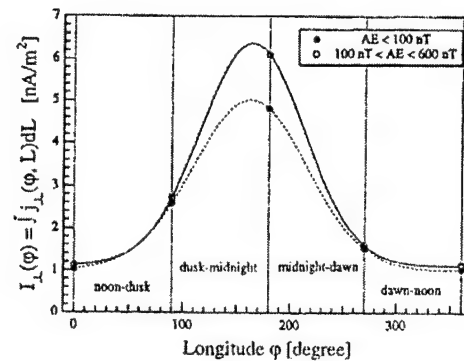


Figure 20. Total ring current density distribution calculated by *De Michelis et al.* [1997] for different *AE* activity ranges. The density curves show both a dawn-dusk and noon-midnight asymmetry with peak density at about 2300 LT.

currents. With magnetic field data from the Polar spacecraft, *Tsyganenko et al.* [1999] reported both a noon-midnight and dawn-dusk asymmetry, with nightside magnetospheric current and duskside sources contributing most to *Dst*. Using AMPTE CCE ion measurements *Greenspan and Hamilton* [2000] showed how the majority of the ring current energy resided on the nightside at storm maximum. ENA images obtained by *Reeves and Henderson* [2001] showed maximum ion fluxes centered in the pre-midnight region (from dusk to a few hours past midnight) within an hour after storm particle injection and expanding both eastward and westward in the hours afterward.

As magnetospheric modeling efforts increased, more modeling studies of the partial ring current system were attempted subsequent to the work of *Harel et al.* [1981a, b]. *Chen et al.* [1982] built theoretical magnetograms from a substorm current model (similar to *Harel et al.* [1981a]) with the same midnight-centered partial current closure of Region 2. *Chen et al.* showed two-thirds of the dawn-dusk asymmetry was due to net Birkeland currents, with one-third from the auroral electrojets. *Sun et al.* [1984]

presented more modeling evidence to support their conclusion the mid-latitude H component was composed of mostly field-aligned current with some ionospheric contribution and very little partial ring current component. *Iyemori* [1990] studied mainly the D component of the mid-latitude asymmetry (in order to remove any ring current effects) and interpreted the results in terms of field-aligned currents. The resulting proposed current system was a combination of a convection-driven Region 1 system and a partial ring current-connected Region 2 system centered in the evening sector. *Takahashi et al.* [1991], using the technique of *Takahashi et al.* [1990], simulated ring current formation by modeling particle trajectories from nightside injections. They explained the partial ring current as injected protons drifting on open drift paths. The divergence of this current then drives field-aligned currents into and out of the ionosphere, which in turn drive ionospheric currents (their model did not include Region 1 currents). The horizontal disturbance asymmetry recovers quickly because when the cross-tail potential decreases, the trapping region expands and particles on open drift paths are then trapped and the population quickly becomes symmetric. With this modeled system, they then estimated the mid-latitude magnetic variations and compared them to those of *Iyemori* [1990]. They found general agreement in the time development of the asymmetric H component and found it mostly influenced by field-aligned and ionospheric currents, but the magnitude of the H asymmetry was overestimated and was, in fact, much larger than Dst (it was suggested some part of Dst must be due to an additional ring current component with no current divergence). *Takahashi et al.* also found the D component agreed with *Iyemori* and it was due to field-aligned and

ionospheric currents. *Stern* [1993], *Tsyganenko* [1993], and *Tsyganenko and Stern* [1996] all computed the asymmetric plasma distribution in the inner magnetosphere to model the magnetic field of the resulting Region 2 and partial ring currents. The current system used was a combination of a symmetric ring current and a quadrupole two-loop system (Figure 21).

But some recent modeling efforts do not necessarily fit the newer ring current model. *Tsyganenko* [2000], revisiting the work of *Tsyganenko* [1993], used the observed asymmetry of trapped particle pressure and anisotropy [from *Lui and Hamilton*, 1992] to derive the asymmetric ring current and corresponding field-aligned currents derived from the current divergence. *Tsyganenko* reported that during quiet times only ~20% of the Region 2 current comes from the partial ring current and the rest comes from the plasma sheet. In a simulation of the ring current by tracing particle trajectories in a time-dependent convection field, *Ebihara and Ejiri* [2000] showed a clear dusk-centered ring current distribution in the main phase of the April 10-11, 1997 storm. The dawn-dusk asymmetry was further confirmed by NOAA-12 particle counts. A clear dusk-side

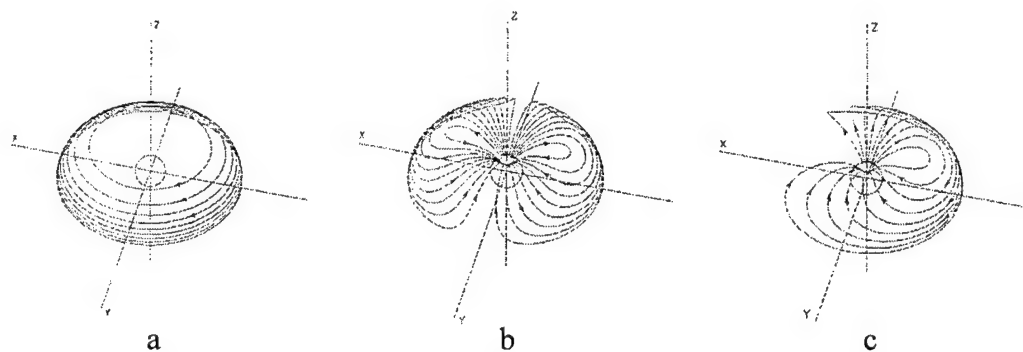


Figure 21. Combination of (a) a symmetric ring current and (b) a two-loop quadrupole system to produce a partial ring current system (c) [*Tsyganenko*, 1993].

asymmetry was also shown in the storm simulations of *Liemohn et al.* [2001].

On the issue of partial ring current contribution to *Dst*, *Siscoe and Crooker* [1974] argued the field-aligned current contribution averaged out to zero and the ionospheric closure (through the eastward electrojet) could produce a positive offset of ~15-20%. In their modeling of magnetospheric currents during magnetic storms, *Alexeev et al.* [1996] determined the partial ring current's contribution to *Dst* is about 20% of the main phase asymmetry. For the March 23-24, 1969 storm for example, the asymmetry strength was ~ 100 nT at the maximum of the main phase, so the maximum partial ring current contribution to *Dst* was ~ 20 nT. *Maltsev et al.* [1996], however, stated the partial ring current did not contribute at all to *Dst*. *McPherron* [1997] qualitatively argued the partial ring current may make *Dst* slightly more negative than if just the symmetric ring current were present, but would sometimes be compensated for by the positive effect of the substorm current wedge. *Kamide et al.* [1998] recognized partial ring current-associated field-aligned currents contribute to *Dst* and, in fact, a decreasing *Dst* in the main phase may indicate the partial ring current, and not the symmetric ring current, is growing. This was echoed by *Liemohn et al.* [1999], *Ebihara and Ejiri* [2000], *Greenspan and Hamilton* [2000], and *Reeves and Henderson* [2001] who all showed the bulk of the *Dst* minimum is due not to the symmetric ring current but to injected plasma drifting on open drift paths (i.e. the equatorial segment of the partial ring current). *Dremukhina et al.* [1999], however, argued the partial ring current contribution averages out and is close to zero. *Grafe* [1999] presented the opposite perspective: there is no symmetric ring current, only an asymmetric ring current that is completely responsible for *Dst* and *DS* (or *ASY*). The

work of *Valdivia et al.* [1999] seems to corroborate this by reproducing the spatial structure of mid-latitude magnetograms by generalizing the DPS relation to use a spatially dependent ring current energy density. *Liemohn et al.* [2001] simulated the near-Earth ion distribution for three storms and found in the main phase, the asymmetric ring current accounted for >80% of *Dst*. Their simulation showed in the main phase, the ring current particles are mostly drifting on open paths (corresponding to increased convection); particles do not become trapped and symmetrically distributed until convection has diminished in the late recovery phase. These findings were based on particle energy calculations, deriving *Dst* from the DPS relation. Much of the latest work [*Liemohn et al.*, 1999; *Grafe*, 1999; *Valdivia et al.*, 1999; *Ebihara and Ejiri*, 2000; *Greenspan and Hamilton*, 2000; *Reeves and Henderson*, 2001; *Liemohn et al.*, 2001] seems to contradict the most current theories by looking only at the equatorial segment (ignoring the field-aligned current contributions, shown earlier to be dominant) and presenting a dusk-centered partial ring current model.

It seems the real picture of the partial ring current is still not clear. While most researchers apparently agree with the midnight-centered model, some recent work [*Ebihara and Ejiri*, 2000; *Liemohn et al.*, 2001] and comments [*Lui et al.*, 1987; *McPherron*, 1997; *Baker et al.*, 2001] still suggest a dusk-centered model. Still unclear is the relationship between the physical mechanism of producing the partial ring current – a duskside drift of injected protons – and the midnight-centered Region 2 closure. Also, if the conclusions of *Harel et al.* [1981b] and *Crooker and Siscoe* [1981] are really true, then it is not the field-aligned current closure of the partial ring current that is important

(as the recent statements above claim), but the net result of the Region 1 and 2 currents that determine the dawn-dusk asymmetry. That would further mean the magnetospheric segment is largely decoupled from the ground signatures and cannot be determined on the basis of surface magnetic records. Another complicating factor is some of the most recent modeling efforts are based not on calculating the effect of the current directly, but on calculating the particle energy and using the DPS relation to get *Dst*, making it difficult to separate out the effects of the symmetric and partial ring currents. Since these two currents are in fact blended into one complex, continuously changing system, it is not always clear how or if the two can be distinguished. For example, instantaneous identification of particles on open versus closed drift paths is nearly impossible.

Field-Aligned Currents

Birkeland [1908, 1913] first proposed field-aligned currents in an effort to explain high-latitude magnetic disturbances (later called polar magnetic substorms). He proposed charges from the sun were diverted along magnetic field lines to produce intense auroral currents, now called the electrojets (Figure 22), and made detailed calculations as to their

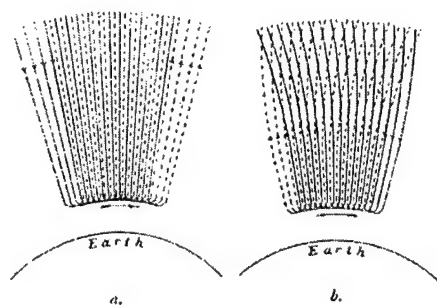


Figure 22. Field-aligned current systems proposed by *Birkeland* [1908] to explain polar magnetic disturbances.

ground magnetic effects. His ideas were disregarded for decades by most other researchers of geomagnetic activity [e.g., *Chapman*, 1918, 1927, 1935; *Vestine*, 1938; *Vestine and Chapman*, 1938; *Silsbee and Vestine*, 1942; *Chapman*, 1952; *Kirkpatrick*, 1952; *Fukushima and Oguti*, 1953; *Akasofu and Chapman*, 1964; *Akasofu et al.*, 1965] who thought polar magnetic disturbances were caused entirely by currents confined to the ionosphere. *Alfvén* [1939, 1940, 1950, 1955] and *Martyn* [1951], however, believed field-aligned currents were necessarily produced by the physics of the ring current and helped drive auroral currents as well as the low-latitude asymmetry. In these theories the possible surface magnetic effects of such field-aligned currents were neglected.

With the advent of more sophisticated methods of studying charged-particle motions in the magnetosphere and ionosphere, many researchers began to invoke field-aligned currents as both an element of the low-latitude asymmetry and as a part of the polar magnetic substorm current system [*Fejer*, 1961; *Boström*, 1964; *Atkinson*, 1967; *Boström*, 1968; *Akasofu and Meng*, 1969; *Bonnevier et al.*, 1970]. In the pioneering work of *Boström* [1964], he considered field-aligned current systems of two possible types: a Birkeland-type system with field-aligned currents at the start and end of the electrojet, and a system with field-aligned current sheets to the north and south of the electrojet (Figure 23). In the second model he assumed the magnetic effect of the field-aligned currents would be cancelled by Pedersen currents and so would create no detectable ground signature.

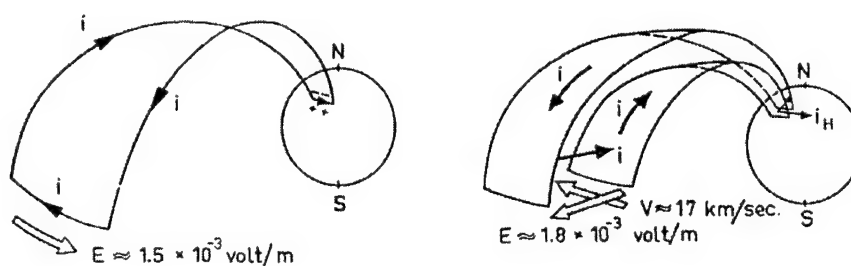


Figure 23. *Boström's* [1964] two types of field-aligned current systems.

Around this same time, observational and theoretical evidence for field-aligned currents began to accumulate [*Zmuda et al.*, 1966, 1967; *Cummings and Dessler*, 1967; *Zmuda et al.*, 1970; *Armstrong and Zmuda*, 1970; *Cloutier et al.*, 1970; *Choy et al.*, 1971]. *Schiold et al.* [1969] used Alfvén's basic ideas about charge separation and the new magnetospheric circulation theories (originally proposed by *Axford and Hines* [1961]) to explain the mechanism of field-aligned currents, which matched the satellite observations of *Zmuda et al.* [1966, 1967]. Their theory produced a field-aligned current sheet system remarkably similar to the Region 1 and Region 2 currents reported several years later. They also proposed these currents would exist even in steady state conditions. With a calculated current intensity of 2×10^6 amps, they found a field-aligned current sheet would produce a surface magnetic field of ~ 100 nT. *Schiold et al.* proposed field-aligned currents be called Birkeland currents since Birkeland was the first to suggest them.

Fukushima [1969, 1976] analyzed substorm current systems and showed field-aligned currents and their associated Pedersen currents would produce no ground magnetic effect with the assumptions of vertical currents (no curvature) and uniform

ionospheric conductivity. *Kamide and Fukushima* [1971], *Fukushima and Kamide* [1973a], and *Fukushima and Kamide* [1973b] calculated the effect of field-aligned currents at the surface and showed 10^6 amps could give several tens of nT (southward) depending on their longitudinal separation. *Kawasaki et al.* [1974] reached a similar result in studying field-aligned substorm current systems. *Crooker and Siscoe* [1974] studied the components of the partial ring current and found significant (up to ~ -100 nT) field-aligned current signatures (see Figure 17).

Theoretical work eventually led to the postulated existence of a substorm current wedge as the cause of substorm activity [e.g., *Akasofu*, 1972; *Kamide and Fukushima*, 1972; *Crooker and McPherron*, 1972; *McPherron et al.*, 1973]. This current system, similar to Boström's type 1 system, included the diversion of magnetotail current along field lines into the auroral ionosphere (Figure 24). *Clauer and McPherron* [1974] looked at the effect of the substorm current wedge at mid-latitudes and determined the field-aligned currents would produce tens of nT in ΔY (positive under the upward current and negative under the downward current) and the equivalent eastward tail closure would produce tens of nT (positive) in ΔH . *Kisabeth and Rostoker* [1977] modeled and examined both of Boström's current systems. For type 1, they found field-aligned currents to have a substantial ΔH effect (~ 300 nT) at the electrojet latitude and dominating ΔH north and south of the current system. The D component was influenced almost exclusively by field-aligned currents [*Bannister and Gough*, 1977; *Hughes and Rostoker*, 1977] and *Kisabeth and Rostoker* showed the magnitude could reach over 100 nT, with the sign depending on the relative distances of the up and down currents. The

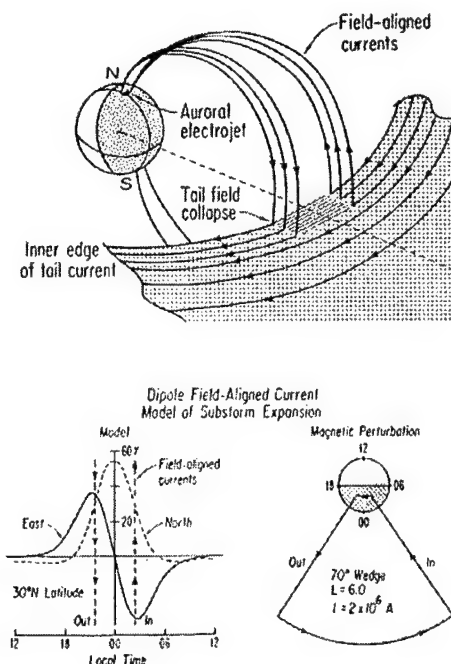


Figure 24. The substorm current wedge (top), its equivalent current system (bottom right), and its magnetic signature at 30° latitude (bottom left) as studied by *Clauer and McPherron* [1974].

contribution to the Z component was ~ 70 nT, although it was dominated by the electrojet. For each field-aligned current sheet in the type 2 system, they found a nearly 200 nT perturbation (positive from the south sheet, negative from the north sheet) in H , a nearly 300 nT perturbation (positive from the south sheet, negative from the north sheet) in D , and ~ 50 nT perturbation in Z (negative from the south sheet, positive from the north sheet).

In addition to the wedge-type substorm current system, satellite observations confirmed a more steady-state dual-sheet structure of field-aligned currents [e.g., *Zmuda and Armstrong*, 1974; *Yasuhara et al.*, 1975; *Sugiura*, 1975; *Sugiura and Potemra*, 1976; *Iijima and Potemra*, 1976a, 1976b, 1978], an extended version of Boström's type 2

system, that became known as the Region 1 and Region 2 currents (Figure 25). It was assumed Region 1 current connected to the distant plasma sheet/boundary layer [Sugiura, 1975; Iijima and Potemra, 1978; Sato and Iijima, 1979; Harel *et al.*, 1981b] and the Region 2 current connected to the partial ring current [Sugiura, 1975; Kamide *et al.*, 1976; Harel *et al.*, 1981b; Chen *et al.*, 1982]. At any one time, then, the total current system could contain components of both types (as in the system suggested by Kamide *et al.* [1976] in Figure 26), be somewhat complex, and contain small-scale structure [e.g., Kamide *et al.*, 1982; Kamide and Baumjohann, 1985]. One problem then became reconciling the substorm wedge picture with observed Region 1 and 2 currents, which are always there. Most decided substorms were a local enhancement of the Region 1 system [Zmuda and Armstrong, 1974; Sugiura, 1975; Iijima and Potemra, 1976a]. Kamide *et al.* [1976] and Chen *et al.* [1982] suggested the substorm current is an enhancement of the overall Region 1, Region 2, Pedersen, and Hall current systems, with a part of Region 1 flowing down on the dawnside, through the westward electrojet, and up through duskside Region 1 current (the substorm current wedge). Most of the downward Region 1 current,

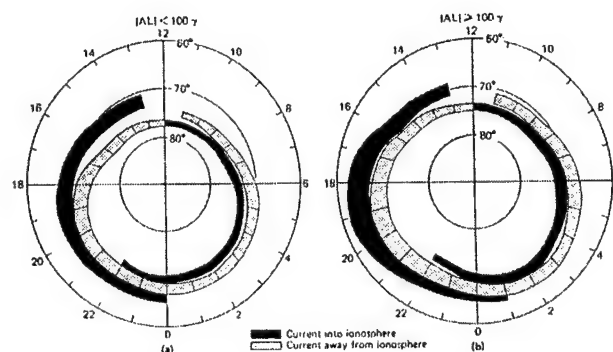


Figure 25. The Region 1 and Region 2 currents reported by Iijima and Potemra [1978].

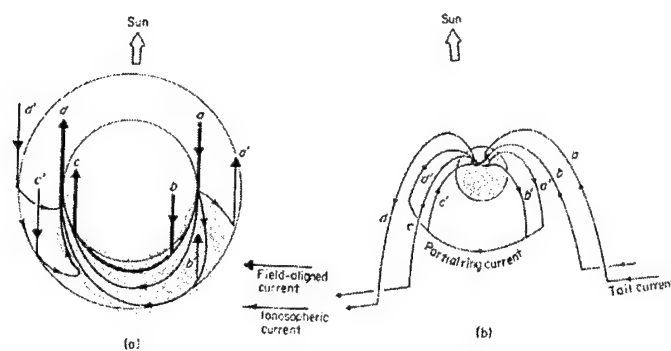


Figure 26. Current system for polar magnetic substorms proposed by *Kamide et al.* [1976].

however, flows through Pedersen currents into the Region 2 current. Though not the most dominant current system physically, the substorm current wedge is the most obvious system in high-latitude surface observations.

Kamide et al. [1981] developed the KRM method to decompose and study these high-latitude currents. They concluded in each local time sector, the north-south Pedersen currents tend to cancel the field-aligned currents. A part of their rationale was the equivalent current systems (constructed from ground magnetic records) do not usually show a significant north-south component to ionospheric currents, although they are known to exist. *Harel et al.* [1981a, 1981b] employed a computer simulation to study substorm currents and decided the net field-aligned current – down at noon and up at midnight, canceling everywhere else – was the primary cause of the low-altitude asymmetry, indicating field-aligned currents could have an impact at all latitudes. *Crooker and Siscoe* [1981] supported this concept and, with a simple wire model, estimated the magnetic disturbance due to these net currents as ~ 30 nT at the equator. As a follow-on effort to Harel et al., *Chen et al.* [1982] also used a computer simulation of

substorm currents to generate theoretical magnetograms. They determined in ΔD at high-latitudes, the north-south Pedersen currents tended to cancel the Region 1 and 2 currents in accordance with *Fukushima* [1969, 1976], even with non-uniform conductivity and curved field lines. At mid-latitudes, however, ΔD tended to be the sum of the competing Region 1 and 2 currents, which individually could create $\sim \pm 100$ nT perturbation. They were also a significant component of mid-latitude ΔH (tens of nT contribution).

Generally, they found the Region 1 and 2 currents made small contributions to ΔZ . At low-latitudes, they found the Region 1 and 2 currents to provide two-thirds of the ΔH asymmetry (~ 10 nT, negative at dusk and positive at dawn). While the total system of Region 1 – Region 2 – Pedersen closure – partial ring current closure carries a large amount of current, the ground signature is modest and only gives significant magnetic perturbations at satellite altitudes (e.g. Triad). The net field-aligned current and substorm current wedge carry less current but produce a larger ground signature. These current systems were summarized by *Chen et al.* in Figure 27. *Sun et al.* [1984] used the KRM method to study mid-latitude H and D disturbances. They found the D variation to depend almost entirely on field-aligned currents and field-aligned currents were also a significant contributor to the H component (tens of nT in both cases). In studying the effect of oblique field-aligned currents, *Tamao* [1986] showed they could produce as much as 80% of the magnetic perturbation of ionospheric currents as compared to vertical currents. *Reddy et al.* [1988] concluded field-aligned currents were the primary cause of low-latitude positive bay disturbances by noting the bays studied were fairly consistent with latitude and the magnetic perturbation increased somewhat with

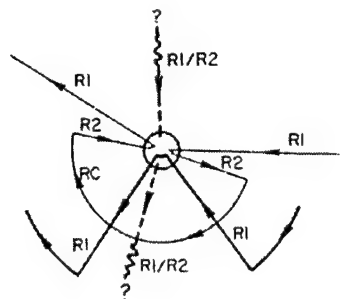


Figure 27. Substorm current system proposed by *Chen et al.* [1982]. It includes the Region 1 and 2 currents, the net Birkeland current at noon and midnight, and the substorm current wedge as a part of the Region 1 system.

increasing latitude, indicating the equatorial electrojet and ring current were not the cause. *Takahashi et al.* [1991] modeled the Region 2 currents by simulating ring current particle injections during a storm, using the calculated ring current divergence to generate the Region 2 currents, which in turn would drive ionospheric currents. These modeled currents were used to calculate magnetic field perturbations at 40° latitude. At the peak of the storm, their model produced field-aligned current H perturbations of ~ 70 nT in the morning sector and ~ -50 nT in the evening sector, D perturbations of ~ 50 nT near midnight and ~ -60 nT near noon, and Z perturbations of ~ 20 nT in the evening sector and ~ -40 nT in the morning sector. *Feldstein* [1992] considered field-aligned currents and electrojets as important contributors to sub-auroral and mid-latitude magnetic effects. In one storm study, they compared the modeled perturbation with and without these currents to the observed perturbations at two observatories: Victoria (lat. 53.9°) and Lvov (lat. 46°). With these currents, the correlation coefficients were 0.91 at Victoria and 0.93 at Lvov. Without these currents, the correlation coefficients were 0.55 at Victoria and 0.9 at Lvov, demonstrating a much greater effect at the higher latitude. In general, they

found their model required inclusion of the high-latitude current system to get good agreement with observations.

While most recent efforts to model field-aligned currents have focused on magnetospheric magnetic fields [e.g., *Stern*, 1993; *Tsyganenko*, 1993; *Tsyganenko and Stern*, 1996; *Nakabe et al.*, 1997; *Perroomian et al.*, 1998; *Tsyganenko*, 2000], a few have tried to determine their effect on *Dst*. *Iyemori and Rao* [1996] computed the effect of the substorm current wedge (10^6 amps, 45° longitudinal extent, tail closure at $15 R_e$) at 30° latitude; the effect of each segment was a few nT. *Iyemori and Rao* argued the average effect of the ionospheric and field-aligned currents were zero and so would have no influence on *Dst*, while the tail segment contributed about 1 nT. In a commentary on *Iyemori and Rao*, *Rostoker et al.* [1997a] remarked the substorm current wedge will generally produce a positive increase in *Dst*. In their words, "The effect of the substorm wedge currents must be considered when addressing the behavior of parameters such as *Dst* and *SYM-H*." Similar statements on the wedge's positive effect on *Dst* were made by *Kamide et al.* [1998]. *McPherron* [1997] recognized the substorm current wedge could contribute to *Dst*, but its narrow longitudinal extent would make that contribution highly variable depending on ground station geometry. *McPherron* concluded the wedge's positive effect would most likely be compensated for by the partial ring current's negative effect. *Friedrich et al.* [1999] studied the effect of the substorm current wedge on *Dst* for various wedge configurations (at longitudinal extents of 15° , 30° , and 90°). The most extreme contribution came from two conjugate wedges of 90° width shifted equatorward to 52.5° latitude and carrying 10^6 amps (Figure 28), with the maximum

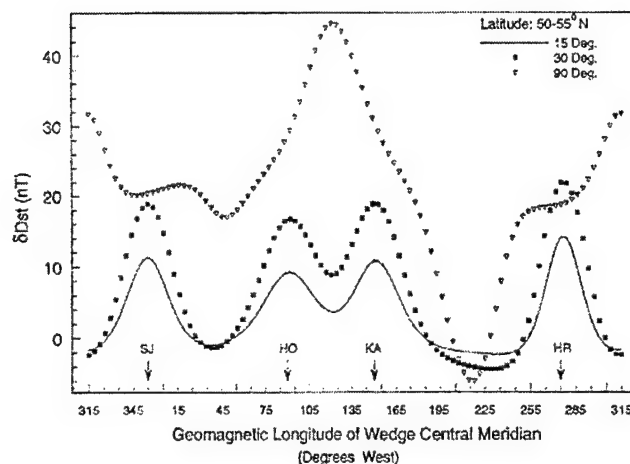


Figure 28. Main phase contributions to 1-minute Dst by conjugate substorm current wedges with ionospheric closure at 52.5° latitude as calculated by *Friedrich et al.* [1999].

contribution being 45 nT. The most dominant contribution was from the tail closure segment. This calculation was made for 1-minute Dst , and the authors estimated the effect on 1-hour Dst to be $\sim 50\%$ less. Overall, they concluded for wedges of less than 30° width, the effect would be in the noise level of Dst , but for extents $\sim 90^\circ$ the effect could be significant, depending on the relative locations of the observatories, with the greatest effect in the expansive phase. According to *Alexeev et al.* [1996] and *Dremukhina et al.* [1999], field-aligned currents contribute only to the low-latitude asymmetry; the contribution to Dst is negligible because by symmetry, they average out to zero in the Dst calculation. *Greenspan and Hamilton* [2000] also concluded that field-aligned currents would most likely not have a major effect on Dst . *Sun and Akasofu* [2000], however, used the KRM method to derive 3-D current systems and consistently calculated contributions of up to 40 nT to Dst by the high-latitude current system, mostly by field-aligned currents.

Other Currents

Induction Currents

In studying the Earth's magnetic variations, *Schuster* [1889] found although most of the variations were due to currents above the Earth's surface, there was also a part originating within the Earth. Schuster attributed this latter part to the interaction of the externally varying magnetic field on the conducting material in the Earth (induction). Modeling the Earth as a uniform conducting sphere did not match observations, however, so Schuster proposed modeling the Earth with a central conducting sphere surrounded by an outer non-conducting shell. *Birkeland* [1913] examined European magnetic records and discovered induction effects ranging from $1/6$ to $1/2$ of the external current effect. He also observed induced currents reached a maximum when the rate of change (not the amplitude) of the perturbing force was greatest. Birkeland further proposed the possibility for localized polar disturbances, induced currents may have a farther reaching effect than the inducing currents, meaning the induced currents could give signatures at lower latitudes that the local auroral currents could not reach. Extending the work of Schuster, *Chapman* [1919b] found the Earth's non-conducting outer shell to extend down to 250 km, and reported for diurnal variations, the internal contribution was about 0.4 times the external contribution, although for only the first harmonic the average value was 0.36. While generally agreeing with these previous results, *Chapman and Whitehead* [1922] found the oceans have the appreciable effect of introducing a thin conducting layer over part of the Earth's surface. *Chapman and Price* [1930] performed a harmonic analysis on average *Dst* and their values for the ratio of internal-to-external contribution

are shown in Table 3. They also took the conductivity model developed from diurnal magnetic variations and applied it to storm time fields, finding the Earth's conductivity was not uniform through the interior region but increased with depth. In addition, Chapman and Price showed different time scales would induce responses from different depths, with magnetic storm fields penetrating deeper because they are aperiodic and slower. *Lahiri and Price* [1939] confirmed the non-uniform conductivity of the Earth's interior, finding increasing conductivity below 250 km and an effective thin conductivity layer at the surface due to the oceans.

Table 3. Ratios of internal-to-external magnetic field components found by various authors. For storms, time is from storm commencement. For *Sq*, time is UT epoch.

	Method	1	3	4	6	8	12	16	18	20	24	28	30	32	36	42	48
Chapman and Price 1930	Storm	.45	.33		.27		.38		.36		.42		.38		.35	.33	.35
Rikitake and Sato 1957	Storm			.66		.65	.23	.39		.37	.37	.33		.32			
Price and Wilkins 1963	<i>Sq</i>			.42		.36	.37	.4									
Anderssen and Seneta 1969	Storm			.77		.74	.38	.37		.35	.48	.31		.30			

Other studies began to confirm there was no simple relation between induced and external currents. *Benkova* [1940] studied *Sq* currents and found an average ratio of 0.48. *Vestine et al.* [1947] calculated the correction of magnetic observations for induction to be 0.9 near the center of the auroral zone, 0.7 near the auroral zone boundary, and 0.6 elsewhere. *Rikitake and Sato* [1957] and *Anderssen and Seneta* [1969] both studied the temporal progression of the induction contribution during storms (Table 3) and found larger contributions earlier in the storm. *Takeuchi and Saito* [1963] showed that the ratio

increases for decreasing period, from 0.36 for a 3-day period to 0.42 for a 3-minute period. *Price and Wilkins* [1964] studied the induction in Sq at various epochs; their results are in Table 3. *Matsushita and Maeda* [1965] also studied the Sq field and decided the ratio was 0.4. According to *Rikitake* [1966], the rapid SSC variation is subject to crustal conductivity anomalies; if these can be ignored, infinite conductivity can be assumed and the ratio of induced to external contributions is 0.5. At the Dst minimum, the ratio is ~ 0.4 . While studying the storm asymmetry, *Langel and Sweeney* [1971] determined the ratio to be 0.38. *Akasofu and Chapman* [1972] noted the maximum effect of induced currents (i.e. infinite conductivity) would be to almost extinguish the Z component while doubling the H component, although in reality the effect would be to increase the horizontal component by $1/3$, indicating a factor of $3/4$ should be used. *Langel and Estes* [1985] used Magsat data to help determine induction contributions for small Dst values (± 20 nT); they came up with a ratio of 0.24 at dusk and 0.29 at dawn. *Langel et al.* [1996] found the induced Sq currents to be 0.6 the intensity of the inducing Sq currents. These varied results are summarized in Table 4.

Studies have also increasingly revealed the complex nature of the Earth's conductivity. *Price* [1967] discussed the complexity and heterogeneity of the Earth's surface conductivity within the first 100 km. He showed for relatively slow variations such as Dst that penetrate much deeper, however, the angular non-uniformity of conductivity was not important, although one must include a surface conducting shell with some effective conductivity to account for this. *Ashour* [1971] and *Park* [1974] noted when the conductivity is finite, there is a time lag in the induction response to

Table 4. Ratios of internal-to-external magnetic field components found by various authors and the corresponding correction factors to remove induction from ΔH .

	Method	H_I/H_E	Factor to remove induction
Birkeland 1913	Storms	.17 to .5	6/7 to 2/3
Chapman 1919	<i>Sq</i>	.37 to .33	.73 to 3/4
Benkova 1940	<i>Sq</i>	.48	.68
Vestine et al. 1947	Storms	.6	5/8
Dessler and Parker 1959	Storms	.5	2/3
Takeuchi and Saito 1963	Storms	.36 to .42	.74 to .70
Matsushita and Maeda 1965		.4	5/7
Rikitake 1966		.4	5/7
Langel and Sweeney 1971		.38	.72
Akasofu and Chapman 1972	Storms	.33	3/4
Langel and Estes 1985	Storms	.24 to .29	.81 to .76
Langel et al. 1996	<i>Sq</i>	.6	5/8

external current changes. *Nopper and Hermance* [1974] studied these time lags for an electrojet and found lags of 5-15 minutes (depending on distance from the electrojet) for a 2-hour period and 2-10 minutes for a 1-hour period. *Kisabeth* [1979] studied the effect of an infinitely conducting Earth on magnetic field measurements and showed a significant effect even on satellite measurements. *Campbell and Schiffmacher* [1988] found evidence of significant lateral heterogeneity in the upper 600 km of the Earth's crust.

As magnetic storm studies increased, researchers began to look for ways to account for induction effects in their calculations and modeling. Despite the wide range and time-dependent nature of internal/external field ratios (Tables 3 and 4), most decided to simply multiply the observed ΔH by 2/3 to remove the field from induced currents [e.g., *Akasofu and Chapman*, 1961; *Siscoe and Crooker*, 1974; *Feldstein*, 1992; *Belova and Maltsev*, 1994; *Alexeev et al.*, 1996; *Maltsev et al.*, 1996; *Dremukhina et al.*, 1999;

Ebihara and Ejiri, 2000; *Ohtani et al.*, 2001] based on the recommendations of *Chapman and Bartels* [1940] and *Dessler and Parker* [1959]. Others, however, have used different values [e.g., $3/4$ by *Greenspan and Hamilton*, 2000]. Induction was neglected in the derivation of the DPS relation by *Dessler and Parker* [1959] and *Schopke* [1966], and in the development of the *Dst* index by *Sugira* [1964] and the *DR* indices by *Kamide and Fukushima* [1971], although Sugira warned, “to deduce the magnetic field of a ring current from our *Dst* values, appropriate corrections must be made for the induced magnetic fields.”

Boström [1971], *Bonnevier et al.* [1970], and *Kisabeth and Rostoker* [1977] all noted using simple factors to remove induction effects could not be done for localized ionospheric currents such as the electrojets. Therefore, in more global and/or auroral studies, simple conductivity models have been used. *Atkinson* [1967] assumed an infinitely conducting Earth in his studies and *Boström* [1971] modeled the magnetic field of substorm currents using a perfect conducting sphere below 100 km. *Boström* noted using a more realistic model with finite conductivity varying with depth would produce similar effects and the overall character of magnetic field perturbations would remain relatively unchanged. *Bonnevier et al.* [1970], *Kisabeth* [1979], *Kamide et al.* [1982], and *Friedrich et al.* [1999] have all used infinite conductivity starting at varying depths.

The rationale for using a simple factor (such as $2/3$) is based on an assumed slowly varying, longitudinally symmetric current system dominated by the zonal spherical harmonic component and penetrates deep into the Earth because of its slow variation [*Chapman and Bartels*, 1940]. In reality, individual magnetograms can show

rapid variations, which may in fact be affected by surface conductivity anomalies in the crust; *Dst* is smooth only because of the averaging process. *Stern* [1984] indicated the $2/3$ factor is only a rough estimate and induced currents actually depend on $\partial B/\partial t$. *Rostoker et al.* [1997b] indicated that induction should have a severe impact on Honolulu (a *Dst* station) since it is near a subsurface conductivity anomaly. *Friedrich et al.* [1999] noted conductivity factors should actually be very complicated because they should depend on local conductivity anomalies and frequency of the disturbance. The situation was perhaps summarized best by *Sugiura* [1964], who stated, "Since *Dst* involves variations with periods of wide range, the effect of magnetic induction in the Earth cannot be accurately estimated by a simple method." Just how much using the simple corrections (or sometimes no correction) affects the accurate interpretation of *Dst* has not been carefully analyzed.

Equatorial Electrojet

Within a belt $\sim 10^\circ$ wide in latitude centered on the magnetic dip equator, significant *H* perturbations occur due to a strong dayside ionospheric current. This current was first reported in ground magnetic measurements by *Egedal* [1947] and named the equatorial electrojet by *Chapman* [1951]. This current can produce perturbations of hundreds of nT within the belt [*Chapman and Raja Rao*, 1965; *Onwumechilli*, 1967; *Forbush and Casaverde*, 1961] but is generally thought not to effect *Dst* since these stations are not located within 10° latitude of the dip equator [*Forbush and Casaverde*, 1961; *Sugiura*, 1964; *Rangarajan*, 1989]. For details on the equatorial electrojet, see *Rastogi* [1989].

Auroral Ionospheric Currents

It is generally assumed that low-latitude magnetic perturbations, and *Dst* in particular, are not affected by auroral currents. This view has been supported by *Rostoker* [1972]. *Fukushima and Kamide* [1973a] concluded that, while auroral currents could contribute to the low-latitude asymmetry, their effect was most likely negligible. *Iyemori and Rao* [1996] concluded ionospheric current effects cancel out in the *Dst* calculation. *Friedrich et al.* [1999] actually calculated the effect of the substorm electrojet on *Dst* and found it to be in the noise level (~few nT).

On the other hand, *Sugiura* [1964] indicated that *Dst* includes some residue from polar disturbances, and *Siscoe and Crooker* [1974] determined the auroral electrojet contribution to *Dst* is typically about 20% that of the ring current. *Mayaud* [1980] indicated auroral variations necessarily interfere with lower latitude measurements. In the theoretical magnetograms of *Chen et al.* [1982], auroral currents had a significant effect on mid-latitude ΔB_z and produced one-third of the low-latitude asymmetry, although they canceled out in the *Dst* calculation. *Sun et al.* [1984] showed ionospheric currents to have an appreciable effect on ΔH all the way down to 10° latitude. *Feldstein* [1992] ascribed the shorter-period low-latitude asymmetry fluctuations to auroral electrojets and the connected field-aligned currents, noting during strong storms the electrojets expand equatorward.

CHAPTER 4

BASICS OF WAVELET ANALYSIS

The Fourier Transform and Its Limitations

The Fourier Transform takes a signal and decomposes it into sinusoidal components of all frequencies. This is done by integrating the signal $f(t)$ against the oscillatory sine and cosine functions over all frequencies:

$$\hat{f}(\omega) = \frac{1}{\sqrt{2\pi}} \int_{-\infty}^{\infty} f(t) e^{-i\omega t} dt$$

In Figure 29, the signal is a superposition of four sinusoidal waves of different frequencies. For this signal, the Fourier Transform does a very good job of finding these frequency components. The difficulty is information is provided in the frequency domain only – no information is available in the time domain. If the signal is periodic, that is not a problem; but if the signal has a time-dependent spectrum, the Fourier Transform cannot

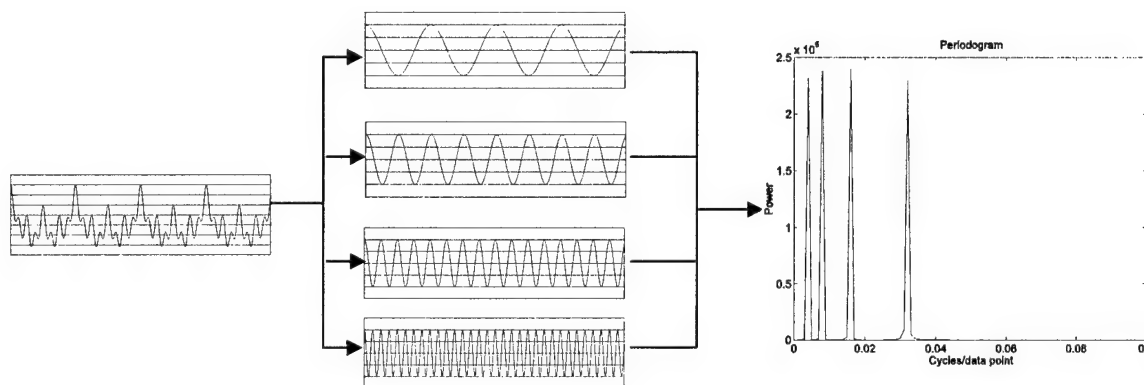


Figure 29. Example showing how a signal composed of sinusoidal components of four frequencies is decomposed by a Fourier Transform. The resulting periodogram can effectively pinpoint the frequency content of the signal.

tell you what frequencies are present at what times (even though that information is apparently present in the amplitude and phase coefficients, there is no straightforward way to extract it). Even worse, if the spectral time dependence is sufficiently complex, the Fourier Transform cannot detect the frequency components at all. Figure 30 shows a Fast Fourier Transform (FFT) applied to sinusoidal signals with increasing frequency. In the first case, the FFT is able to identify the frequency components. In the second case, where the frequencies are somewhat lower, the FFT is not as effective in identifying the frequencies. For signals with impulsive inputs, the Fourier Transform will give a broad continuum of spectral content, which gives little information about the impulsive aspects of the signals. An example of this is seen in Figure 31.

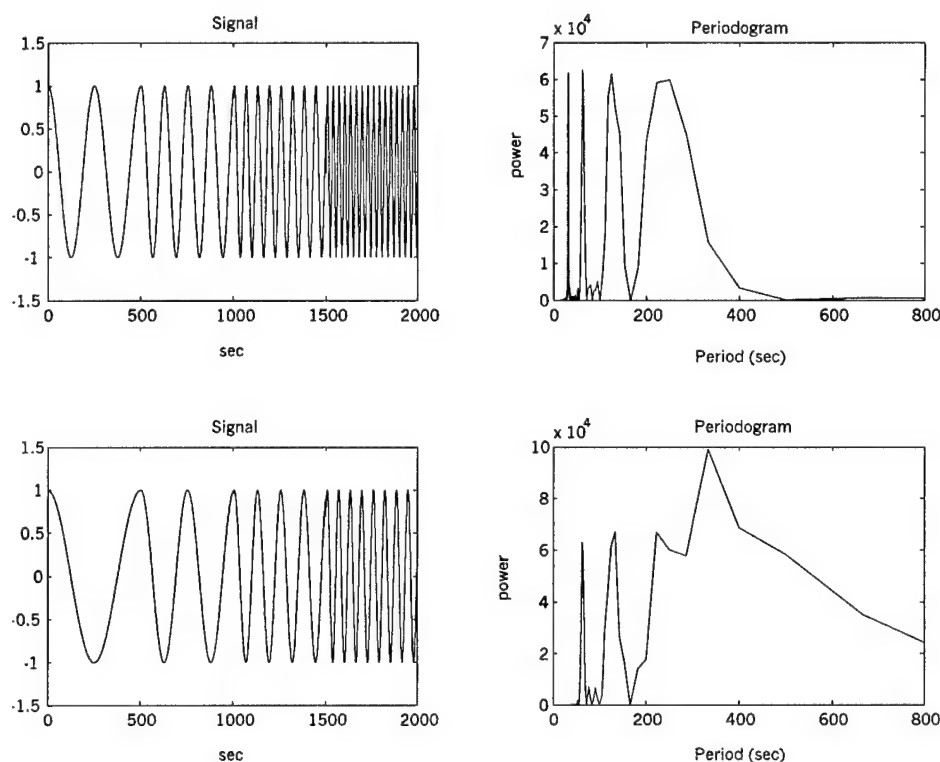


Figure 30. Periodograms derived from performing a Fast Fourier Transform (FFT) on sinusoidal signals with progressively increasing frequencies.

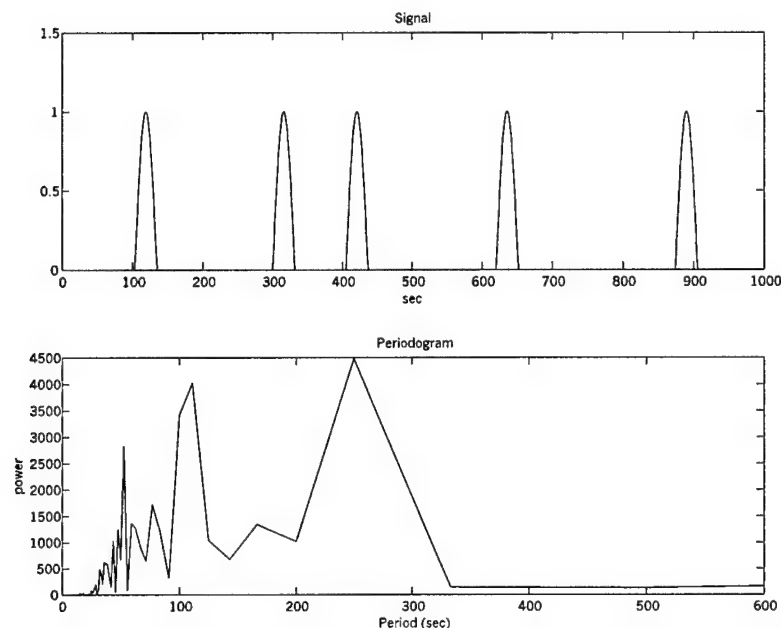


Figure 31. Signal composed of impulses and the resulting FFT periodogram.

The Short-Time Fourier Transform and Its Limitations

The Short-Time Fourier Transform (STFT) is a technique that modifies the Fourier Transform in order to provide some information on frequency content as a function of time. With the Short-Time Fourier Transform,

$$STFT_f^w(\tau, \omega) = \int_{-\infty}^{\infty} f(t)w^*(t - \tau)e^{-i\omega t} dt$$

the signal is divided into sections (windows), and each section is analyzed for its frequency content. The window function w performs this windowing – it could be a simple step function or a smoothed function like a Gaussian. This will give information in the frequency domain and the time domain, so we know how the frequency changes in time. With the choice of window function, you also choose the frequency vs. time resolution. A narrow window gives you good time resolution but poor frequency

resolution, while for a wide window, the opposite is true. Examples of this effect can be seen in Figures 32 and 33. In Figure 32, a sinusoidal signal with increasing frequency is analyzed. In this case, a narrow window allows identification of the breakpoints in frequency, but the frequency specification is somewhat broad. With a wide window, the frequencies are better specified, but their locations in time are much more uncertain.

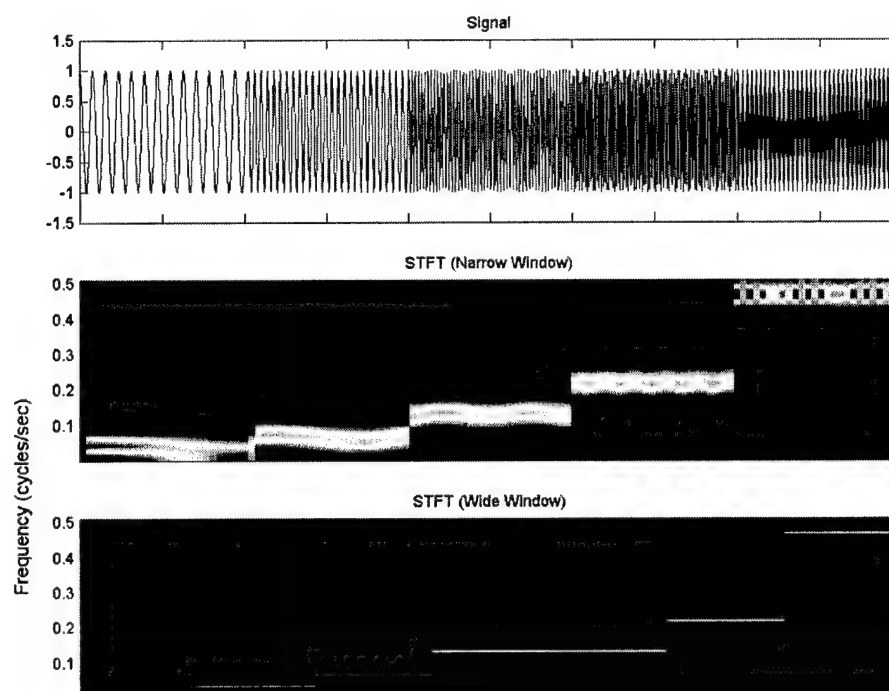


Figure 32. Analysis of a sinusoidal signal of increasing frequency with the Short Time Fourier Transform (STFT) with two different window sizes.

Figure 33 shows analysis of a two-frequency signal with two imbedded spikes. The narrow window identifies the spike quite well, but again the frequency specification is poor. A wide window once again allows good frequency specification, but the spikes are not detected at all. This fixed resolution with window choice makes the STFT an inaccurate and inefficient method of time-frequency localization since what is normally

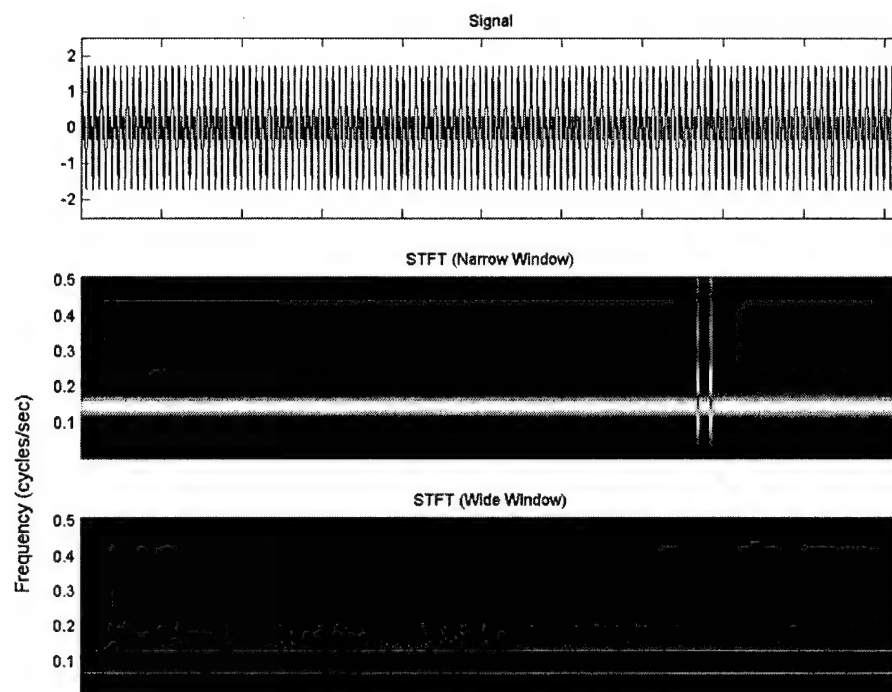


Figure 33. STFT with two different windows of a two-frequency signal with two imbedded impulses.

desired is to analyze the signal with large window and see gross features (low frequencies) and with a small window and see small features (high frequencies). A further limitation is that within the window used to break up the signal, the signal is still assumed to contain a relatively constant frequency spectrum. For signals with complicated spectral content that require a multi-resolution analysis technique, the STFT is inadequate.

Wavelet Analysis

Continuous Wavelet Transform (CWT)

The continuous wavelet transform is given by

$$CWT_f^\psi(\tau, s) = \frac{1}{\sqrt{|s|}} \int_{-\infty}^{\infty} f(t) \psi^*\left(\frac{t - \tau}{s}\right) dt$$

where $f(t)$ is the function to be analyzed and $\psi_{s,\tau}(t)$ is known as the mother wavelet – mother implying it is a prototype for generating other comparative functions, and wavelet meaning small wave. Unlike the infinite sine and cosine functions of the Fourier Transform, the mother wavelet is finite in time. Over the integration, the parameters τ (translation) and s (scale) move the wavelet in time and make the wavelet larger or smaller in order to compare it to the function $f(t)$. In effect, the integral decomposes the signal into a combination of scaled and translated versions of the mother wavelet. Figure 34 shows the Second Derivative Gaussian Wavelet (more popularly known as the Mexican Hat Wavelet) and how the variation of the translation and scale parameters allows various versions of the wavelet to be compared to the signal – in this case a simple sinusoidal wave. The result of the integration is a two-dimensional matrix of coefficients (similar to correlation coefficients) as a function of translation and scale. An example of CWT coefficients of a sinusoidal signal analyzed by the Mexican Hat Wavelet is in Figure 35. Absolute values have been plotted as this usually conveys the information better. Notice the analysis is able to identify the frequency of the signal (scale is inversely proportional to frequency, so increasing scale means lower frequencies). In practice, the analyzed signal is not continuous (as in the discrete values of geomagnetic

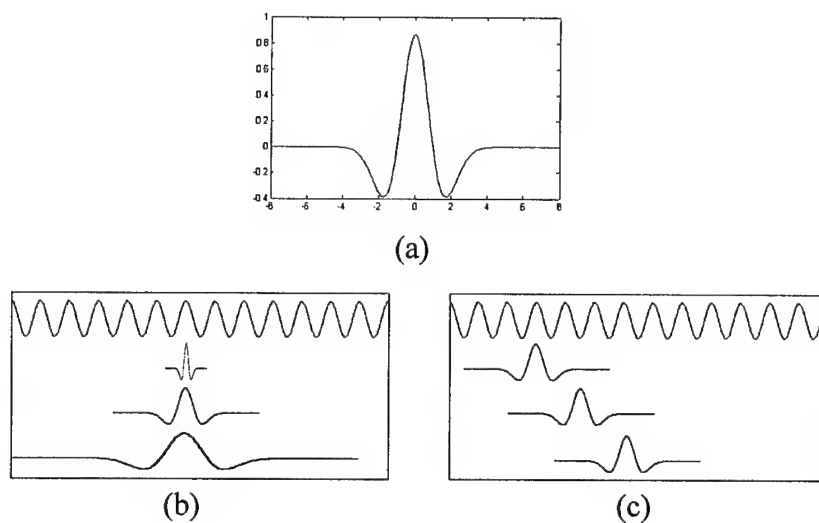


Figure 34. (a) The Second Derivative Gaussian, or Mexican Hat, Wavelet. The effect of (b) scale and (c) translation upon the Mexican Hat Wavelet when compared to a sinusoidal signal.

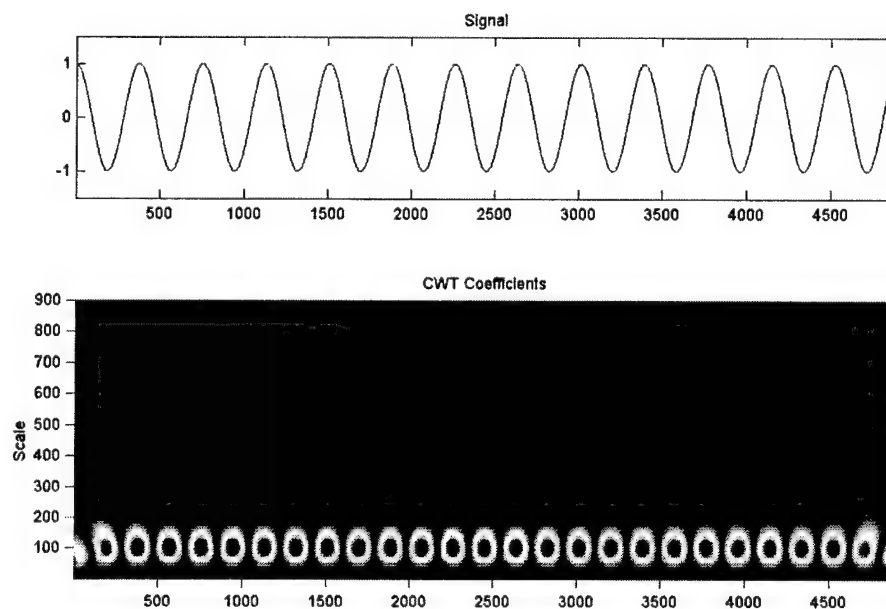


Figure 35. Absolute value of the CWT coefficients resulting from analyzing a sinusoidal signal with the Mexican Hat wavelet.

data) and so a discrete version is adopted where the integral becomes a summation over all the data points.

There are an infinite number of possible wavelets that can be used, the only requirement being:

$$\int_{-\infty}^{\infty} \psi(t) dt = 0 ,$$

which is necessary to ensure the wavelet transform has an inverse. Different wavelets have different strengths and some different wavelets are shown in Figure 36. The Mexican Hat wavelet is used for individual event localization, the Morlet wavelet favors spectral accuracy of oscillations, the 1st-derivative Gaussian wavelet is good at finding gradients, and the Haar wavelet detects discontinuities. For each wavelet, a specific scale value can generally be correlated to a specific characteristic frequency, or pseudo-frequency. The relationship is inversely proportional and can be obtained by finding the

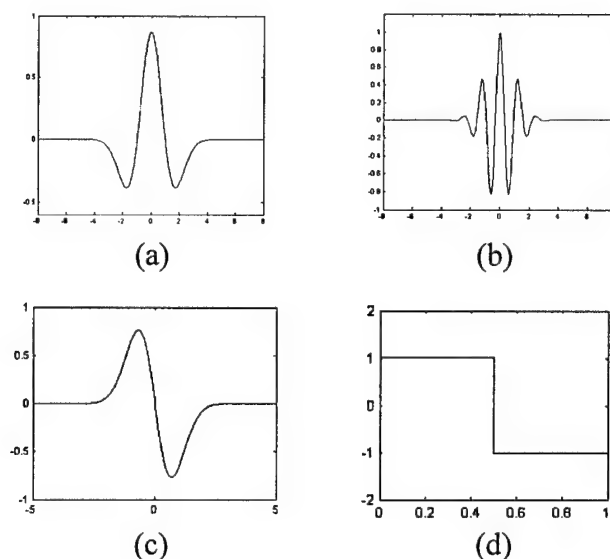


Figure 36. Some possible wavelets: (a) Mexican Hat wavelet, (b) Morlet wavelet, (c) 1st-derivative Gaussian wavelet, and (d) Haar wavelet.

equivalent Fourier period for the wavelet scale [Meyers *et al.*, 1993; Torrence and Compo, 1998]. A CWT of a sinusoidal signal with increasing frequency is shown in Figure 37 – the frequency (scale) content and frequency cutoff times can be clearly seen. A CWT of a signal with aperiodic impulses is shown in Figure 38. The Mexican Hat wavelet is able to locate the impulses and can even provide an associated scale, which can then give a related pseudo-frequency. In Figure 39, a more complicated signal is analyzed. This signal contains a constant low frequency, an increasing high frequency, and several discontinuities. The CWT with the Morlet wavelet easily identifies all of these features. The strength of CWT is it can perform multi-resolution analysis – it gives good time resolution at high frequencies and good frequency resolution at low frequencies.

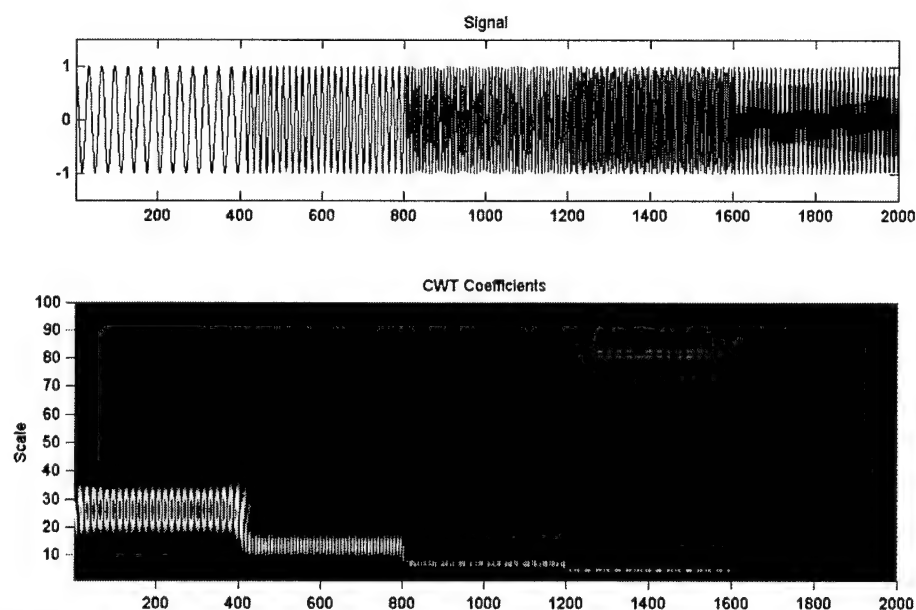


Figure 37. CWT analysis of a sinusoidal signal of increasing frequency using the Morlet wavelet.

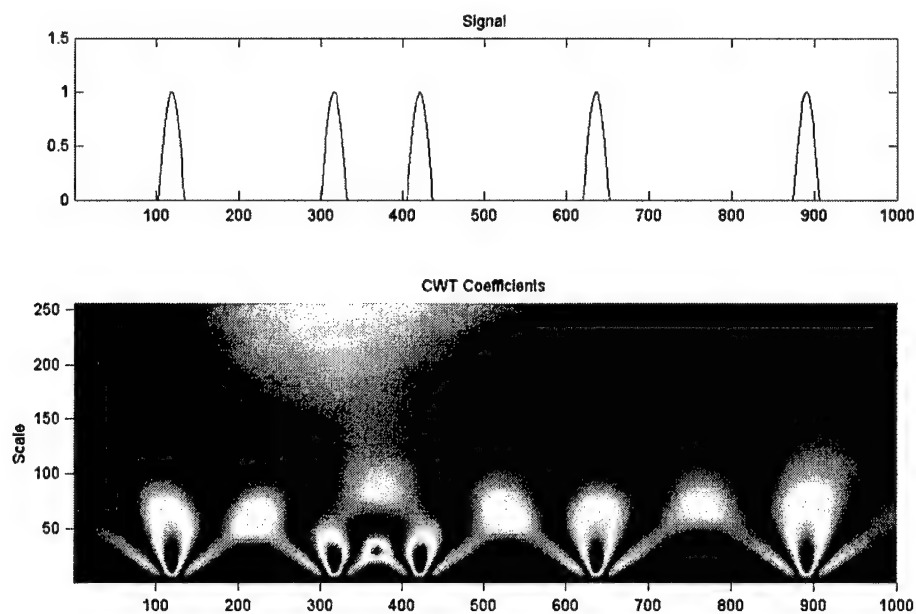


Figure 38. Absolute value of the CWT coefficients resulting from analyzing an aperiodic impulsive signal with the Mexican Hat wavelet.

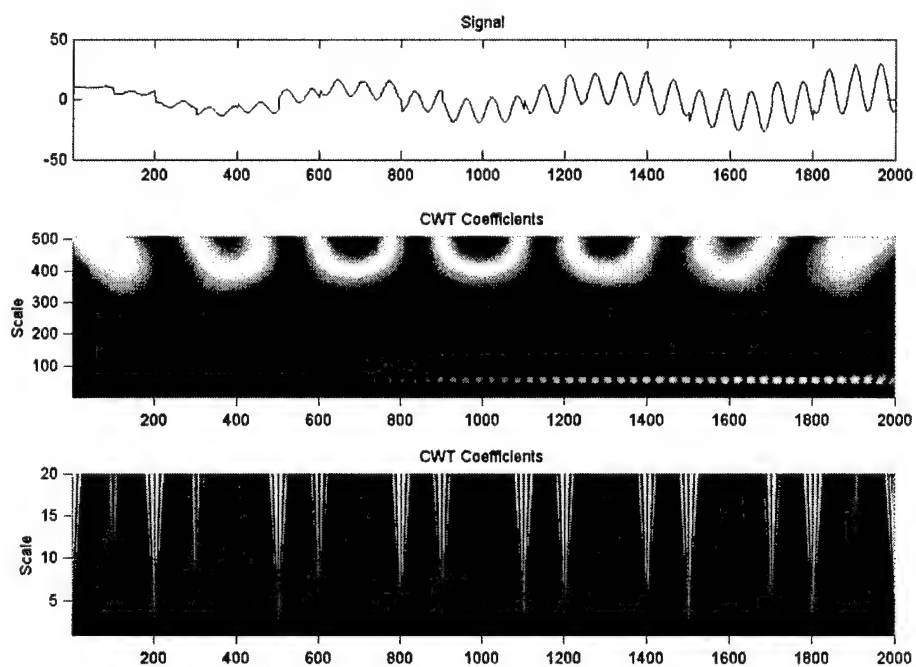


Figure 39. Absolute value of the CWT coefficients resulting from analyzing a signal containing a steady low frequency, an increasing high frequency, and several discontinuities. The analysis was performed with the Morlet wavelet.

Discrete Wavelet Transform (DWT)

This is distinctly different from the discrete version of the CWT. Although visually revealing, the CWT analysis at all scales and times turns out to be very redundant as far as signal reconstruction is concerned. The analysis can be just as accurate if the signal is analyzed with scale and translation values that are powers of two (dyadic). This process is the Discrete Wavelet Transform (DWT) and is equivalent to passing the signal through a series of high- and low-pass filters. This decomposition can then be used for reconstruction (exact reconstruction is possible), compression, filtering, and de-noising of signals. Chapter 3 of *Chan* [1995] and Chapter 5 of *Boggess and Narcowich* [2001] discuss the mathematics and algorithms of the DWT in great detail. The requirements for wavelets used in DWT are greater: the wavelet basis must be orthogonal, and the wavelet must have compact support, or:

$$\int_{-\infty}^{\infty} |\psi(t)|^2 dt < \infty.$$

A specialized application of the DWT is de-noising signals using the Stationary Wavelet Transform (SWT). The SWT uses the same basic deconstruction of the DWT, but restores translation invariance which is lost under the DWT by averaging several de-noised signals [*Coifman and Donoho*, 1995]. It also suppresses some artificial artifacts, such as Gibbs phenomena around discontinuities, that can appear in the DWT.

CHAPTER 5

WAVELET ANALYSIS OF LOW- AND MID-LATITUDE DATA

Storm Data Selection

In order to analyze the contributions to magnetic field measurements during magnetic storms, I selected four magnetic storm periods from the Jan-Jun 1979 data set. The intent was to focus the analysis on the data from the individual stations rather than an index like *SYM H* since the individual magnetograms more closely represent direct measurements of actual physical processes. The criteria used for storm selection were:

- 1) *Dst* below -100 nT (of which there were five) so the strongest storms are analyzed; and
- 2) no more than one of the six stations with data gaps near storm maximum, making analysis impossible (four of the five meeting the first criteria). The periods selected are summarized in Table 5. The 5-minute resolution data sets were chosen to be 1024 data points long (a length of 85 hours, 20 minutes) due the DWT requirement of data sets having a total number of data points equal to a power of two, and considering the sets must be long enough to include the entire storm period (which can cover several days). Plots of the data for these periods are shown in Figures 40-43. In some cases, data gaps were subsequently filled in with interpolated values in order to enable wavelet analysis.

Table 5. Time periods selected for study from the Jan-Jun 1979 data set.

Time Period Covered	Minimum <i>Dst</i> (nT)
0000 UT/20 Feb 79 – 1315 UT/23 Feb 79	-107
0030 UT/10 Mar 79 – 1345 UT/13 Mar 79	-140
1725 UT/2 Apr 79 – 0640 UT/6 Apr 79	-202
0000 UT/24 Apr 79 – 1315 UT/27 Apr 79	-149

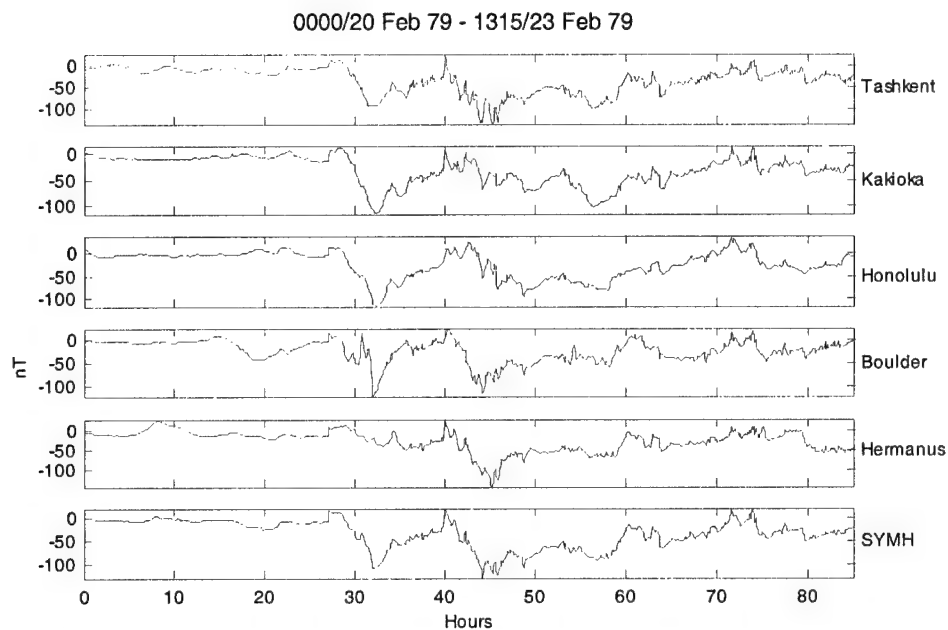


Figure 40. Magnetograms and *SYMH* for the period 0000 UT/20 Feb 79 – 1315 UT/23 Feb 79.

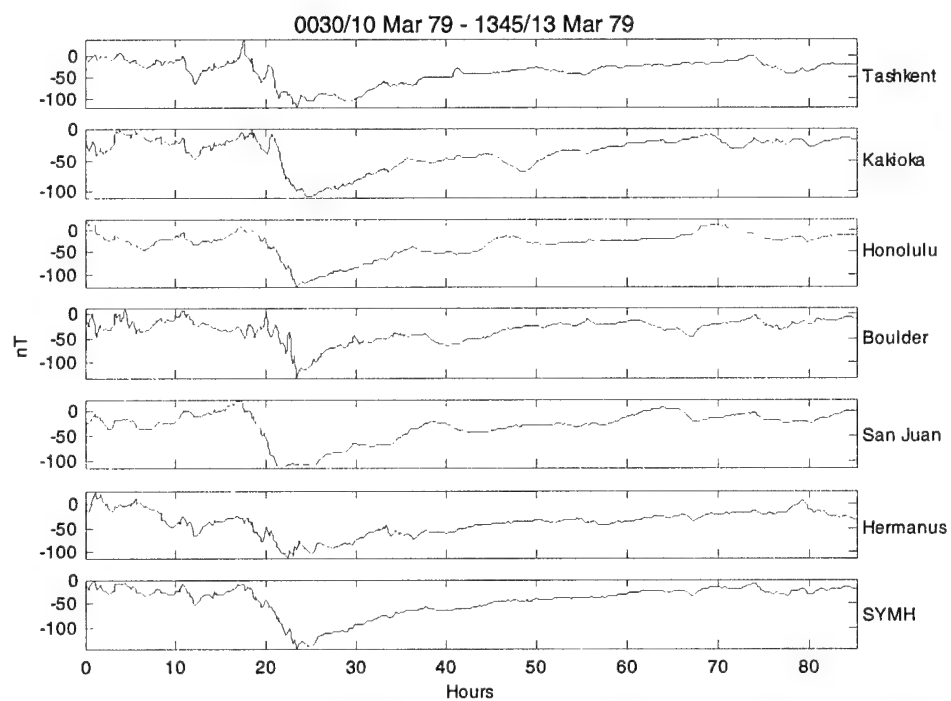


Figure 41. Magnetograms and *SYMH* for the period 0030 UT/10 Mar 79 – 1345 UT/13 Mar 79.

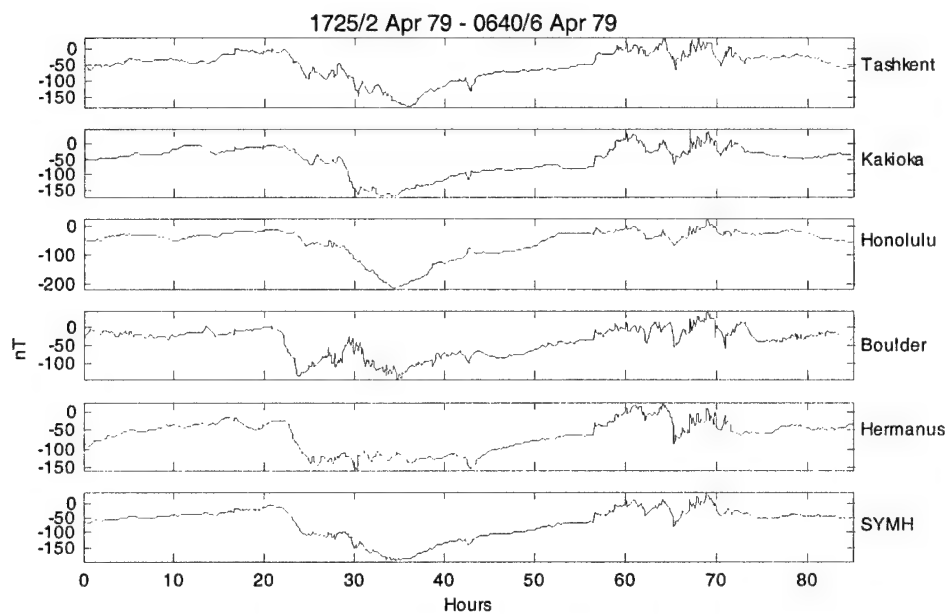


Figure 42. Magnetograms and *SYMH* for the period 1725 UT/2 Apr 79 – 0640 UT/6 Apr 79.

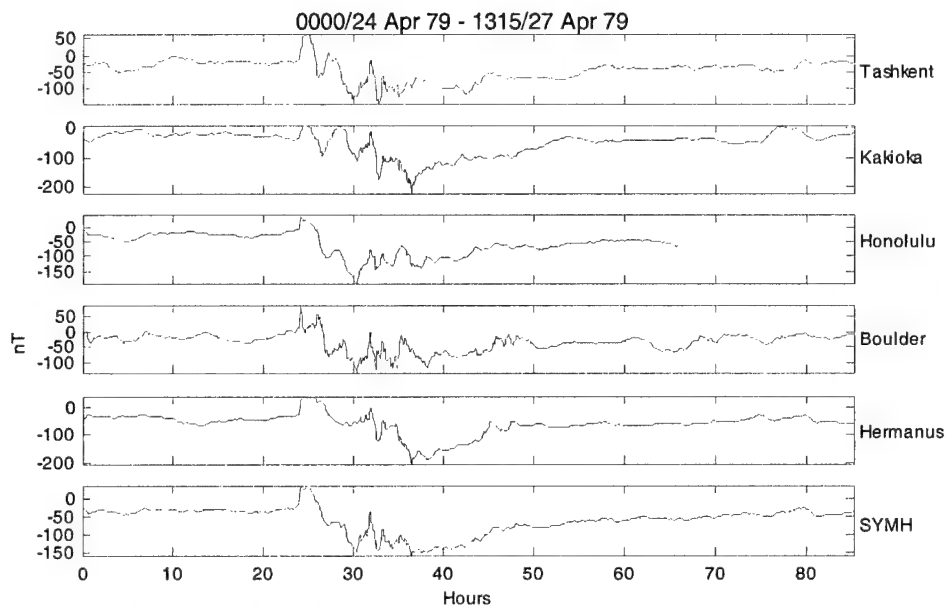


Figure 43. Magnetograms and *SYMH* for the period 0000 UT/24 Apr 79 – 1315 UT/27 Apr 79.

Wavelet Analysis of Magnetograms

Procedure

A CWT analysis was performed on the individual magnetograms using the Reverse Biorthogonal 2.8 wavelet. This wavelet, pictured in Figure 44, is similar to the Mexican Hat wavelet (and so is suited to detection of impulsive events) but is sharper, and was chosen in order to correspond better to the spiky nature of the signals. These and all subsequent wavelet analyses were performed using MATLAB. The resulting CWT coefficients (absolute values) for pseudo-periods up to 20 hours are shown in Figures 45-48 for the selected storm periods. In the following analyses, one must keep in mind a pseudo-period corresponds to a complete oscillation, with both a positive and a negative phase. If we are interested in single impulsive events (as is the physical nature of most of our currents), the characteristic time will be one-half of the corresponding pseudo-period.

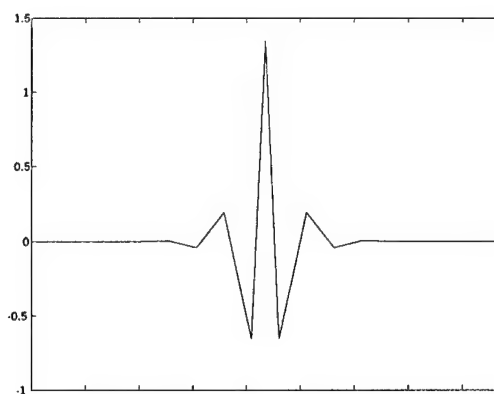


Figure 44. The Reverse Biorthogonal 2.8 wavelet.

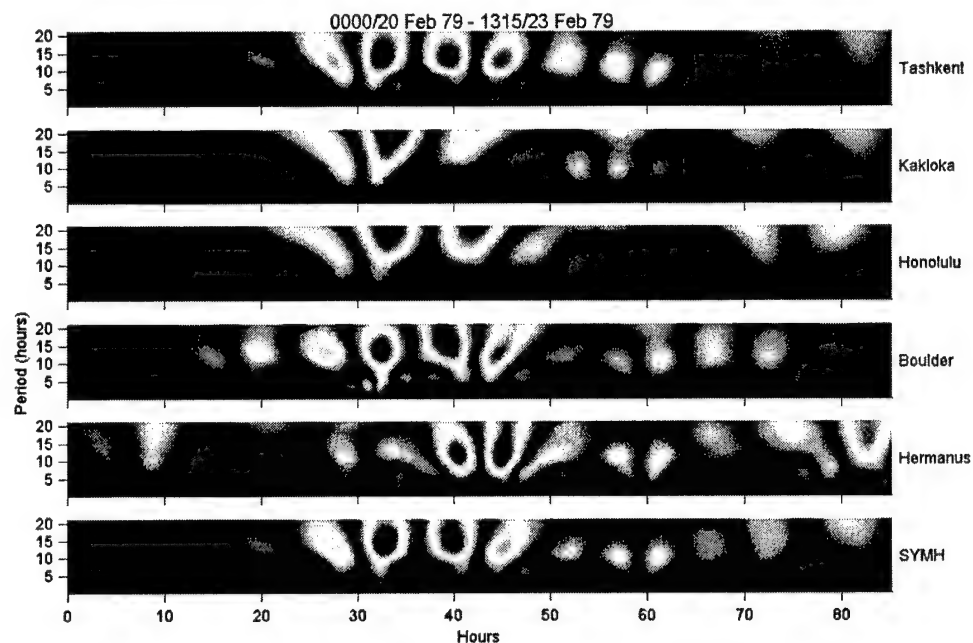


Figure 45. Absolute value of the CWT coefficients for the 20-23 Feb 79 storm. Pseudo-periods up to 20 hours are shown.

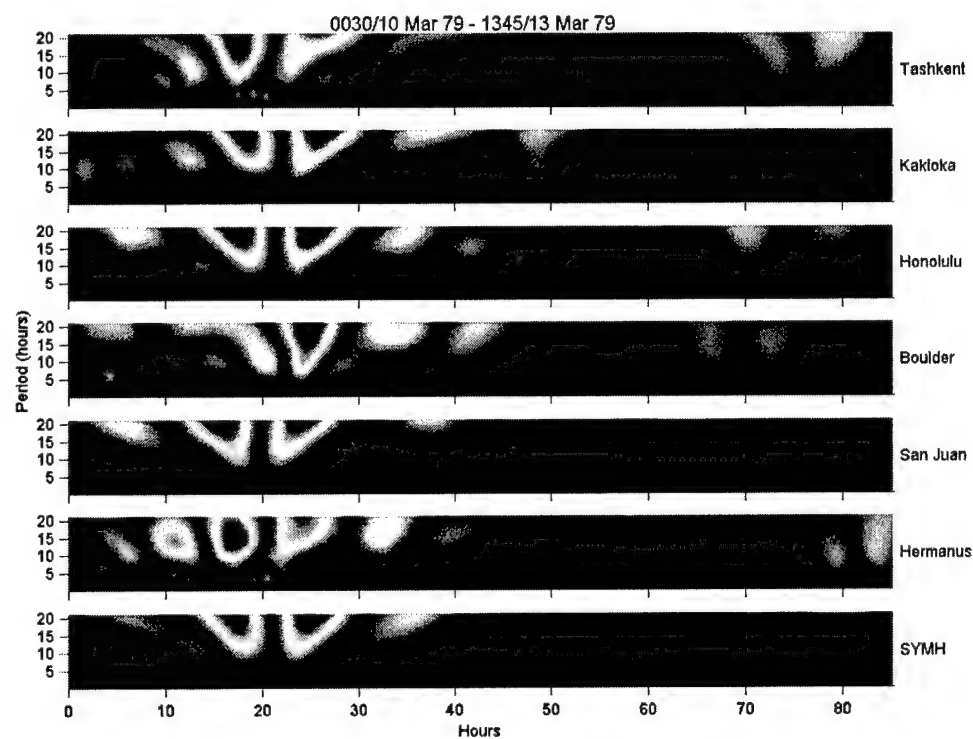


Figure 46. Absolute value of the CWT coefficients for the 10-13 Mar 79 storm. Pseudo-periods up to 20 hours are shown.

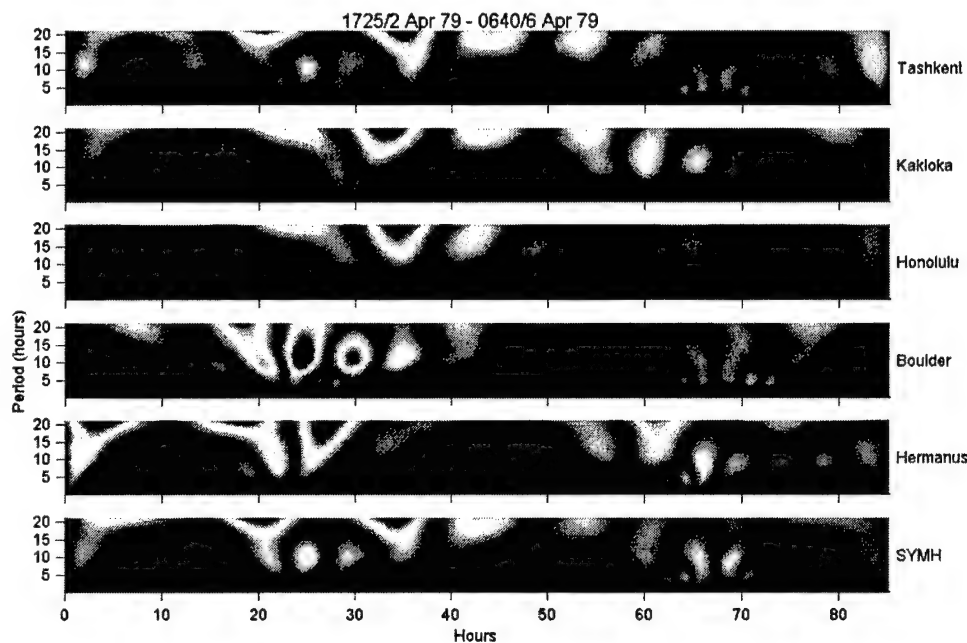


Figure 47. Absolute value of the CWT coefficients for the 2-6 Apr 79 storm. Pseudo-periods up to 20 hours are shown.

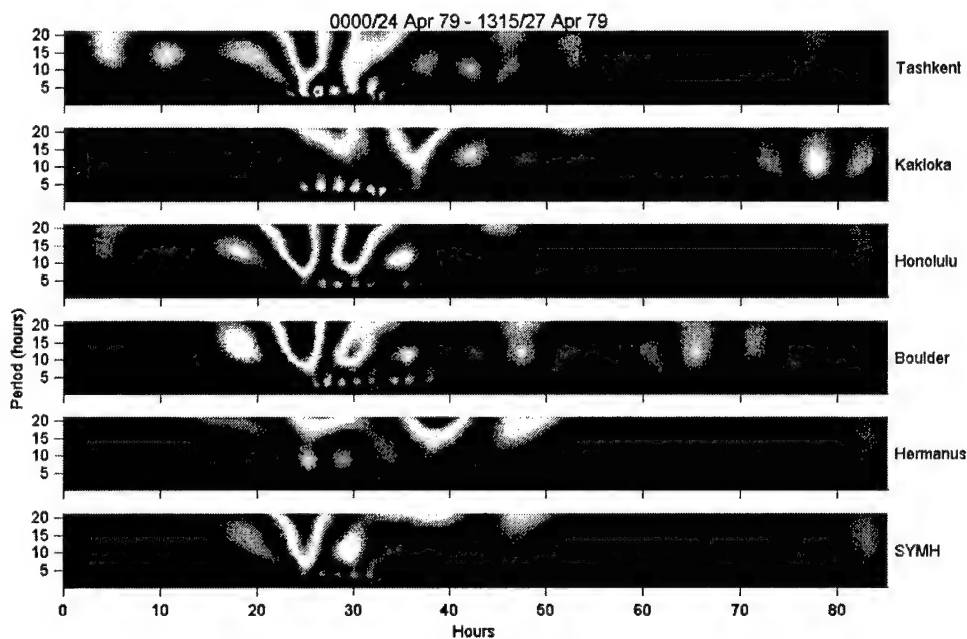


Figure 48. Absolute value of the CWT coefficients for the 24-27 Apr 79 storm. Pseudo-periods up to 20 hours are shown.

Spectral Information

In general, there appear to be two primary characteristic pseudo-periods present in the magnetograms in Figures 45-48. One is in the 10-20 hour range, the other around 3 to 5 hours (this component is especially clear in Figure 48). To highlight the higher frequency component better, the coefficients for periods of 1 to 5 hours are shown in Figures 49-52.

These higher frequency inputs tend to precede the lowest H excursion and are generally confined to the region around the storm main phase, but also appear prominently in some non-storm periods that are still somewhat active (for example, see the period between 60 and 70 hours in Figures 42, 47, and 51). Power in this frequency range is evident to some degree in all magnetograms and even appears in *SYMH*. It would be reasonable to conclude this component is due to substorm activity since the lifetime of substorms is typically 2 to 3 hours. Wavelet analysis has allowed us to clearly isolate this characteristic component in the magnetograms.

Another way to view the spectral content of the signals is with the time-average of the square of the CWT coefficients at each scale (or pseudo-period). This will give an approximate (non-normalized) power spectrum for the signal. The pseudo-power spectra were computed for the four storm periods using the Morlet wavelet and the results are shown in Figures 53 and 54 (the Morlet wavelet was used since it isolates spectral components more clearly). The maximum period detectable by the analysis was 52 hours. In the plots, specific frequency components clearly exist, but are not consistent from storm to storm. This is most likely due to the fact that each storm has a distinctly

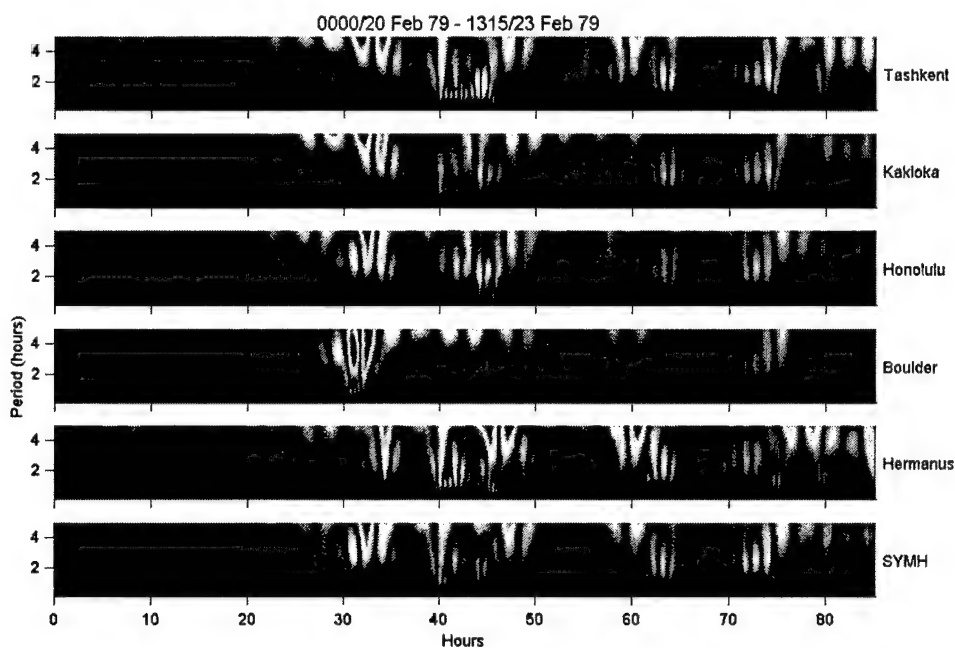


Figure 49. Absolute value of the CWT coefficients for the 20-23 Feb 79 storm. Pseudo-periods up to 5 hours are shown.

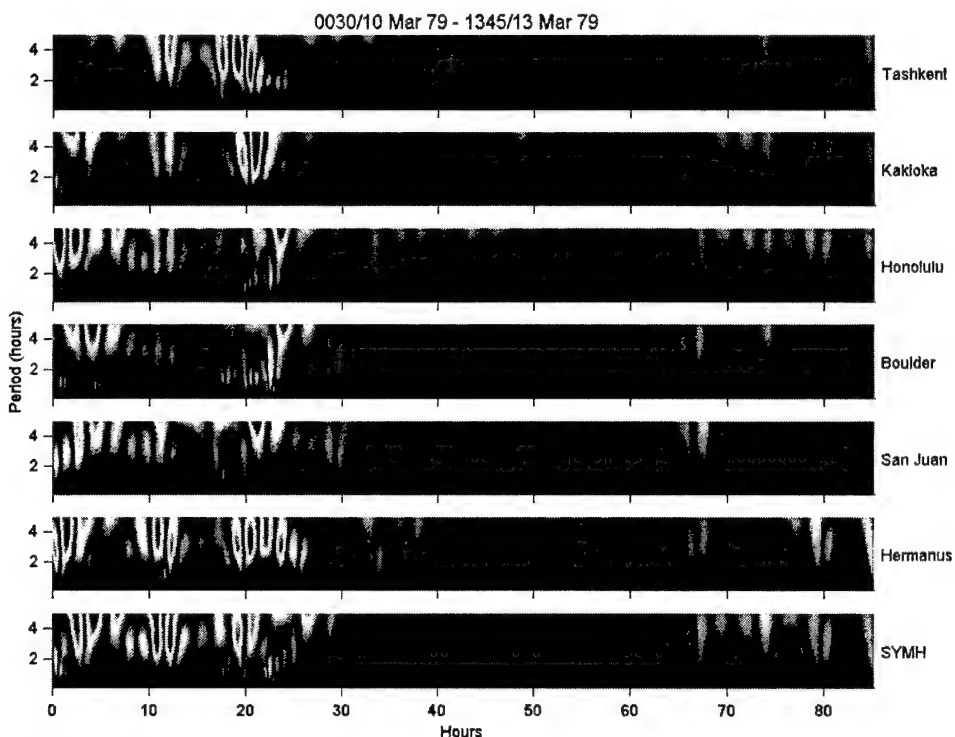


Figure 50. Absolute value of the CWT coefficients for the 10-13 Mar 79 storm. Pseudo-periods up to 5 hours are shown.

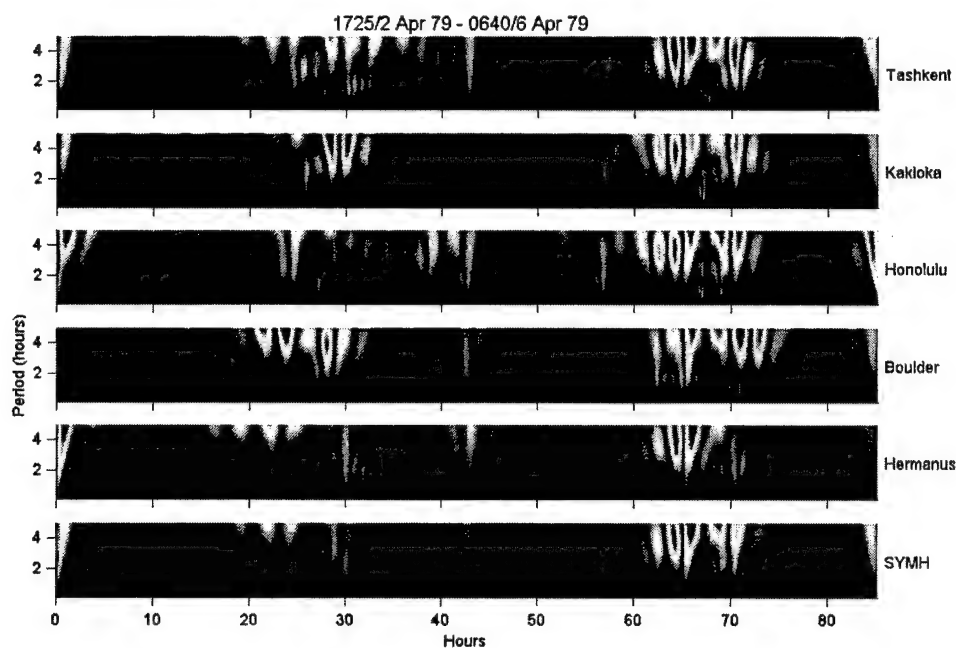


Figure 51. Absolute value of the CWT coefficients for the 2-6 Apr 79 storm. Pseudo-periods up to 5 hours are shown.

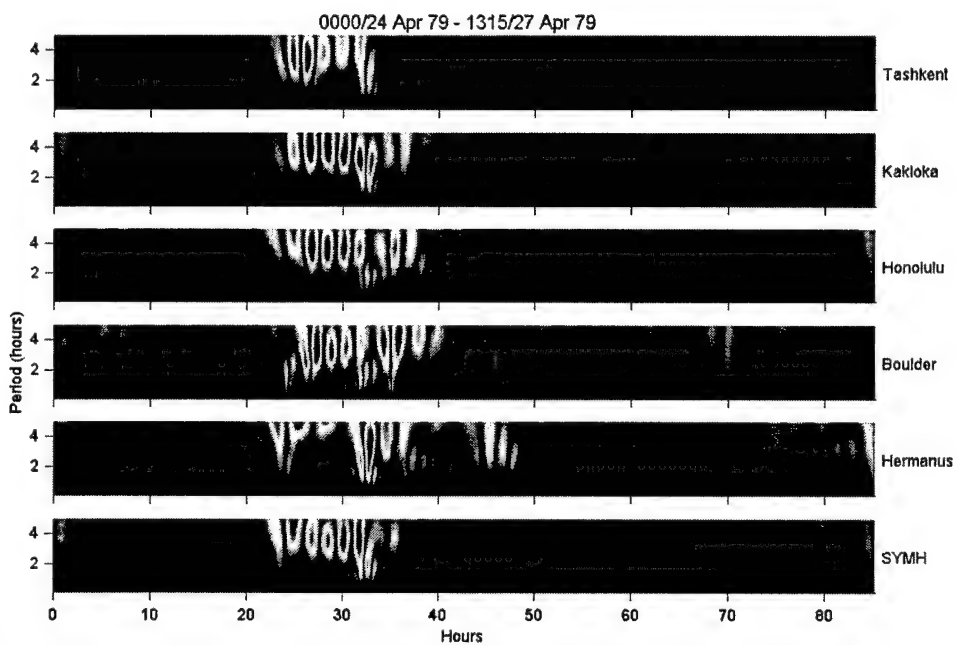


Figure 52. Absolute value of the CWT coefficients for the 24-27 Apr 79 storm. Pseudo-periods up to 5 hours are shown.

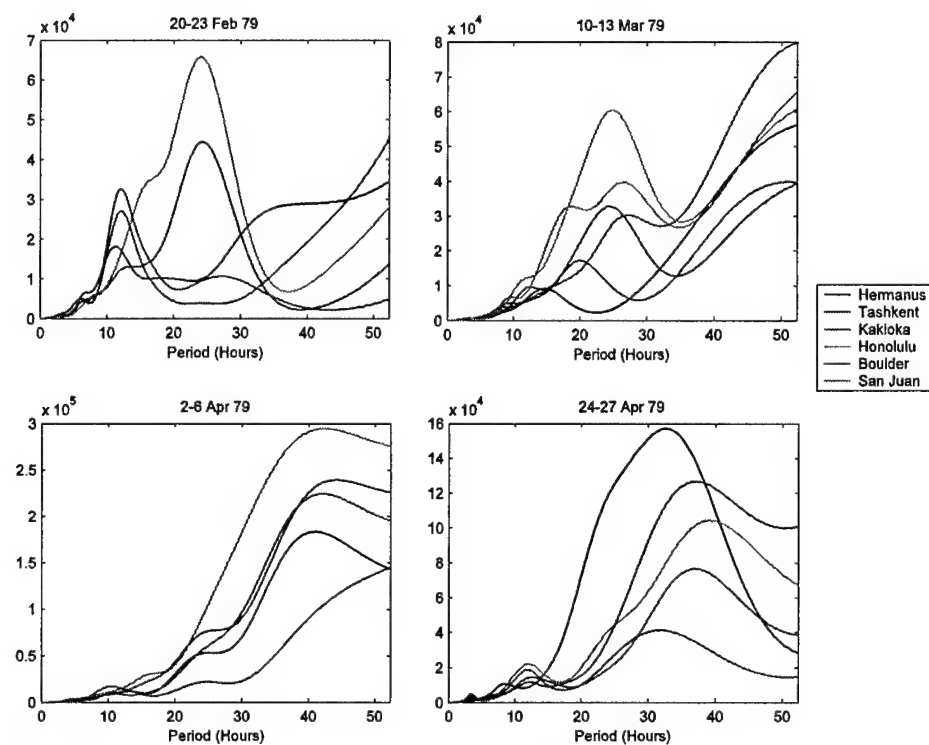


Figure 53. Time average of the square of the CWT coefficients for pseudo-periods up to 52 hours.

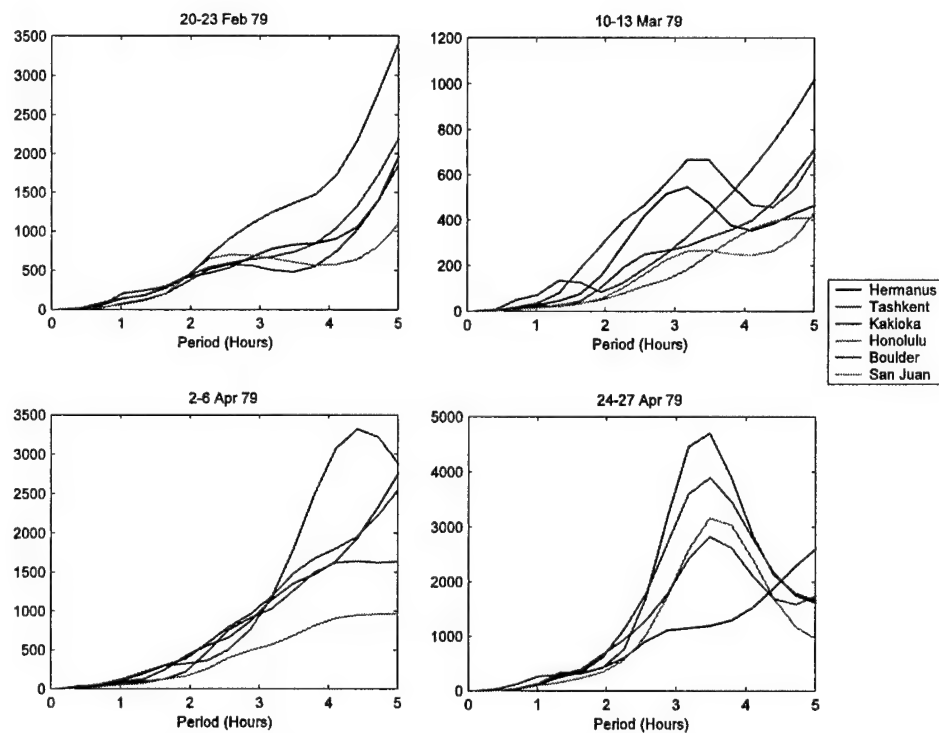


Figure 54. Time average of the square of the CWT coefficients for pseudo-periods up to 5 hours.

different character. They also are not consistent from station to station most of the time. This is most likely due to spatial distribution of stations and the oftentimes local nature of some of the currents involved.

The 20-23 Feb 79 storm shows signs of components at about 2.5 hours, 12 hours, and 24 hours, but are not consistent at all sites. The 10-13 Mar 79 storm, with a more classic shape, has inputs at about 3 hours, 10-15 hours, 20-25 hours, and possibly another peak beyond 50 hours. The 2-6 Apr 79 storm shows components at about 4-6 hours, 10 hours, 20-25 hours, and 40-45 hours. The 24-27 Apr 79 storm has clear inputs at 3-4 hours, 12 hours, and 30-40 hours. An FFT power spectrum of these same magnetograms (Figure 55) shows nearly identical spectral components, providing independent verification of these results. The lowest frequency components (periods of 30 hours and

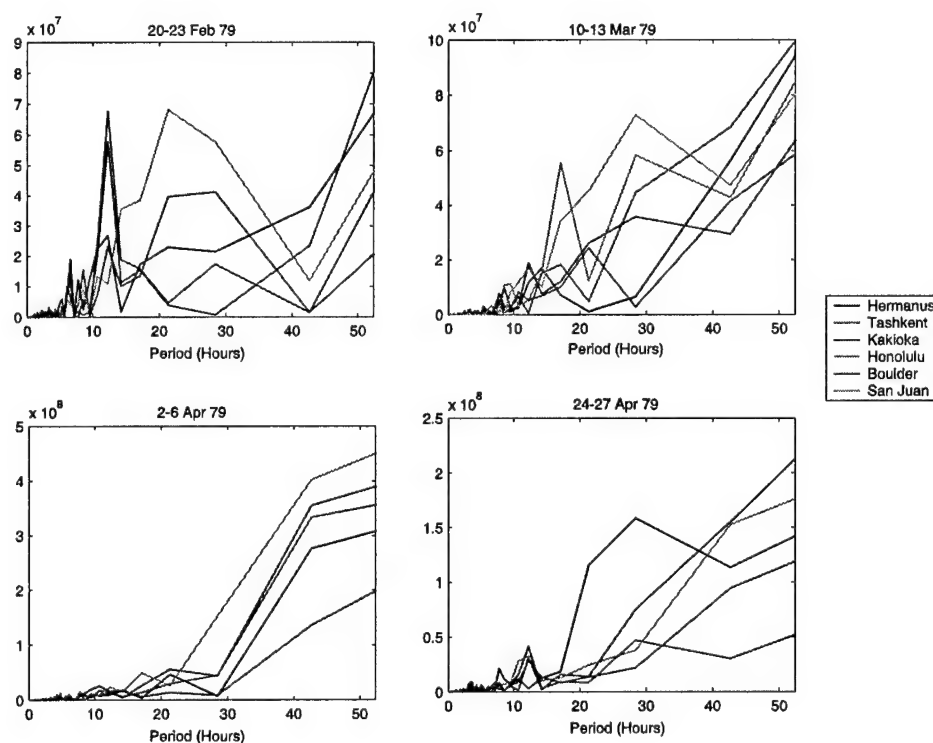


Figure 55. FFT of the four storm times for periods up to 52 hours.

greater) have the greatest consistency between stations and are most likely driven by the large-scale ring current intensification. The highest frequency part (3-6 hour period) is most likely related to substorm activity, although it is not obvious how this may be since at these stations, the auroral electrojets are not measurable. The middle frequencies (12-25 hour periods) have a less clear origin. The 24 hour pseudo-period could relate to the partial ring current, which would give a 24 hour oscillatory signal as the station rotates around the Earth.

Separation of High and Low Frequencies Using the SWT

The DWT is especially suited to the filtering of signals by the suppression of selected scales in the reconstruction of the decomposed signal. One way this can be used is to remove the highest frequencies from a signal to recover only the low-frequency component. Figure 56 represents the low-frequency approximations representing a denoising of the magnetograms using the SWT version of the DWT with periods < 36 hours removed. The higher-frequency variations removed represent impulsive events with a characteristic time of approximately 18 hours (or pseudo-periods less than 36 hours). The resulting approximations were then corrected for an equivalent equatorial current by dividing the reconstructed signal by the cosine of the latitude. These approximations are quite smooth and generally appear symmetric. When the next level of coefficients (18 hour period) are added, the reconstructed magnetograms start to show a character more asymmetric and similar to the 'classic' *Dst* storm shape (Figure 57). This would seem to confirm the lowest frequency part of the magnetograms are due to the slowly-varying

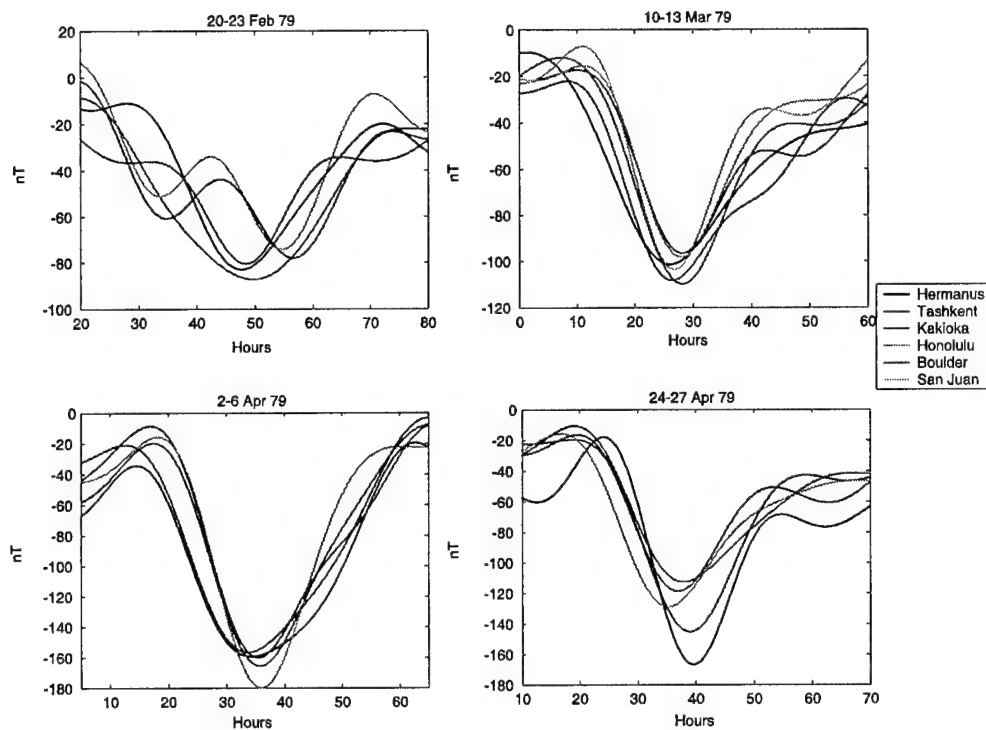


Figure 56. Reconstructed magnetograms with only periods > 36 hours retained.

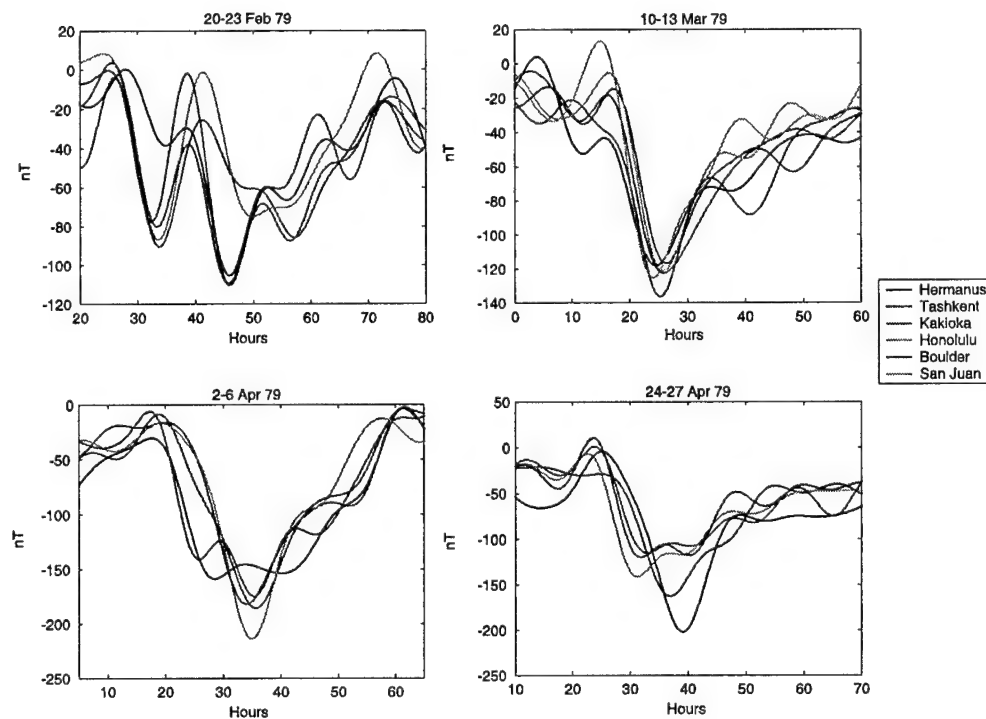


Figure 57. Reconstructed magnetograms with only periods > 18 hours retained.

symmetric ring current, but both the >30 hour component and the 24 hour component must be included to form the expected *Dst* shape.

CHAPTER 6

WAVELET ANALYSIS OF HIGH-LATITUDE DATA

Substorm Current Wedge and Electrojet Theory

It has been known for some time when solar wind changes produce a geomagnetic storm, defined as the low-latitude magnetic perturbation lasting tens of hours, the changes also produce rapid (on the order of minutes to hours) auroral current variations known as substorms. With auroral currents being much more localized, the magnetic effect of these current variations are only seen in magnetometers at high latitude. As discussed in Chapter 3, the substorm current wedge (Figure 24) has become a popular model for the substorm current system. In this depiction, current is diverted from the magnetotail, along field lines, and into the ionosphere in both hemispheres to drive the westward electrojet in the auroral region.

In reality, the situation is more complex. The westward electrojet has two components: one is controlled by magnetospheric convection (the directly driven component) and one is controlled by the diversion of tail current into the electrojet via the substorm current wedge (the unloading component) [Rostoker *et al.*, 1987; Kamide and Kokubun, 1996; Baker *et al.*, 1997; Sun *et al.*, 2000]. The unloading component has a shorter characteristic time scale (~15 minutes to an hour) than the directly driven time scale of several hours [Kamide and Kokubun, 1996; Rostoker *et al.*, 1997; L. Zhu, private communication, 2002] so it may be possible to distinguish between the two components in high-latitude magnetograms using wavelet analysis.

Separation of Electrojet Components via DWT

Based on the time scale differences between the directly driven and unloading components, I attempted to use the SWT denoising technique to separate the two components. Table 6 shows the DWT analysis levels and the corresponding scales, pseudo-periods, and impulse widths for the Reverse Biorthogonal 2.8 wavelet based on a sampling rate of 1 minute.. I decided to remove levels 7 and below in the reconstructed magnetogram with the idea that, by removing impulses of 1.8 hours or greater, the reconstruction should represent the directly driven component. The residual (levels 1-7), then, should contain only the unloading component. An example of this procedure applied to the Leirvogur magnetogram for the 24-27 Apr 79 period is shown in Figure 58. The top plot is the original magnetogram, the middle represents the reconstructed signal with levels 7 and below removed, and the bottom is the residual. The middle represents an approximation of the directly driven component and the bottom represents an approximation of the unloading component.

Table 6. Level and scale information for DWT analysis on 1-minute data using the Reverse Biorthogonal 2.8 wavelet.

Level	Scale	Pseudo-Period	Impulse Width
1	2	3.4 min	1.7 min
2	4	6.8 min	3.4 min
3	8	13.6 min	6.8 min
4	16	27.2 min	13.6 min
5	32	54.4 min	27.2 min
6	64	1.8 hrs	54.4 min
7	128	3.6 hrs	1.8 hrs
8	256	7.3 hrs	3.6 hrs
9	512	14.6 hrs	7.3 hrs

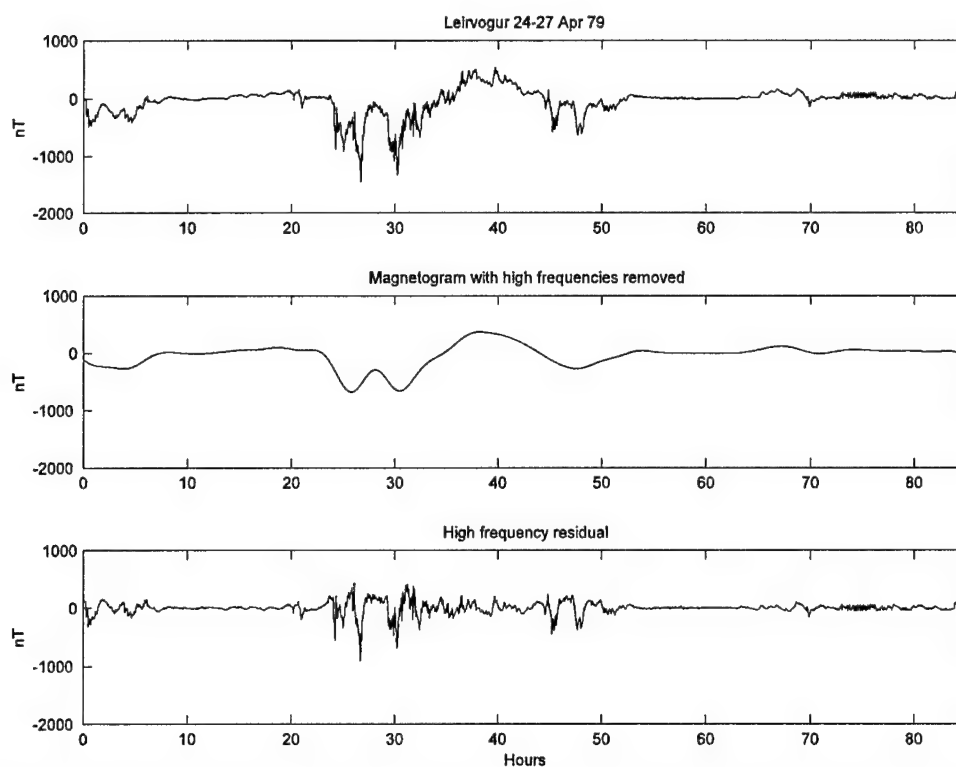


Figure 58. Leirvogur magnetogram analyzed with the SWT denoising technique to remove high frequencies.

To determine how close this approximation really is, we can compare the results to an individual event to see if it makes sense. Figure 59 shows a multiple-onset substorm event with two impulsive unloading events superimposed on a slower varying directly driven background. The SWT denoising analysis is able to separate the slowly varying component (middle plot) and the high-frequency unloading events (bottom plot). In this example the denoising technique seems to successfully separate the two components.

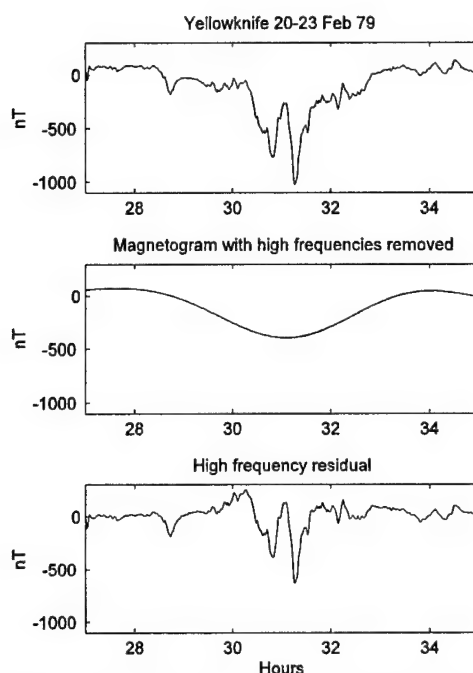


Figure 59. Example of how the SWT denoising separates the directly driven (middle) and unloading (bottom) components from a substorm signature (top).

Substorm Current Wedge Calculations

Current Wedge Signatures at Low Latitude

Although the localized electrojets will produce no significant magnetic signatures at low- and mid-latitudes, the other segments of the substorm current wedge may be detectable. The disruption of tail current (magnetically equivalent to eastward wedge current closure) and the field-aligned currents may produce significant magnetic perturbations at these latitudes (see Chapter 3). Specifically, it is generally believed near midnight, a strong positive perturbation will be seen that will gradually decrease as you move east or west and turn negative as you move outside the wedge [Clauer and McPherron, 1974; McPherron *et al.*, 1997; Y. Kamide, personal communication, 2002]. This situation is summarized in Figure 60 where the X component is approximately the

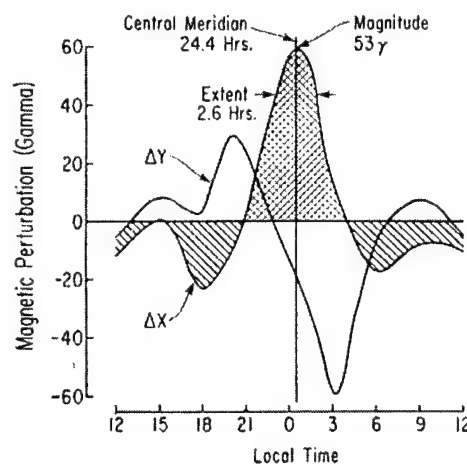


Figure 60. Example of a mid-latitude local time profile of a substorm [Clauer and McPherron, 1974].

same as the H perturbation. Based on this view, we would expect substorm signatures to appear in the data set as:

- 1) High-latitude electrojet signatures appearing as intense (hundreds to thousands of nT), rapid negative perturbations near local midnight, possibly extending several hours east or west depending upon the longitudinal extent of the wedge.
- 2) Low- and mid-latitude positive perturbations (tens of nT) near local midnight, on the order of an hour, superimposed on any other variations present.
- 3) Less intense negative perturbations at low- and mid-latitudes a few hours away from midnight, depending upon the longitudinal extent of the wedge.

An example of one such set of signatures is shown in Figure 61 for a substorm at approximately 1200 UT on 4 Apr 79. The high-latitude station College (~0215 LT) shows the largest electrojet signature (Figure 61a), but signatures are also seen at Barrow (~0130 LT) and Cape Wellen (~0040LT) (Figure 61c). Because of the localized nature

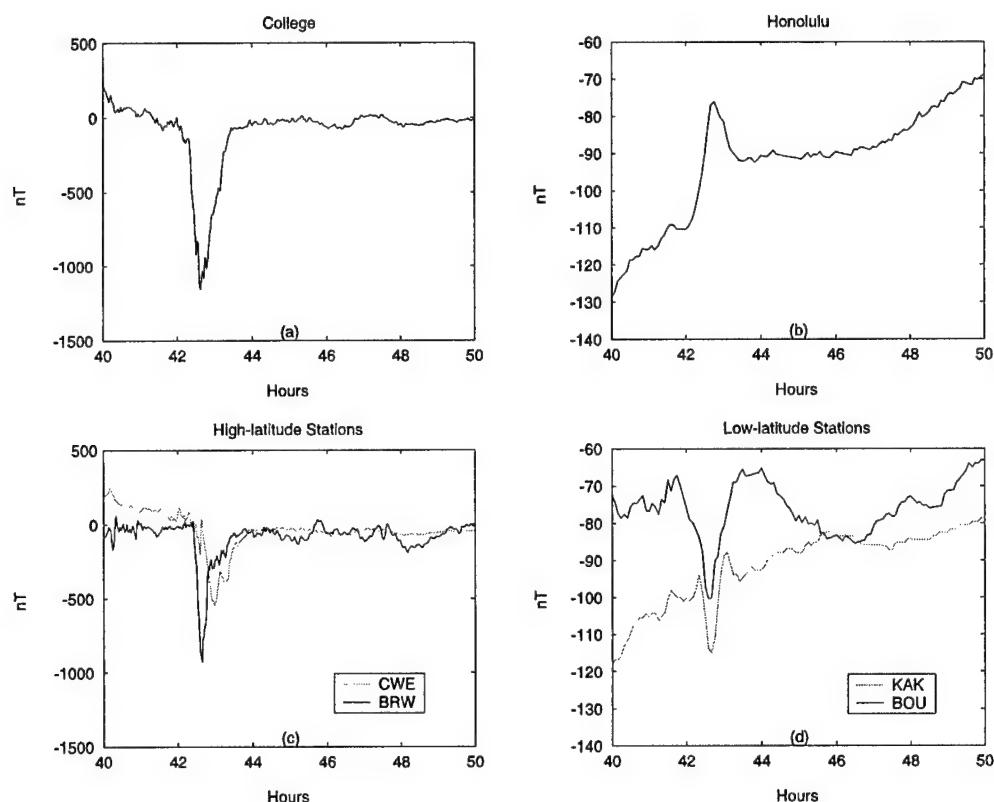


Figure 61. Multiple signatures of a substorm found in magnetograms during the 2-6 Apr 79 storm. (a) and (c) show the influence of the westward electrojet while the perturbations in (b) and (d) are produced by the combination of tail current disruption and field-aligned currents.

of the electrojet, the strongest signature at College does not necessarily mean the electrojet is strongest there, only that it's closest. At low- and mid-latitudes, Honolulu (~0130 LT) shows a clear positive wedge signature, indicating it is inside the wedge (Figure 61b). Boulder (~0500 LT) and Kakioka (~2120 LT) show corresponding negative signatures indicating they are outside of the wedge (Figure 61d). From the magnetograms, then, we can determine this wedge has a longitudinal extent of somewhere between 30° and 100° , which is consistent with expected wedge widths [L. Zhu, private communication, 2002].

Self-Consistent Current Wedge Calculations

In order to determine if these (and similar) signatures are indeed caused by the substorm current wedge, I performed calculations to see if the measurements could self-consistently match a theoretical substorm current wedge configuration. Calculations were made with the following simplifying assumptions:

1) In order to connect the ionospheric and tail current segments, a dipolar magnetic field model was used. While approximately true close to the Earth, as you move further down the magnetotail, the field becomes non-dipolar. The dipole field formula [$r = 1.024/\sin^2(90 - \theta)$, r is distance of tail current (in R_e), θ is latitude of electrojet (assumed to be at a height of 150 km)] enables us to uniquely specify a tail current distance from the Earth that corresponds to a specific electrojet latitude; however, these calculations in general will place the tail current closer to the Earth than in the actual case.

2) The low-latitude positive magnetic perturbation is caused by the disruption of tail current. While the field-aligned current will have some effect, by only using measurements close to midnight (2230 to 0130 LT), the field-aligned current effect will be minimized.

3) The tail current segment of the wedge is approximated by a line current. The tail current is generally considered as flowing from dawn to dusk across the magnetotail, but near the inner edge some curvature could exist as it merges with the ring current close to the Earth. This should not cause an appreciable change in the results.

4) The entire tail current wedge segment is converted to electrojet current (1/2 to each hemisphere).

5) The electrojet is modeled as an infinite east-west sheet current 500 km wide at a height of 150 km (the height actually varies but within this range the results will not vary much). For stations under the electrojet near midnight, assuming infinite length should not negligibly change the result.

6) Induction is 1/3 of low- and high-latitude ΔH . As seen in Chapter 3, induction is much more complex than can be accounted for by a simple factor (especially at high-latitude), but without any other information, this is the best we can do.

7) The wedge is centered at midnight and is between 30° and 120° in width.

8) The electrojet is confined to latitudes between 68° and 50° . This is consistent with observation.

9) To determine the location of the low-latitude stations in relation to the tail current, magnetic latitude and geographic longitude are used. This is consistent with other studies of this type.

The procedure I developed is as follows:

1) Find examples of positive low-latitude perturbations near midnight (must be associated with high electrojet activity) and the corresponding high-latitude magnetogram(s) that show electrojet activity (all examples came from the four storm periods used previously).

2) Use additional high- and low-latitude magnetograms to determine the range of possible wedge widths.

3) Determine the magnitude of the high-latitude perturbation(s) caused by the electrojet and correct for induction.

4) Determine the approximate magnitude of the low-latitude perturbation by comparison to the background baseline. Correct the perturbation for induction and find the equatorial equivalent.

5) I developed a computer program to take the corrected low-latitude perturbation and go through an iterative process of determining the magnitude of tail current causing the perturbation at various distances from the Earth (for a given wedge width), determining the corresponding electrojet current, and finding the wedge configuration(s) (identified by the latitude of the electrojet and wedge width), if any, that would produce the specified high-latitude perturbation (there are two possible results depending on if the electrojet was north or south of the station).

Current Wedge Calculation Results

From the four storm periods, there were nine events with eighteen pairs of low- and high-latitude data points that were useable for current wedge calculations. This does not represent the total number of substorms during these times, only the ones meeting the specific criteria. Table 7 shows the data used; for the high-latitude stations, ΔH is the unloading component determined by wavelet analysis. The results of the current wedge calculations are shown in Figure 62 as a plot of Kp versus the latitude of the electrojet that matches the observations (if there were two possible latitudes, I took the one that either matched another calculation in the same event or the one that was more physically reasonable). In this plot the data points represent the median wedge width and the bars

Table 7. Data selected for current wedge calculations.

Date/Time (UT)	Kp	LL Station	LL ΔH (nT)	HL Station	HL ΔH (nT)	Wedge Size (°)
21 Feb 79/7:00	7-	BOU	104	FCC	-430	40-90
				YLK	-383	
				PBQ	-549	
21 Feb 79/7:30	7-	BOU	90	FCC	-431	40-90
				YLK	-631	
				PBQ	-709	
22 Feb 79/6:15	5-	BOU	40	FCC	-746	30-40
22 Feb 79/8:15	5-	BOU	17	FCC	-291	60-80
				YLK	-413	
10 Mar 79/18:30	4+	TKT	60	DIK	-356	30-80
4 Apr 79/12:00	5-	HON	25	CMO	-817	30-100
				BRW	-738	
				CWE	-404	
25 Apr 79/11:00	7	HON	80	CMO	-1003	90-120
				BRW	-713	
25 Apr 79/21:00	6-	HER	40	LRV	-444	100-120
26 Apr 79/0:00	6-	HER	40	LRV	-368	60-120
				NAQ	-312	

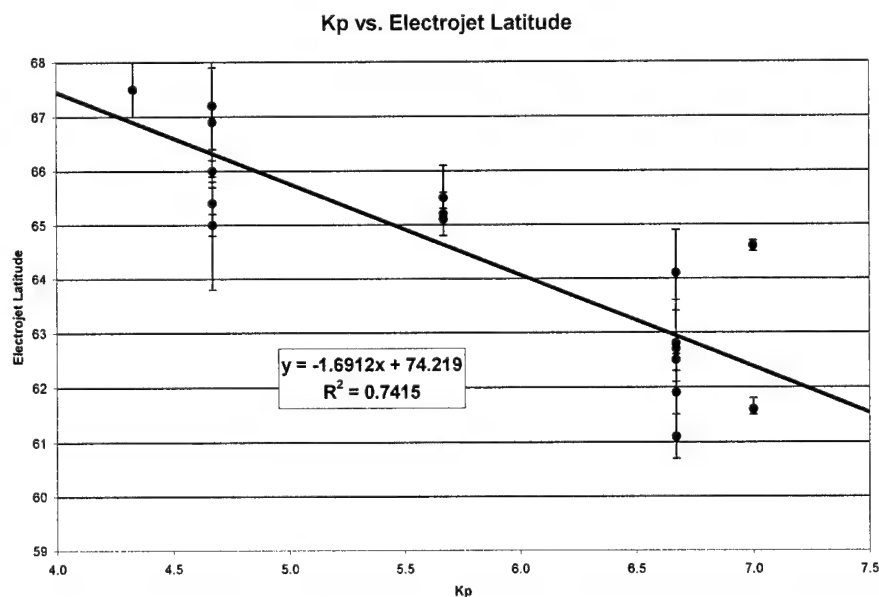


Figure 62. Plot of K_p versus the electrojet latitudes that provide a self-consistent current wedge solution to the low- and high-latitude measurements in Table 7. The least-squares fit line and details are also shown.

on either side represent the maximum and minimum values based on the estimated possible wedge widths. The plot also shows the least-squares linear fit to the data.

Two results are evident. The first is in every case, the spatially separate measurements converge to a solution that provides a physically reasonable wedge configuration. This shows the assumptions as to the cause of the noted perturbations are physically reasonable. The second result is the relationship between the calculated electrojet latitude and Kp . In general, it is expected as geomagnetic activity levels increase (as measured, for instance, by Kp), the electrojet moves equatorward [Feldstein, 1992]. This is exactly the trend seen in Figure 62. Figure 63 shows the locations of the tail current portion of the wedge and represents a mapping of the calculated median

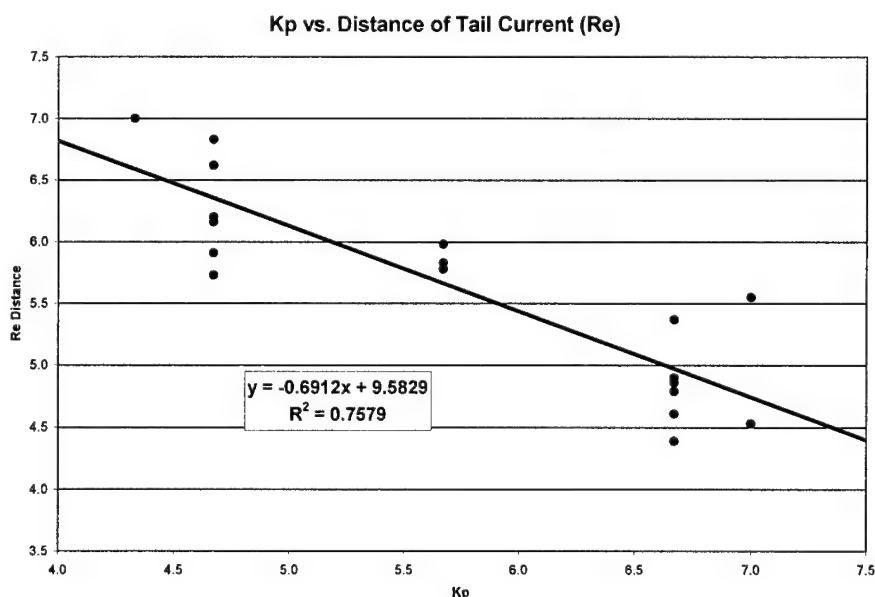


Figure 63. Plot of Kp versus the median distance of the wedge tail current closure corresponding to the electrojet latitudes calculated in Figure 62. This represents a simple mapping of the electrojet latitude to the equatorial plane using the dipole field formula. The least-squares fit line and details are also shown.

electrojet latitudes to the equatorial plane using the dipole field formula. These locations seem to be in the right range for the inner edge of the tail current.

The corresponding electrojet current intensities for these calculations (at median wedge widths) are shown in Figure 64. These values are consistent with observed values for the electrojet current (~millions of amps) and also show a trend toward increasing current intensity with increasing geomagnetic activity (Kp), which is what one would expect. This provides further confirmation that the basic premise of the calculations was reasonable.

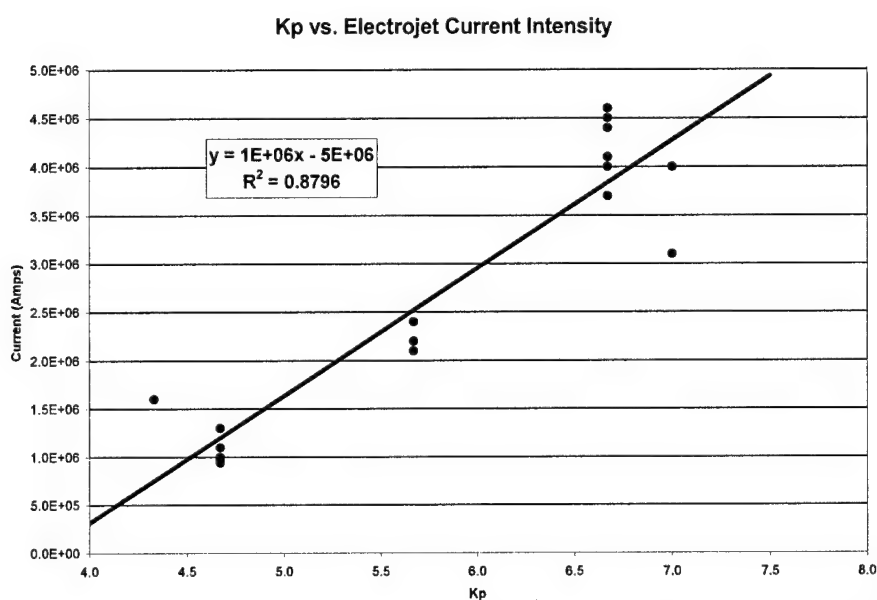


Figure 64. Plot of Kp versus the median electrojet current intensity values that provide a self-consistent current wedge solution to the low-and high-latitude measurements in Table 7. The least-squares fit line and details are also shown.

CHAPTER 7

CONCLUSIONS AND FURTHER STUDY

Conclusions

For decades researchers have speculated on the composition of *Dst* and of the magnetograms that constitute its basis. We have seen wavelet analysis is a promising tool in the effort to determine the physical processes that produce these signals. Wavelet analysis is able to deconstruct these signals and effectively identify components of different time scales present in the signal. With an initial application of wavelet analysis to magnetograms, we have been able to generally identify components associated with the symmetric ring current (>30 hours), substorm currents (~ 3 -6 hours), and another component (~ 12 -25 hours) with less clear origin, but attributable to the partial ring current. As these components are even seen in *SYM-H*, it is unlikely that all but the lowest frequencies are removed in the simple averaging process used to construct the 1-hour *Dst*.

Although some attempts have been made to separate the directly driven and unloading components of substorm activity [e.g., *Sun et al.*, 2000], no method has been universally accepted. Wavelet analysis offers a technique (via DWT) of separating components and partially reconstructing signals based on characteristic scales. Since the directly driven and unloading components have different time scales, this technique provides approximations of the two components. Application of this method has produced satisfactory results when our analyzed signals is compared to what would be expected.

Although the low- and mid-latitude magnetic signatures of substorms have been known and studied for some time, no quantitative calculations of currents and wedge configurations have ever been made based on magnetic observations. Starting with the hypothesis low-latitude positive perturbations (on the order of an hour near midnight) are associated with the tail current segment of the substorm current wedge, our calculations have succeeded in showing paired low- and high-latitude measurements match expected current wedge configurations. Moreover, the calculated electrojet latitudes and current intensities fit with trends expected during increasing levels of geomagnetic activity. Also, these results confirm the high frequency component of low- and mid-latitude magnetograms seen in wavelet analysis is probably related to substorms.

Areas For Further Study

Some possible areas to pursue related to this research are:

- 1) Further analyzing low- and mid-latitude storm data in more detail with wavelet analysis. The versatility of wavelet analysis allows one to extract more information than has been done here. Applying wavelets of different properties and shapes, as well as using complex wavelets, may allow for a more detailed analysis and better identification of spectral content. More work could be done in studying the individual DWT level coefficients and applying various filtered reconstructions to separate components.

- 2) Understanding the differences between DWT coefficient selection and SWT denoising. SWT denoising was used in this study but DWT coefficient selection may be more versatile in the ability to separate components. A better appreciation of how these

two techniques differ, and which one is more applicable to time-series data, is crucial to continued component separation using wavelet analysis.

3) Studying the effect of the various magnetogram components on *Dst*. The focus of this study was on 5-minute data, so the implications for the 1-hour *Dst* index is not entirely certain. Since we have evidence of multi-scale components present in the magnetograms used to construct *Dst*, and even in the high time resolution *Dst* (*SYM-H*), more study is needed to determine exactly how these components remain in the *Dst* formulation.

4) Broadening the scope of substorm current wedge calculations. More detailed work could be done in using more spatially separate measurements and more accurate magnetic field models to locate and specify the current wedge. Space-based measurements could be used to independently verify the results. If this procedure is verified as producing accurate wedge approximations, methods could be developed to provide real-time approximations of the current wedge configuration. This would address a longstanding problem in the magnetospheric research community.

5) Verifying the usefulness of wavelet analysis in identifying the directly driven and unloading components in high-latitude measurements. These two components may not be independent of each other, which complicates the picture [*Kamide et al.*, 1996]. Additional study would provide a better understanding of the validity of wavelet analysis in this area and of the possible relationships between these two components.

6) Analyzing solar wind data. Since all of these processes are driven by the solar wind, wavelet analysis of solar wind data in comparison to magnetograms may yield new insights into the relationships of the various current systems involved.

REFERENCES

- Akasofu, S.-I., The ring current and the outer atmosphere, *J. Geomag. Res.*, 65, 535, 1960.
- Akasofu, S.-I., Magnetospheric substorms: a model, in *Solar-Terrestrial Physics/Leningrad 1970*, part 3, ed. by E. R. Dryer and J. G. Roederer, pp. 131-151, D. Reidel, Dordrecht, Netherlands, 1972.
- Akasofu, S.-I. and S. Chapman, The ring current, geomagnetic disturbance, and the Van Allen radiation belts, *J. Geomag. Res.*, 66, 1321, 1961.
- Akasofu, S.-I., J. C. Cain, and S. Chapman, The magnetic field of a model radiation belt, numerically computed, *J. Geomag. Res.*, 66, 4013, 1961.
- Akasofu, S.-I. and S. Chapman, On the asymmetric development of magnetic storm fields in low and middle latitudes, *Planet. Space Sci.*, 12, 607, 1964.
- Akasofu, S.-I., S. Chapman, and C.-I. Meng, The polar electrojet, *J. Atmos. Terr. Phys.*, 27, 1275, 1965.
- Akasofu, S.-I. and S. Chapman, The normality of the SD variation at Huancayo and the asymmetry of the main phase of geomagnetic storms, *Planet. Space Sci.*, 15, 205, 1967a.
- Akasofu, S.-I. and S. Chapman, A systematic shift of the DS axis, *Planet. Space Sci.*, 15, 937, 1967b.
- Akasofu, S.-I. and C.-I. Meng, Low latitude negative bays, *J. Atmos. Terr. Phys.*, 30, 227, 1968.
- Akasofu, S.-I. and C.-I. Meng, A study of polar magnetic substorms, *J. Geomag. Res.*, 74, 293, 1969.
- Akasofu, S.-I. and S. Chapman, *Solar-Terrestrial Physics*, Clarendon Press, Oxford, 1972.
- Alexeev, I. I., Regular magnetic field in the earth's magnetosphere, *Geomagn. Aeron.*, 18, 656, 1978.
- Alexeev, I. I., E. S. Belenkaya, V. V. Kalegaev, Y. I. Feldstein, and A. Grafe, Magnetic storms and magnetotail currents, *J. Geomag. Res.*, 101, 7737, 1996.

Alfvén, H., A theory of magnetic storms and of the aurora, *Kgl. Sv. Vetenskapsakad. Handl., Ser. 3, 18(3)*, 1, 1939.

Alfvén, H., A theory of magnetic storms and of the aurora, II and III, *Kgl. Sv. Vetenskapsakad. Handl., Ser. 3, 18(9)*, 1, 1940.

Alfvén, H., *Cosmical Electrodynamics*, Oxford Univ. Press, London and New York, 1950.

Alfvén, H., On the electric field theory of magnetic storms, *Tellus*, 7, 50, 1955.

Anderssen, R. S. and E. Seneta, New analysis for the geomagnetic *Dst* field of the magnetic storm on June 18-19, 1936, *J. Geomag. Res.*, 74, 2768, 1969.

Apel, J. R., S. F. Singer, and R. C. Wentworth, Effects of trapped particles on the geomagnetic field, *Adv. Geophys.*, 9, 131, 1962.

Armstrong, J. C. and A. J. Zmuda, Field-aligned current at 1100 km in the auroral region measured by satellite, *J. Geomag. Res.*, 75, 7122, 1970.

Arykov, A. A. and Y. P. Maltsev, Contribution of various sources to the geomagnetic storm field, *Geomagn. Aeron.*, 33, 771, 1994 (English Translation).

Arykov, A. A., and Y. P. Maltsev, Direct-driven mechanism for geomagnetic storms, *Geophys. Res. Lett.*, 23, 1689, 1996.

Ashour, A. A., The evaluation of the field of the currents induced in the earth by an external field whose distribution is known numerically, *Radio Sci.*, 6, 171, 1971.

Atkinson, G., An approximate flow equation for geomagnetic flux tubes and its application to polar substorms, *J. Geomag. Res.*, 72, 5373, 1967.

Axford, W. I. and C. O. Hines, A unifying theory of high-latitude geophysical phenomena and geomagnetic storms, *Can. J. Phys.*, 39, 1433, 1961.

Axford, W. I., H. E. Petschek, and G. L. Siscoe, Tail of the magnetosphere, *J. Geomag. Res.*, 70, 1231, 1965.

Baker, D. N., A. J. Klimas, D. Vassiliadis, T. I. Pulkkinen, and R. L. McPherron, Reexamination of driven and unloading aspects of magnetospheric substorms, *J. Geomag. Res.*, 102, 7169, 1997.

Baker, D. N., N. E. Turner, and T. I. Pulkkinen, Energy transport and dissipation in the magnetosphere during geomagnetic storms, *J. Atmos. Terr. Phys.*, 63, 421, 2001.

- Bannister, J. R. and D. I. Gough, Development of a polar magnetic substorm: a two-dimensional magnetometer array study, *Geophys. J. R. astr. Soc.*, 51, 75, 1977.
- Beard, D. B., The interaction of the terrestrial magnetic field with the solar corpuscular radiation, *J. Geomag. Res.*, 65, 3559, 1960.
- Beard, D. B., The interaction of the terrestrial magnetic field with the solar corpuscular radiation, *J. Geomag. Res.*, 67, 477, 1962.
- Behannon, K. W. and N. F. Ness, Magnetic storms in the earth's magnetic tail, *J. Geomag. Res.*, 71, 2327, 1966.
- Belova, E. G. and Y. P. Maltsev, Supplementary sources of geomagnetic depression during the geomagnetic storm of 8-9 February 1986, *J. Atmos. Terr. Phys.*, 56, 1011, 1994.
- Benkova, N. P., Spherical harmonic analysis of the *Sq* variations, May-August 1933, *Terr. Magn. Atmos. Electr.*, 45, 425, 1940.
- Birkeland, K., *The Norwegian Aurora Polaris Expedition, 1902-1903, Vol. I, On the cause of magnetic storms and the origin of terrestrial magnetism, Section 1*, H. Aschehoug & Co., Christiania, 1908.
- Birkeland, K., *The Norwegian Aurora Polaris Expedition, 1902-1903, Vol. I, On the cause of magnetic storms and the origin of terrestrial magnetism, Section 2*, H. Aschehoug & Co., Christiania, 1913.
- Bogges, A. and F. J. Narcowich, *A First Course in Wavelets With Fourier Analysis*, Prentice Hall, Upper Saddle River, NJ, 2001.
- Bogott, F. H. and F. S. Mozer, ATS-5 observations of energetic proton injection, *J. Geomag. Res.*, 78, 8113, 1973.
- Bonnevier, B., R. Boström, and G. Rostoker, A three-dimensional model current system for polar magnetic substorms, *J. Geomag. Res.*, 75, 107, 1970.
- Boström, R., A model of the auroral electrojets, *J. Geomag. Res.*, 69, 4983, 1964.
- Boström, R., Currents in the ionosphere and magnetosphere, *Ann. Geophys.*, 24, 681, 1968.
- Boström, R., The magnetic field of three-dimensional magnetospheric model current systems and currents induced in the ground, *Acta Poly. Scand.*, 77, 1, 1971.

- Burton, R. K., R. L. McPherron, and C. T. Russell, An empirical relationship between interplanetary conditions and *Dst*, *J. Geomag. Res.*, 80, 4204, 1975.
- Cahill, L. J., Inflation of the inner magnetosphere during a magnetic storm, *J. Geomag. Res.*, 71, 4505, 1966.
- Cahill, L. J., Magnetosphere inflation during four magnetic storms in 1965, *J. Geomag. Res.*, 75, 3778, 1970.
- Campbell, W. H., The field levels near midnight at low and equatorial geomagnetic stations, *J. Atmos. Terr. Phys.*, 35, 1127, 1973.
- Campbell, W. H., Geomagnetic storms, the *Dst* ring-current myth and lognormal distributions, *J. Atmos. Terr. Phys.*, 58, 1171, 1996.
- Campbell, W. H. and E. R. Schiffmacher, Upper mantle electrical conductivity for seven subcontinental regions of the earth, *J. Geomag. Geoelectr.*, 40, 1387, 1988.
- Chan, Y. T., *Wavelet Basics*, Kluwer Academic Publishers, Boston, 1995.
- Chapman, S., An outline of a theory of magnetic storms, *Proc. Roy. Soc. London, Ser. A*, 95, 61, 1918.
- Chapman, S., Terrestrial magnetic variations and their connection with solar emissions which are absorbed in the earth's outer atmosphere, *Trans. Cambridge Phil. Soc.*, 22, 341, 1919a.
- Chapman, S., The solar and lunar diurnal variations of terrestrial magnetism, *Phil. Trans.*, A218, 1, 1919b.
- Chapman, S., On certain average characteristics of world wide magnetic disturbance, *Proc. Roy. Soc. London, Ser. A*, 115, 242, 1927.
- Chapman, S., The electric current-systems of magnetic storms, *Terr. Magn. Atmos. Electr.*, 40, 349, 1935.
- Chapman, S., The equatorial electrojet as detected from the abnormal electric current distribution above Huancayo, Peru, and elsewhere, *Arch. Meteorol. Geophys. Bioklimatol.*, 4, 368, 1951.
- Chapman, S., The morphology of geomagnetic storms: an extension of the analysis of *DS*, the disturbance local-time inequality, *Ann. Geophys.*, 5, 481, 1952.

- Chapman, S. and T. T. Whitehead, The influence of electrically conducting material within the earth on various phenomena of terrestrial magnetism, *Trans. Phil. Soc. Cambridge*, 22, 463, 1922.
- Chapman, S. and A. T. Price, The electric and magnetic state of the interior of the earth as inferred from terrestrial magnetic variations, *Phil. Trans. Roy. Soc. London*, A229, 427, 1930.
- Chapman, S. and V. C. A. Ferraro, A new theory of magnetic storms: part 1, the initial phase, *Terr. Magn. Atmos. Electr.*, 36, 77 and 171, 1931.
- Chapman, S. and V. C. A. Ferraro, A new theory of magnetic storms: part 1, the initial phase, *Terr. Magn. Atmos. Electr.*, 37, 147 and 421, 1932.
- Chapman, S. and V. C. A. Ferraro, A new theory of magnetic storms: part II – The main phase, *Terr. Magn. Atmos. Electr.*, 38, 79, 1933.
- Chapman, S. and J. Bartels, *Geomagnetism*, Clarendon Press, Oxford, 1940.
- Chapman, S. and V. C. A. Ferraro, The theory of the first phase of a geomagnetic storm, *Terr. Magn. Atmos. Electr.*, 45, 245, 1940.
- Chapman, S. and V. C. A. Ferraro, The geomagnetic ring current: its radial stability, *Terr. Magn. Atmos. Electr.*, 46, 1, 1941.
- Chapman, S. and K. S. Raja Rao, The H and Z variations along and near the equatorial electrojet in India, Africa and the Pacific, *J. Atmos. Terr. Phys.*, 27, 559, 1965.
- Chen, C.-K., R. A. Wolf, M. Harel, and J. L. Karty, Theoretical magnetograms based on quantitative simulation of a magnetospheric substorm, *J. Geomag. Res.*, 87, 6137, 1982.
- Choe, J. Y. and D. B. Beard, The compressed geomagnetic field as a function of dipole tilt, *Planet. Space Sci.*, 22, 595, 1974.
- Choe, J. Y., D. B. Beard, and E. C. Sullivan, Precise calculation of the magnetosphere surface for a tilted dipole, *Planet. Space Sci.*, 21, 485, 1973.
- Choy, L. W., R. L. Arnoldy, W. Potter, P. Kintner, and L. J. Cahill, Jr., Field-aligned currents near an auroral arc, *J. Geomag. Res.*, 76, 8279, 1971.
- Clauer, C. R. and R. L. McPherron, Mapping the local time-universal time development of magnetospheric substorms using mid-latitude magnetic observations, *J. Geomag. Res.*, 79, 2811, 1974.

- Clauer, C. R. and R. L. McPherron, On the relationship of the partial ring current to substorms and the interplanetary magnetic field, *J. Geomag. Geoelectr.*, 30, 195, 1978.
- Clauer, C. R. and R. L. McPherron, The relative importance of the interplanetary electric field and magnetospheric substorms on partial ring current development, *J. Geomag. Res.*, 85, 6747, 1980.
- Cloutier, P. A., H. R. Anderson, R. J. Park, R. R. Vondrak, R. J. Spiger, and B. R. Sandel, Detection of geomagnetically aligned currents associated with an auroral arc, *J. Geomag. Res.*, 75, 2595, 1970.
- Coifman, R. R. and D. L. Donoho, Translation-invariant de-noising, *Lecture Notes in Statist.*, 103, 125, 1995.
- Crooker, N. U., High-time resolution of the low-latitude asymmetric disturbance in the geomagnetic field, *J. Geomag. Res.*, 77, 773, 1972.
- Crooker, N. U. and G. L. Siscoe, A study of the geomagnetic disturbance field asymmetry, *Radio Sci.*, 6, 495, 1971.
- Crooker, N. U. and R. L. McPherron, On the distinction between the auroral electrojet and the partial ring current systems, *J. Geomag. Res.*, 77, 6886, 1972.
- Crooker, N. U. and G. L. Siscoe, Model geomagnetic disturbance from asymmetric ring current particles, *J. Geomag. Res.*, 79, 589, 1974.
- Crooker, N. U. and G. L. Siscoe, Birkeland currents as the cause of the low-latitude asymmetric disturbance field, *J. Geomag. Res.*, 86, 11,201, 1981.
- Cummings, W. D., Asymmetric ring currents and the low-latitude disturbance daily variation, *J. Geomag. Res.*, 71, 4495, 1966.
- Cummings, W. D. and A. J. Dessler, Field-aligned currents in the magnetosphere, *J. Geomag. Res.*, 72, 1007, 1967.
- Daglis, I. A., R. M. Thorne, W. Baumjohann, S. Orsini, The terrestrial ring current: origin, formation, and decay, *Rev. Geophys.*, 37, 407, 1999.
- Data Book 21*, WDC-C2 for Geomagnetism, Kyoto, Japan, 1992.
- Davis, T. N. and M. Sugiura, Auroral electrojet activity index *AE* and its universal time variation, *J. Geomag. Res.*, 71, 785, 1966.

- De Michelis, P., I. A. Daglis, and G. Consolini, Average terrestrial ring current derived from AMPTE/CCE-CHEM measurements, *J. Geomag. Res.*, 102, 14,103, 1997.
- Dessler, A. J. and E. N. Parker, Hydromagnetic theory of geomagnetic storms, *J. Geomag. Res.*, 64, 2239, 1959.
- Dremukhina, L. A., Y. I. Feldstein, I. I. Alexeev, V. V. Kalegaev, and M. E. Greenspan, Structure of the magnetospheric magnetic field during magnetic storms, *J. Geomag. Res.*, 104, 28,351, 1999.
- Dungey, J. W., The steady state of the Chapman-Ferraro problem in two dimensions, *J. Geomag. Res.*, 66, 1043, 1961.
- Ebihara, Y. and M. Ejiri, Simulation study on fundamental properties of the storm-time ring current, *J. Geomag. Res.*, 105, 15,843, 2000.
- Ebihara, Y. and M. Ejiri, Reply to "comment on 'simulation study fundamental properties of the storm-time ring current' by Y. Ebihara and M. Ejiri, *J. Geomag. Res.*, 106, 6323, 2001.
- Egedal, J., The magnetic diurnal variation of the horizontal force near the magnetic equator, *Terr. Magn. Atmos. Electr.*, 52, 449, 1947.
- Fejer, J. A., The effects of energetic trapped particles magnetospheric motions and ionospheric currents, *Can. J. Phys.*, 39, 1409, 1961.
- Fejer, J. A., Theory of the geomagnetic daily disturbance variations, *J. Geomag. Res.*, 69, 123, 1964.
- Feldstein, Y. I., Modelling of the magnetic field of magnetospheric ring current as a function of interplanetary medium parameters, *Space Sci. Rev.*, 59, 83, 1992.
- Feldstein, Y. I., A. Grafe, V. Y. Pisarsky, A. Prigansova and P. V. Sumaruk, Magnetic field of the magnetospheric ring current and its dynamics during magnetic storms, *J. Atmos. Terr. Phys.*, 52, 1185, 1990.
- Ferraro, V. C. A., An approximate method of estimating the size and shape of the stationary hollow carved out in a neutral ionized stream of corpuscles impinging on the geomagnetic field, *J. Geomag. Res.*, 65, 3951, 1960a.
- Ferraro, V. C. A., Theory of sudden commencements and of the first phase of a magnetic storm, *Revs. Modern Phys.*, 32, 934, 1960b.

Fok, M.-C., R. A. Wolf, R. W. Spiro, and T. E. Moore, Comprehensive computational model of earth's ring current, *J. Geomag. Res.*, 106, 8417, 2001.

Forbush, S. E., On cosmic ray effects associated with magnetic storms, *Terr. Magn. Atmos. Electr.*, 43, 203, 1938.

Forbush, S. E. and M. Casaverde, *Equatorial Electrojet in Peru*, Carnegie Inst. of Washington Pub. 620, 1961.

Frank, L. A., Direct detection of asymmetric increases of extraterrestrial 'ring current' proton intensities in the outer radiation zone, *J. Geomag. Res.*, 75, 1263, 1970.

Friedrich, E., G. Rostoker, M. G. Connors, and R. L. McPherron, Influence of the substorm current wedge on the *Dst* index, *J. Geomag. Res.*, 104, 4567, 1999.

Fukushima, N., Equivalence in ground geomagnetic effect of Chapman-Vestine's and Birkeland-Alfvén's electric current-systems for polar magnetic storms, *Rep. Ionos. Space Res. Jap.*, 23, 219, 1969.

Fukushima, N., Polar magnetic substorms, *Planet. Space Sci.*, 20, 1443, 1972.

Fukushima, N., Generalized theorem for no ground magnetic effect of vertical currents connected with Pedersen currents in the uniform-conductivity ionosphere, *Rep. Ionos. Space Res. Jap.*, 30, 35, 1976.

Fukushima, N. and T. Oguti, Polar magnetic storms and geomagnetic bays, *Rep. Ionos. Space Res. Jap.*, 7, 137, 1953.

Fukushima, N. and Y. Kamide, Partial ring current models for worldwide geomagnetic disturbance, *Rev. Geophys. Space Phys.*, 11, 795, 1973a.

Fukushima, N. and Y. Kamide, Contribution of field aligned current to geomagnetic bays and Sq fields: a comment on partial ring-current models, *Radio Sci.*, 8, 1013, 1973b.

Gonzalez, W. D., B. T. Tsurutani, A. L. C. Gonzalez, E. J. Smith, F. Tang, and S.-I. Akasofu, Solar wind-magnetosphere coupling during intense magnetic storms (1978-1979), *J. Geomag. Res.*, 94, 8835, 1989.

Grafe, A., Anomalous *DS*-variation in equatorial latitudes during geomagnetic storms, *Planet. Space Sci.*, 22, 991, 1974.

Grafe, A., Are our ideas about *Dst* correct?, *Ann. Geophys.*, 17, 1, 1999.

- Grafe, A., Y. I. Feldstein, V. I. Pisarski, N. M. Rudneva, P. Ochabova, and A. Prigantsova, The local time asymmetry of the geomagnetic disturbance field at low latitudes and its dependence upon the interplanetary activity, *J. Geomag. Geoelectr.*, **38**, 1183, 1986.
- Greenspan, M. E. and D. C. Hamilton, A test of the Dessler-Parker-Sckopke relation during magnetic storms, *J. Geomag. Res.*, **105**, 5419, 2000.
- Halderson, D. W., D. B. Beard, and J. Y. Choe, Corrections to "the compressed geomagnetic field as a function of dipole tilt," *Planet. Space Sci.*, **23**, 887, 1975.
- Hamilton, D. C., G. Gloeckler, F. M. Ipavich, W. Stüdemann, B. Wilken and G. Kremser, Ring current development during the great geomagnetic storm of February 1986, *J. Geomag. Res.*, **93**, 14,343, 1988.
- Harel, M., R. A. Wolf, P. H. Reiff, R. W. Spiro, W. J. Burke, F. J. Rich, and M. Smiddy, Quantitative simulation of a magnetospheric substorm, 1. model logic and overview, *J. Geomag. Res.*, **86**, 2217, 1981a.
- Harel, M., R. A. Wolf, R. W. Spiro, P. H. Reiff, C.-K. Chen, W. J. Burke, F. J. Rich, and M. Smiddy, Quantitative simulation of a magnetospheric substorm, 2. comparison with observations, *J. Geomag. Res.*, **86**, 2242, 1981b.
- Hines, C. O., Comment on "on the geomagnetic storm effect," *J. Geomag. Res.*, **62**, 491, 1957.
- Hines, C. O. and E. N. Parker, Statement of differences regarding the ring-current effect, *J. Geomag. Res.*, **63**, 691, 1958.
- Hines, C. O. and L. R. O. Storey, Time constants in the geomagnetic storm effect, *J. Geomag. Res.*, **63**, 671, 1958.
- Hoffman, R. A. and P. A. Bracken, Magnetic effects of the quiet-time proton belt, *J. Geomag. Res.*, **70**, 3541, 1965.
- Hughes, T. J. and G. Rostoker, Current flow in the magnetosphere and ionosphere during periods of moderate activity, *J. Geomag. Res.*, **82**, 2271, 1977.
- Iijima, T. and T. A. Potemra, The amplitude distribution of field-aligned currents at northern high latitudes observed by Triad, *J. Geomag. Res.*, **81**, 2165, 1976a.
- Iijima, T. and T. A. Potemra, Field-aligned currents in the dayside cusp observed by Triad, *J. Geomag. Res.*, **81**, 5971, 1976b.

Iijima, T. and T. A. Potemra, Large-scale characteristics of field-aligned currents associated with substorms, *J. Geomag. Res.*, **83**, 599, 1978.

Iijima, T., T. A. Potemra, and L. J. Zanetti, Large-scale characteristics of magnetospheric equatorial currents, *J. Geomag. Res.*, **95**, 991, 1990.

Iyemori, T., Storm-time magnetospheric currents inferred from mid-latitude geomagnetic field variations, *J. Geomag. Geoelectr.*, **42**, 1249, 1990.

Iyemori, T. and D. R. K. Rao, Decay of the *Dst* field of geomagnetic disturbance after substorm onset and its implication to storm-substorm relation, *Ann. Geophys.*, **14**, 608, 1996.

Jordanova, V. K., C. J. Farrugia, L. Janoo, J. M. Quinn, R. B. Torbert, K. W. Ogilvie, R. P. Lepping, J. T. Steinberg, D. J. McComas, and R. D. Belian, October 1995 magnetic cloud and accompanying storm activity: ring current evolution, *J. Geomag. Res.*, **103**, 79, 1998.

Jorgensen, A. M., H. E. Spence, M. G. Henderson, G. D. Reeves, M. Sugiura, and T. Kamei, Global energetic neutral atom (ENA) measurements and their association with the *Dst* index, *Geophys. Res. Lett.*, **24**, 3173, 1997.

Kalegaev, V. V. and A. Dmitriev, Magnetosphere dynamics under disturbed conditions on 23-27 November, 1986, *Adv. Space Res.*, **26**, 117, 2000.

Kamide, Y. and N. Fukushima, Analysis of magnetic storms with *DR*-indices for equatorial ring current field, *Rep. Ionos. Space Res. Jap.*, **25**, 125, 1971.

Kamide, Y. and N. Fukushima, Positive geomagnetic bays in evening high-latitudes and their possible connection with partial ring current, *Rep. Ionos. Space Res. Jap.*, **26**, 79, 1972.

Kamide, Y., F. Yasuhara, and S.-I. Akasofu, A model current system for the magnetospheric substorm, *Planet. Space Sci.*, **24**, 215, 1976.

Kamide, Y., A. D. Richmond, and S. Matsushita, Estimation of ionospheric electric fields, ionospheric currents, and field-aligned currents from ground magnetic records, *J. Geomag. Res.*, **86**, 801, 1981.

Kamide, Y., B.-H. Ahn, S.-I. Akasofu, W. Baumjohann, E. Friis-Christensen, H. W. Kroehl, H. Maurer, A. D. Richmond, G. Rostoker, R. W. Spiro, J. K. Walker, and A. N. Zaitzev, Global distribution of ionospheric and field-aligned currents during substorms as determined from six IMS meridian chains of magnetometers: initial results, *J. Geomag. Res.*, **87**, 8228, 1982.

- Kamide, Y. and W. Baumjohann, Estimation of electric fields and currents from International Magnetospheric Study magnetometer data for the CDAW 6 intervals: implications for substorm dynamics, *J. Geomag. Res.*, *90*, 1305, 1985.
- Kamide, Y. and S. Kokubun, Two-component auroral electrojet: importance for substorm studies, *J. Geomag. Res.*, *101*, 13,027, 1996.
- Kamide, Y., W. Sun, and S.-I. Akasofu, The average ionospheric electrodynamics for the different substorm phases, *J. Geomag. Res.*, *101*, 99, 1996.
- Kamide, Y., W. Baumjohann, I. A. Daglis, W. D. Gonzalez, M. Grande, J. A. Joselyn, R. L. McPherron, J. L. Phillips, E. G. D. Reeves, G. Rostoker, A. S. Sharma, H. J. Singer, B. T. Tsurutani and V. M. Vasyliunas, Current understanding of magnetic storms: storm-substorm relationships, *J. Geomag. Res.*, *103*, 17,705, 1998.
- Kavanaugh, L. D., J. W. Freeman, Jr., and A. J. Chen, Plasma flow in the magnetosphere, *J. Geomag. Res.*, *73*, 5511, 1968.
- Kawasaki, K. and S.-I. Akasofu, Low-latitude DS component of geomagnetic storm field, *J. Geomag. Res.*, *76*, 2396, 1971.
- Kawasaki, K., C.-I. Meng, and Y. Kamide, The development of three-dimensional current system during a magnetospheric substorm, *Planet. Space Sci.*, *22*, 1471, 1974.
- Kertz, W., Ring current variations during the IGY, *Ann. Int. Geophys. Year*, *35*, 49, 1964.
- Kirkpatrick, C. B., On current systems proposed for S_D in the theory of magnetic storms, *J. Geomag. Res.*, *57*, 1952.
- Kisabeth, J. L., On calculating magnetic and vector potential fields due to large-scale magnetospheric current systems and induced currents in an infinitely conducting earth, in *Quantitative Modeling of Magnetospheric Processes*, *Geophys. Monogr. Ser.*, vol. 21, ed. by W. P. Olson, pp. 473-498, AGU, Washington D.C., 1979.
- Kisabeth, J. L. and G. Rostoker, Modelling of three-dimensional current systems associated with magnetospheric substorms, *Geophys. J. R. Astr. Soc.*, *49*, 655, 1977.
- Lahiri, B. N. and A. T. Price, electromagnetic induction in non-uniform conductors, and the determination of the conductivity of the earth from terrestrial magnetic variations, *Phil. Trans. Roy. Soc. London*, *A237*, 509, 1939.
- Langel, R. A. and R. E. Sweeney, Asymmetric ring current at twilight local time, *J. Geomag. Res.*, *76*, 4420, 1971.

- Langel, R. A. and R. H. Estes, Large-scale, near-field magnetic fields from external sources and the corresponding induced internal field, *J. Geomag. Res.*, 90, 2487, 1985.
- Langel, R. A., T. J. Sabaka, R. T. Baldwin, and J. A. Conrad, The near-earth magnetic field from magnetospheric and quiet-day ionospheric sources and how it is modeled, *Phys. Earth Planet. Int.*, 98, 235, 1996.
- Liemohn, M. W., J. U. Kozyra, V. K. Jordanova, G. V. Khazanov, M. F. Thomsen, and T. E. Cayton, Analysis of early phase ring current recovery mechanisms during geomagnetic storms, *Geophys. Res. Lett.*, 26, 2845, 1999.
- Liemohn, M. W., J. U. Kozyra, M. F. Thomsen, J. L. Roeder, G. Lu, J. E. Borovsky, and T. E. Cayton, Dominant role of the asymmetric ring current in producing the stormtime *Dst**, *J. Geomag. Res.*, 106, 10,883, 2001.
- Lindemann, F. A., Note on the theory of magnetic storms, *Phil. Mag.*, 38, 669, 1919.
- Lui, A. T. Y., W. McEntire and S. M. Krimigis, Evolution of the ring current during two magnetic storms, *J. Geomag. Res.*, 92, 7459, 1987.
- Lui, A. T. Y. and D. C. Hamilton, Radial profiles of quiet time magnetospheric parameters, *J. Geomag. Res.*, 97, 19,325, 1992.
- Lyons, L. R., and D. J. Williams, A source for the geomagnetic storm main phase ring current, *J. Geomag. Res.*, 85, 523, 1980.
- Maltsev, Y. P., A. A. Arykov, E. G. Belova, B. B. Gvozdevsky, and V. V. Safargaleev, Magnetic flux redistribution in the storm time magnetosphere, *J. Geomag. Res.*, 101, 7697, 1996.
- Martyn, D. F., The theory of magnetic storms and auroras, *Nature*, 167, 92, 1951.
- Matsushita, S. and H. Maeda, On the geomagnetic solar quiet daily variation field during the IGY, *J. Geomag. Res.*, 70, 2535, 1965.
- Mayaud, P. N., *Derivation, Meaning, and Use of Geomagnetic Indices*, *Geophys. Monogr. Ser.*, vol 22, AGU, Washington D.C., 1980.
- McPherron, R. L., The role of substorms in the generation of magnetic storms, in *Magnetic Storms*, *Geophys. Monogr. Ser.*, vol. 98, ed. by B. T. Tsurutani, W. D. Gonzalez, Y. Kamide, and J. K. Arballo, pp. 131-147, AGU, Washington D.C., 1997.

- McPherron, R. L., C. T Russell, and M. P. Aubry, Satellite studies of magnetospheric substorms on August 15, 1968, 9. Phenomenological model for substorms, *J. Geomag. Res.*, 78, 3131, 1973.
- Mead, G. D., Deformation of the geomagnetic field by the solar wind, *J. Geomag. Res.*, 69, 1181, 1964.
- Mead, G. D., and D. B. Beard, Shape of the geomagnetic field solar wind boundary, *J. Geomag. Res.*, 69, 1169, 1964.
- Meyers, S. D., B. G. Kelly, and J. J. O'Brien, An introduction to wavelet analysis in oceanography and meteorology: with application to the dispersion of yanai waves, *Mon. Wea. Rev.*, 121, 2858, 1993.
- Midgley, J. E., Perturbation of the geomagnetic field – a spherical harmonic expansion, *J. Geomag. Res.*, 69, 1197, 1964.
- Midgley, J. E. and L. Davis, Calculation by a moment technique of the perturbation of the geomagnetic field by the solar wind, *J. Geomag. Res.*, 68, 5111, 1963.
- Moos, N. A. F., *Magnetic Observations Made at the Government Observatory, Bombay, for the Period 1846 to 1905 and Their Discussion*, Government Central Press, Bombay, 1910.
- Nakabe, S., T. Iyemori, M. Sugiura, and J. A. Slavin, A statistical study of the magnetic field structure in the inner magnetosphere, *J. Geomag. Res.*, 102, 17,571, 1997.
- Noël, S., Decay of the magnetospheric ring current: a Monte Carlo simulation, *J. Geomag. Res.*, 102, 2301, 1997.
- Nopper, Jr., R. W. and J. F. Hermance, Phase relations between polar magnetic substorm fields at the surface of a finitely conducting earth, *J. Geomag. Res.*, 79, 4799, 1974.
- Ogilvie, K. W., L. F. Burlaga, and T. D. Wilkerson, Plasma observations on Explorer 34, *J. Geomag. Res.*, 73, 6809, 1968.
- Ohtani, S., M. Nosé, G. Rostoker, H. Singer, A. T. Y. Lui, and M. Nakamura, Storm-substorm relationship: contribution of the tail current to *Dst*, *J. Geomag. Res.*, 106, 21,199, 2001.
- Olson, W. P., The shape of the tilted magnetopause, *J. Geomag. Res.*, 74, 5642, 1969.
- Olson, W. P., Variations in the earth's surface magnetic field from the magnetopause current system, *Planet. Space Sci.*, 18, 1471, 1970.

Olson, W. P., A model of the distributed magnetospheric currents, *J. Geomag. Res.*, 79, 3731, 1974.

Onwumechilli, C. A., Geomagnetic Variations in the Equatorial Zone, in *Physics of Geomagnetic Phenomena*, vol. 1, ed. by S. Matsushita and W. H. Campbell, pp.425-507, Academic Press, New York, 1967.

Park, D., magnetic field at the earth's surface produced by a horizontal line current, *J. Geomag. Res.*, 79, 4802, 1974.

Parker, E. N., On the geomagnetic storm effect, *J. Geomag. Res.*, 61, 625, 1956.

Parker, E. N., The gross dynamics of a Hydromagnetic gas cloud, *Suppl. Astrophys. J.*, 3, 51, 1957a.

Parker, E. N., Newtonian development of the dynamical properties of ionized gases of low density, *Phys. Rev.*, 107, 924, 1957b.

Parker, E. N., Electrical conductivity in the geomagnetic storm effect, *J. Geomag. Res.*, 63, 437, 1958a.

Parker, E. N., Inadequacy of ring-current theory for the main phase of a geomagnetic storm, *J. Geomag. Res.*, 63, 683, 1958b.

Parker, E. N., Interaction of the solar wind with the geomagnetic field, *Phys. Fluids*, 1, 171, 1958c.

Parker, E. N., Nonsymmetric inflation of a magnetic dipole, *J. Geomag. Res.*, 71, 4485, 1966.

Peroomian, V., L. R. Lyons, and M. Schulz, Inclusion of shielded Birkeland currents in a model magnetosphere, *J. Geomag. Res.*, 103, 151, 1998.

Piddington, J. H., Geomagnetic storm theory, *J. Geomag. Res.*, 65, 93, 1960.

Piddington, J. H., A hydromagnetic theory of geomagnetic storms, *Geophys. J. Roy. Astr. Soc.*, 7, 183, 1962.

Piddington, J. H., Theories of the geomagnetic storm main phase, *Planet. Space Sci.*, 11, 1277, 1963.

Price, A. T., Electromagnetic induction within the earth, in *Physics of Geomagnetic Phenomena*, vol. 1, ed. by S. Matsushita and W. H. Campbell, pp.235-298, Academic Press, New York, 1967.

Price, A. T. and G. A. Wilkins, New methods for the analysis of geomagnetic fields and their application to the *Sq* field of 1932-3, *Phil. Trans. Roy. Soc. London*, A256, 31, 1963.

Rangarajan, G. K., Indices of geomagnetic activity, in *Geomagnetism*, vol. 3, ed. by J. A. Jacobs, pp. 323-384, Academic Press, London, 1989.

Rastogi, R. G., The equatorial electrojet: magnetic and ionospheric effects, in *Geomagnetism*, vol. 3, ed. by J. A. Jacobs, pp. 461-525, Academic Press, London, 1989.

Reddy, C. A., S. Ajith Kumar, and V. V. Somayajulu, An observational test for the ionospheric or magnetospheric origin of night-time geomagnetic positive bays at low and mid latitudes, *Planet. Space Sci.*, 36, 1149, 1988.

Reeves, G. D. and M. G. Henderson, The storm-substorm relationship: ion injections in geosynchronous measurements and composite energetic neutral atom images, *J. Geomag. Res.*, 106, 5833, 2001.

Rikitake, T., *Electromagnetism and the Earth's Interior, Developments in Solid Earth Geophysics 2*, Elsevier, Amsterdam, 1966.

Rikitake, T. and S. Sato, The geomagnetic *Dst* field of the magnetic storm on Jun 18-19, 1936, *Bull. Earthq. Res. Inst., Tokyo Univ.*, 35, 7, 1957.

Roeder, J. L., J. F. Fennell, M. W. Chen, M. Grande, S. Livi, and M. Schulz, CRRES observations of stormtime ring current ion composition, *AIP Conf. Proc.*, 383, 131, 1996a.

Roeder, J. L., J. F. Fennell, M. W. Chen, M. Schulz, M. Grande, and S. Livi, CRRES observations of the composition of the ring-current ion populations, *Adv. Space Res.*, 17, 17, 1996b.

Roelof, E. C., Energetic neutral atom image of a storm-time ring current, *Geophys. Res. Lett.*, 14, 652, 1987.

Roelof, E. C., Remote sensing of the ring current using energetic neutral atoms, *Adv. Space Res.*, 9, 12,195, 1989.

Rostoker, G., Geomagnetic Indices, *Rev. Geophys. Space Phys.*, 10, 935, 1972.

Rostoker, G., S.-I. Akasofu, W. Baumjohann, Y. Kamide, and R. L. McPherron, The roles of direct input of energy from the solar wind and unloading of stored magnetotail energy in driving magnetospheric substorms, *Space Sci. Rev.*, **46**, 93, 1987.

Rostoker, G., W. Baumjohann, W. Gonzalez, Y. Kamide, S. Kokubun, R. L. McPherron, and B. T. Tsurutani, Comment on "decay of the *Dst* field of geomagnetic disturbance after substorm onset and its implication to storm-substorm relation", *Ann. Geophys.*, **15**, 848, 1997a.

Rostoker, G., E. Friedrich and M. Dobbs, Physics of magnetic storms, in *Magnetic Storms, Geophys. Monogr. Ser.*, vol. 98, ed. by B. T. Tsurutani, W. D. Gonzalez, Y. Kamide, and J. K. Arballo, pp. 149-160, AGU, Washington D.C., 1997b.

Sato, T. and T. Iijima, Primary sources of large-scale Birkeland currents, *Space Sci. Rev.*, **24**, 1879, 347, 1979.

Schild, M. A., J. W. Freeman, and A. J. Dessler, A source for field-aligned currents at auroral latitudes, *J. Geomag. Res.*, **74**, 247, 1969.

Schmidt, A., Erdmagnetismus, in *Encyklopädie der Mathematischen Wissenschaften*, Band IV, i, B, 10, pp. 265-396, Leipzig, 1917 (in German).

Schuster, A., The diurnal variation of terrestrial magnetism, *Phil. Trans.*, **A180**, 467, 1889.

Sckopke, N., A general relation between the energy of trapped particles and the disturbance field near the earth, *J. Geomag. Res.*, **71**, 3125, 1966.

Silsbee, H. C. and E. H. Vestine, Geomagnetic bays, their frequency and current-systems, *Terr. Magn. Atmos. Electr.*, **47**, 195, 1942.

Singer, S. F., A new model of magnetic storms and aurorae, *Trans. Am. Geophys. Union*, **38**, 175, 1957.

Siscoe, G. L., A unified treatment of magnetospheric dynamics with applications to magnetic storms, *Planet. Space Sci.*, **14**, 947, 1966.

Siscoe, G. L., V. Formisano, and A. J. Lazarus, A calibration of the magnetosphere, *JGR*, **73**, 4869, 1968.

Siscoe, G. L. and N. U. Crooker, On the partial ring current contribution to *Dst*, *J. Geomag. Res.*, **79**, 1110, 1974.

- Smith, E. J., P. J. Coleman, D. L. Judge, and C. P. Sonett, Characteristics of the extraterrestrial current system: Explorer VI and Pioneer V, *J. Geomag. Res.*, 65, 1858, 1960.
- Spreiter, J. R. and B. R. Briggs, Theoretical determination of the form of the boundary of the solar corpuscular stream produced by interaction with the magnetic dipole field of the earth, *J. Geomag. Res.*, 67, 37, 1962.
- Stern, D. P., Energetics of the magnetosphere, *Space Sci. Rev.*, 39, 193, 1984.
- Stern, D. P., A simplified model of Birkeland currents, *J. Geomag. Res.*, 98, 5691, 1993.
- Störmer, C., Physique du globe, *CR Hebd. Acad. Sci.*, 151, 736, 1910 (in French).
- Störmer, C., *The Polar Aurora*, Clarendon Press, Oxford, 1955.
- Su, S. Y. and A. Konradi, Magnetic field depression at the earth's surface calculated from the relationship between the size of the magnetosphere and the *Dst* values, *J. Geomag. Res.*, 80, 195, 1975.
- Sugiura, M., Hourly values of equatorial *Dst* for the IGY, *Ann. Int. Geophys. Year*, 35, 9, 1964.
- Sugiura, M., Rotation of the low-latitude *DS* field and westward drift of a partial ring current, *Geophys. J. R. astr. Soc.*, 15, 23, 1968.
- Sugiura, M., Identifications of the polar cap boundary and the auroral belt in the high-altitude magnetosphere: a model for field-aligned currents, *J. Geomag. Res.*, 80, 2057, 1975.
- Sugiura, M. and S. Chapman, The average morphology of geomagnetic storms with sudden commencements, *Abh. Akad. Wiss. Göttingen Math. Phys. Kl.*, 4, 1, 1960.
- Sugiura, M. and T. A. Potemra, Net field-aligned currents observed by Triad, *J. Geomag. Res.*, 81, 2155, 1976.
- Sun, W., B.-H. Ahn, S.-I. Akasofu and Y. Kamide, A comparison of the observed mid-latitude magnetic disturbance fields with those reproduced from the high-latitude modeling current system, *J. Geomag. Res.*, 89, 10,881, 1984.
- Sun, W. and S.-I. Akasofu, On the formation of the storm-time ring current belt, *J. Geomag. Res.*, 105, 5411, 2000.

- Sun, W., W.-Y. Xu, and S.-I. Akasofu, An improved method to deduce the unloading component for magnetospheric substorms, *J. Geomag. Res.*, 105, 13,131, 2000.
- Swift, D. W., Possible consequences of the asymmetric development of the ring current belt, *Planet. Space Sci.*, 15, 835, 1967.
- Swift, D. W., Further possible consequences of the asymmetric development of the ring current belt – effect of variations in ionospheric conductivity, *Planet. Space Sci.*, 16, 329, 1968.
- Takahashi, S., T. Iyemori and M. Takeda, A simulation of the storm-time ring current, *Planet. Space Sci.*, 38, 1133, 1990.
- Takahashi, S., M. Takeda and Y. Yamada, Simulation of storm-time partial ring current and the dawn-dusk asymmetry of geomagnetic variation, *Planet. Space Sci.*, 39, 821, 1991.
- Takeuchi, H. and M. Saito, Electromagnetic induction within the earth, *J. Geomag. Res.*, 68, 6287, 1963.
- Tamao, T., Direct contribution of oblique field-aligned currents to ground magnetic fields, *J. Geomag. Res.*, 91, 183, 1986.
- Tonks, L., Particle transport, electric currents, and pressure balance in a magnetically immobilized plasma, *Phys. Rev.*, 97, 1443, 1955.
- Torrence, C. and G. P. Compo, A practical guide to wavelet analysis, *Bull. Am. Met. Soc.*, 79, 61, 1998.
- Tsyganenko, N. A., Global quantitative models of the geomagnetic field in the cislunar magnetosphere for different disturbance levels, *Planet. Space Sci.*, 35, 1347, 1987.
- Tsyganenko, N. A., A global analytical representation of the magnetic field produced by the region 2 Birkeland currents and the partial ring current, *J. Geomag. Res.*, 98, 5677, 1993.
- Tsyganenko, N. A., Modeling the inner magnetosphere: the asymmetric ring current and region 2 Birkeland currents revisited, *J. Geomag. Res.*, 105, 27,739, 2000.
- Tsyganenko, N. A. and D. P. Stern, Modeling the global magnetic field of the large-scale Birkeland current systems, *J. Geomag. Res.*, 101, 27,187, 1996.
- Tsyganenko, N. A., G. Le, C. T. Russell, and T. Iyemori, A study of the inner magnetosphere based on data of Polar, *J. Geomag. Res.*, 104, 10,275, 1999.

Turner, N. E., D. N. Baker, T. I. Pulkkinen, and R. L. McPherron, Evaluation of the tail current contribution to *Dst*, *J. Geomag. Res.*, *105*, 5431, 2000.

Turner, N. E., D. N. Baker, T. I. Pulkkinen, J. L. Roeder, J. F. Fennell, and V. K. Jordanova, Energy content in the storm time ring current, *J. Geomag. Res.*, *106*, 19,149, 2001.

Valdivia, J. A., D. Vassiliadis, A. Klimas, A. S. Sharma, and K. Papadopoulos, Spatiotemporal activity of magnetic storms, *J. Geomag. Res.*, *104*, 12,239, 1999.

Vasyliunas, V. M., Comment on "simulation study fundamental properties of the storm-time ring current" by Y. Ebihara and M. Ejiri, *J. Geomag. Res.*, *106*, 6321, 2001.

Verzariu, P., M. Sugiura, and I. B. Strong, Geomagnetic field variations caused by changes in the quiet-time solar wind pressure, *Planet. Space Sci.*, *20*, 1909, 1972.

Vestine, E. H., Asymmetrical characteristics of the earth's magnetic disturbance-field, *Terr. Magn. Atmos. Electr.*, *43*, 261, 1938.

Vestine, E. H. and S. Chapman, The electric current-system of geomagnetic disturbance, *Terr. Magn. Atmos. Electr.*, *43*, 351, 1938.

Vestine, E. H., L. Laporte, I. Lange, and W. E. Scott, *The Geomagnetic Field, Its Description and Analysis*, Carnegie Inst. of Washington Pub. 580, 1947.

Williams, D. J., The earth's ring current: causes, generation, and decay, *Space Sci. Rev.*, *34*, 223, 1983.

Williams, D. J., Dynamics of the earth's ring current: theory and observation, *Space Sci. Rev.*, *42*, 375, 1985.

Williams, D. J., Ring current and radiation belts, *Rev. Geophys.*, *25*, 570, 1987.

Wrenn, G. L., Persistence of the ring current, *Geophys. Res. Lett.*, *16*, 891, 1989.

Yasuhara, F., Y. Kamide, and S.-I. Akasofu, Field-aligned and ionospheric currents, *Planet. Space Sci.*, *23*, 1355, 1975.

Yokoyama, N. and Y. Kamide, Statistical nature of geomagnetic storms, *J. Geomag. Res.*, *102*, 14,215, 1997.

Zmuda, A. J., J. H. Martin, and F. T. Heuring, Transverse magnetic disturbances at 1100 kilometers in the auroral region, *J. Geomag. Res.*, *71*, 5033, 1966.

Zmuda, A. J., F. T. Heuring, and J. H. Martin, Dayside magnetic disturbances at 1100 kilometers in the auroral oval, *J. Geomag. Res.*, 72, 1115, 1967.

Zmuda, A. J., J. C. Armstrong, and F. T. Heuring, Characteristics of transverse magnetic disturbances observed at 1100 kilometers in the auroral oval, *J. Geomag. Res.*, 75, 4757, 1970.

Zmuda, A. J. and J. C. Armstrong, The diurnal flow pattern of field-aligned currents, *J. Geomag. Res.*, 79, 4611, 1974.

CURRICULUM VITAE

William B. Cade III
(July 2002)

EDUCATION:

BS in Physics, Texas A&M University, College Station, Texas (1987).

BS in Meteorology, Texas A&M University, College Station, Texas (1988).

MS in Physics, Utah State University, Logan, Utah (1993).

PhD in Physics, Utah State University, Logan, Utah (expected 2002).

EXPERIENCE:

Atmospheric and Space Environmental Forecaster, 4th Weather Wing (United States Air Force), Cheyenne Mountain Weather Support Unit (1989-1991).

Space Weather Operations Officer, Air Force Space Command, Directorate of Operations (1993-1996).

Assistant Professor of Aerospace Studies, Air Force ROTC, Texas A&M University (1996-1999).

PUBLICATIONS:

[REDACTED] A correlative comparison of the ring current and auroral electrojets using geomagnetic indices, *J. Geomag. Res.*, 100, 97, 1995.

[REDACTED] A wavelet analysis of storm-substorm relationships, in *Storm-Substorm Relationship, Geophys. Monogr. Ser.* (accepted)

PRESENTATIONS:

[REDACTED] Wavelet analysis and possible geophysical applications, Fall Meeting, American Geophysical Union, San Francisco, CA, 2001.